

PROJECT 1: CHARACTERISING THE NEURAL POTENTIAL OF DENTAL PULP MESENCHYMAL
STEM CELLS IN COMPARISON TO OTHER MESENCHYMAL STEM CELL SOURCES FOR NEURAL
STEM CELL GENERATION

AND

PROJECT 2: INVESTIGATING THE ROLE OF THE DYNAMIC SYNAPTIC CLEFT SIZE AND ITS ROLE
IN PLASTIC PROCESSES

By

SIMON FOALE

A thesis submitted to the University of Birmingham for the degree of

MASTER OF RESEARCH in BIOMEDICAL RESEARCH



UNIVERSITY OF
BIRMINGHAM

School of Dentistry

School of Clinical and Experimental Medicine

College of Medical and Dental Sciences

University of Birmingham

August 2014



UNIVERSITY OF
BIRMINGHAM

University of Birmingham Research Archive

e-theses repository

This unpublished thesis/dissertation is copyright of the author and/or third parties. The intellectual property rights of the author or third parties in respect of this work are as defined by The Copyright Designs and Patents Act 1988 or as modified by any successor legislation.

Any use made of information contained in this thesis/dissertation must be in accordance with that legislation and must be properly acknowledged. Further distribution or reproduction in any format is prohibited without the permission of the copyright holder.



UNIVERSITY OF
BIRMINGHAM



*Characterising the neural potential
of dental pulp mesenchymal stem
cells in comparison to other
mesenchymal stem cells sources for
neural stem cell generation*

Simon Foale

1005702

This project is submitted in partial fulfilment of the requirements for the award of the MRes

School of Dentistry

Supervisor: Dr Ben Scheven & Dr Wendy Leadbeater

Contents

1 Introduction.....	1
1.1 Endogenous neural stem cells	1
1.1.1 Endogenous neural stem cells for <i>in vitro</i> neural stem cell population generation	2
1.2 Embryonic stem cells	3
1.3 Mesenchymal stem cells.....	4
1.3.1 Adipose and Bone Marrow stem cells.....	4
1.3.2 Dental Pulp stem cells	5
1.4 Neurospheres.....	6
1.5 Characterising neural spheres	7
1.6 Study rationale and hypothesis	8
1.7 Aims.....	9
2 Materials and Methods	10
2.1 Animals and solutions	10
2.2 Cell Lines and isolation.....	11
2.2.1 Adipose stem cell isolation.....	11
2.2.2 Bone Marrow stem cell isolation	11
2.2.3 Dental pulp stem cell isolation	12
2.3 Cell culturing	12

2.3.1 Mesenchymal stem cell culturing	12
2.3.2 Induction to neural stem cells and subsequent culturing.....	13
2.4 Polymerase chain reaction (PCR)	13
2.4.2 Primers	14
2.4.3 PCR procedure.....	14
2.5 Immunofluorescence	15
2.5.1 Antibodies	15
2.5.2 Immunohistochemistry	15
2.5.3 Immunocytochemistry	16
2.6 Analysis	18
2.6.1 PCR	18
2.6.2 Microscopy	19
3 Results	20
3.1 Seeding density of spheroids	20
3.2 Neural/mesenchymal marker expression in murine teeth	20
3.3 Growth patterns of mesenchymal stem cell populations and spheres.....	23
3.4 Immunocytochemistry of mesenchymal cells	26
3.5 Immunocytochemistry of neurosphere cultures	30
3.6 Semi-quantitative polymerase chain reaction analysis	33

4 Discussion	37
4.1 Sphere formation capabilities.....	37
4.2 Neural phenotypes of MSC derived spheres	38
4.3 Mesenchymal characteristics of MSC derived spheres	39
4.4 Limitations.....	40
4.5 Future directions and implications	42
5. Conclusions.....	43
6. Bibliography.....	44

List of figures

1. Example of a neurosphere.....	page 7
2. Example of confluent mesenchymal stem cells.....	page 12
3. Example of PCR bands run on an agarose gel.....	page 18
4. Comparison of different seeding densities.....	page 19
5. Immunohistochemistry stains of dental pulp tissue.....	page 21
6. Optical microscopy of passage two mesenchymal stem cell populations...	page 23
7. Representative spheres from different mesenchymal stem cell sources....	page 24
8. Spheres from 96 well plates.....	page 25
9. Sphere grown on bacterial grade plates.....	page 26
10. CD146/nestin stains of mesenchymal stem cell populations.....	page 27
11. CD133/Stro-1 stains of mesenchymal stem cell populations.....	page 28
12. P75 stains of mesenchymal stem cell populations.....	page 29
13. CD146/nestin stains of neurospheres.....	page 30
14. CD133/Stro-1 stains of neurospheres.....	page 32
15. Semi-quantitative PCR analysis of adipose derived populations.....	page 34
16. Semi-quantitative PCR analysis of bone marrow derived populations.....	page 34
17. Semi-quantitative PCR analysis of dental pulp derived populations.....	page 34
18. Comparisons of semi-quantitative analysis of neurospheres.....	page 35

Tables

1. Primer list.....	page 13
2. Antibody list.....	page 14

Acknowledgements

Sincerest thanks must go to the entire team in the Dental school for their help and guidance throughout the project. The encouragement and advice from Dr Scheven and Dr Leadbeater has been important for this project to come together. Gratitude must also be expressed to Gay Smith and Michelle Holder for their patience and instruction with training. I am indebted to them all, whose help has been invaluable throughout this project.

Abstract

Loss of neurons can have huge implications. A beneficial therapy would be to generate novel neurons *in vitro* for replacement therapies. This requires the expansion of neural stem cell (NSC) populations, however accessing NSCs is a dangerous procedure. Other stem cell sources can develop neural characteristics when treated in a specific manner. Dental pulp stem cells (DPSCs) are neural crest derived and are closely related to NSCs so should readily convert when stimulated to do so. This study focused on characterizing the neural induced stem cells from three mesenchymal stem cell sources, adipose, bone marrow and dental pulp. This was achieved through semi-quantitative PCR analysis and immunofluorescence staining. DPSCs were found to show the fewest mesenchymal signs prior to induction, however both adipose and bone marrow stem cells showed a reduction in expression of markers of mesenchymal origin. Nestin, a NSC marker was not found upregulated in any sample however another marker of NSCs, CD133 was found to upregulate slightly. This study suggests that CD133 and vimentin (a mesenchymal marker used) could be promising target to indicate neural/mesenchymal phenotypes. The data does not clearly suggest one cell source is more viable for neural induction due to low sample sizes.

1 Introduction

Damage or loss of neurons can result in significant morbidity or mortality. There are numerous diseases which can result in the loss or degradation of neurons or neurotoxicity, such as Parkinson's disease, Alzheimer's disease, as well as any form of trauma to the nervous system (Thies and Bleiler 2013, Nussbaum and Ellis 2003, Stoica *et al* 2014, Li *et al* 2008). The social and economic consequences for both the injured individual and society are huge (PriebeGM. 2007). Current treatments cannot bring about recovery, but simply focus on limiting further damage and improving quality of life.

A potential therapy would be to generate novel neurons *in vitro* which can then be transplanted *in vivo*. Additionally, specific *in vitro* neuron populations could be used to investigate the mechanisms of neurodegenerative disease and drug interactions, reducing the need for expensive animal models (Zeng *et al.* 2004) (Phillips *et al.* 2009). To generate novel *in vitro* neurons, a source of neural stem cells (NSCs) is required.

1.1 Endogenous neural stem cells

It was originally believed that the adult mammal CNS did not possess the ability to generate any novel neural stem cells. Altman (1962) originally found evidence that after inducing electrolytic brain lesions in adult rats, a neuronal subpopulation was able to take up radioactive nucleoside thymidine- H^3 , a marker of mitotic division. Extremely restricted neurogenesis is now known to occur in two regions in the adult mammal, the subventricular zone surrounding the ventricles and the subgranular zone within the hippocampus (Geuna *et al* 2001). In the subventricular zone, the generated neurons are transported down the rostral

migratory stream to the olfactory bulb. Here they mature and rebuild the local population of interneurons required for the olfactory process (Alvarez-Buylla and Garcia-Verdugo 2002). Subgranular zone novel neurons migrate to the dentate gyrus of the hippocampus where they have been suggested to have a role in learning or depression however more conclusive data are needed to confirm these findings (Monje *et al* 2002, Kempermann *et al* 2004). Interestingly, there is also evidence that these cells have the capacity to increase regeneration after injury (Jin 2001), as shown by increased BrdU staining after focal ischaemia. Despite these sources of NSCs, there has never been any sign of functional integration and repair of the CNS following trauma or after neurodegeneration.

1.1.1 Endogenous neural stem cells for *in vitro* neural stem cell population generation

Endogenous neural stem cells would be extremely promising for treating neurodegenerative disorders or neurotrauma as they can be sourced from a patients' own tissue, circumventing the risk of immune rejection. The cells are already primed to become the neurons and it has arguably been demonstrated that NSCs have an innate ability to repair the damaged CNS which fails *in vivo* (Jin *et al* 2001). Additionally, it has been shown that treatment with epidermal growth factor (EGF) and basic fibroblast growth factor (FGF-2) supplements in an appropriate growth media is sufficient to induce upregulation of these cells for both murine and human populations (Laywell *et al* 2000, Reynolds and Weiss 1992, Chaichana *et al* 2006).

If a procedure can be developed to induce specific differentiation, then these NSCs could have therapeutic benefit. This approach is being investigated by a number of sources for treating many neurodegenerative disorders, with mixed results (Kulbatski *et al* 2005, Cave *et*

al 2014). There are limitations to the use of neural stem cells. As stated earlier, the cells are only found within deep structures of the mammalian brain. Invasive surgeries have to be used to collect the cells. As a result, there is a high risk of haemorrhage or infection associated with collection.

1.2 Embryonic stem cells

Another viable stem cell source for generating neural stem cells, are embryonic stem cells (ESCs). ESCs are promising because of their pluripotency (Abranches *et al* 2009). There a number of studies which have looked into ESCs ability to convert into neurons with mixed results. Zeng *et al* (2004) were able to generate neuron-like cells which expressed tyrosine hydroxylase, an enzyme used in the creation of dopamine, as well as a number of other neuronal markers indicating some specific neural differentiation has been induced. However it is not clear whether these cells still expressed the phenotype of neural, embryonic or other endogenous dopamine producing cells. Low cell survival was observed after transplantation into rats raising concerns over the integration. Other studies have also shown the presence of neuronal markers in ESC derived cells treated in a neural growth protocol, indicating their ease for differentiating down a neural pathway (Zhang *et al*. 2001).

ESCs, despite their advantages have a number of limitations. Sourcing the cells remains difficult and controversial (Ethics Committee of the American Society for Reproductive Medicine 2013, Fox *et al* 2010). Additionally, it has been suggested that their high pluripotency creates an increased risk of tumourgenicity when compared to other stem cell sources (Li *et al* 2008, Zeng *et al* 2004). Finally, as the cells are not patient specific, there is a risk of a detrimental immune response (Krystkowiak *et al* 2007).

1.3 Mesenchymal stem cells

Another possible exogenous source of developing neural stem cell is to use mesenchymal stem cells (MSCs). MSCs are stem cells of stromal origin which have multiple sources, such as the adipose, bone marrow, dental pulp and umbilical cord tissue, and are able to differentiate into a number of cell types. They are promising for neuroregenerative treatments due to ease of growth and differentiation (Forostyak, *et al* 2013, Caplan 2005). MSCs can be obtained easily from a patient, avoiding the need for immunosuppression (Anderlini *et al* 2001).

1.3.1 Adipose and Bone Marrow stem cells

Previous studies have shown that both bone marrow and adipose mesenchymal stem cells (BMSCs and ADSCs respectively) can increase expression of neural markers, whilst retaining markers of pluripotency after neural induction protocols (Heo *et al* 2013, Safford *et al* 2002, Xu *et al* 2008). Fox *et al* (2010) have shown that human BMSCs, following a neural conversion procedure, produce action potential-like behaviour. The neural-like cells also respond to L-glutamate with a calcium influx, indicating a neural phenotype. Functional benefit has been shown after incorporation of neural induced BMSCs into a site of neuronal injury, however the mechanisms behind this are unclear (Heo *et al* 2013). Additionally, both BMSCs and ADSCs are easy to access and replenish endogenously, making them an attractive target for therapeutic treatments (Safford *et al*. 2002).

1.3.2 Dental Pulp stem cells

Dental pulp stem cells (DPSCs) are promising MSCs for neural induction. Both DPSCs and neural stem cells are neural crest derived, shown by expression of the neural crest marker

P75, and appear to follow a similar differentiation pathway (Janebodini *et al* 2011). Both DPSCs and their derivatives show a neural phenotype endogenously. Odontoblast, derivatives of DPSCs, express the expected epithelial markers however it has also been shown that they also express the neural stem cell marker nestin (Farahani *et al* 2011). Farahani *et al* (2011) also showed that odontoblasts express the N-methyl-d-aspartate (NMDA) receptor and the transient receptor potential vanilloid subfamily member 1 (TRPV1), two receptors which are primarily in neurons.

DPSCs express a number of neuronal stem cell and neuron markers such as nestin, Sox2, Mash1 and β III-tubulin as well as multiple others (Young *et al* 2013). Evidence has shown that dental pulp stem cells are able to endogenously secrete neurotrophic factors at a greater production than other MSC types *in vitro* (Mead *et al*. 2013). When stimulated to differentiate, previous studies have shown that DPSCs are able to generate neural phenotypes, expressing voltage gated channels and appearing to express axonal and dendritic-like processes. These cells however did not show action potential-like behaviour (Ellis *et al* 2014).

Human dental pulp is easily extracted from teeth and upregulated without invasive techniques (Kerkis and Caplan 2012). They also show a high degree of pluripotency and have (Huang *et al* 2008).

1.4 Neurospheres

The upregulation of neural stem cells has predominantly been through the production of a free-floating, heterogeneous spheroid structure of the stem cells, known as a neurosphere

(figure 1) (Scuteri *et al.* 2011). These spheres expand in solution and when seeded onto an adhesive surface in favourable conditions, differentiate into the three main primary cell types within the CNS; neurons, astrocytes and oligodendrocytes. A number of techniques have been used to grow neurospheres, especially when using non-neural stem cells, (Chaichana *et al* 2006). Most studies tend to use a combination of 20% (w/v) epidermal growth factor (EGF) and basic fibroblast growth factor (FGF-2, Heo *et al* 2013), although there is debate about the requirement of FGF-2 (Abraham *et al* 2013). Serum has been shown to encourage differentiation (Gil-Perotin *et al* 2013), so supplements have been used including Neurobasal medium and B27 supplements. Of the two supplements, B27 appears to encourage higher rates of cell survival and aid the sphere generation (Brewer *et al* 1994).

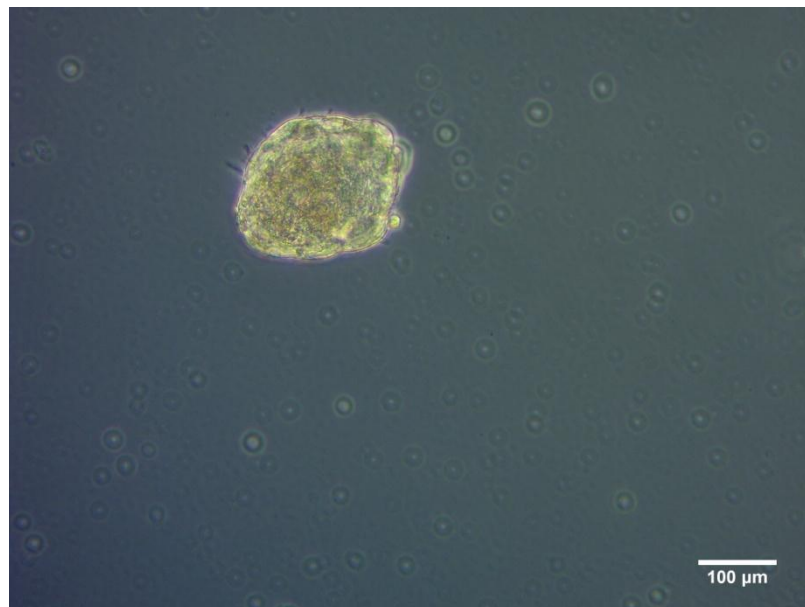


Figure 1: An example of a neurosphere taken by optical microscopy. Scale bars represent 100 μm

1.5 Characterising neural spheres

A number of methods have been used to characterise neural cells *in vitro*. Some studies have shown an ability of NSCs to pass currents, through expression of K^+ currents, however this

has only been shown in a limited example of human embryonic neural stem cells lines (Cho *et al* 2002) and thus it is not clear how translatable this research is.

One method that can be used to examine NSCs is looking at the expression profile of biomarkers. A number of markers have been proposed. Nestin is the traditional neural stem cell marker (Darabi *et al* 2013, Zwart *et al* 2008). It is an intermediate filament found in the dividing NSCs and has been shown to downregulate and be replaced upon maturation (Lin *et al* 2006). Another potential NSC marker is transmembrane protein CD133. CD133 has been reported in a number of cell types, however previous reports indicate that MSCs do not endogenously express the marker unless encouraged to convert to a NSC. A weakness with this marker is that it has been reported in neural progenitor cells (Li *et al.* 2013, Vogel *et al.* 2003, Yang *et al.* 2012). A number of other markers of NSCs have been proposed such as Mushashi1, neurofilament 68 and GFAP, however there were weaknesses in that these markers have also been observed in subpopulations of MSCs or in mature neurons (Darabi *et al* 2013) (Zwart *et al* 2008).

MSC markers can also be utilised to show a conversion from a mesenchymal phenotype. Possible markers include the transmembrane protein CD146 (Covas *et al* 2008, Crisan *et al* 2008), the intermediate filament vimentin (Mani *et al* 2008, Satelli and Li 2011) and the transmembrane protein endoglin/CD105 (Ninagawa *et al* 2011), all of which have been reported to be absent in NSCs.

1.6 Study rationale and hypothesis

The ethics, difficulty of extraction and risk of tumourgenicity have made the use of NSCs and ESCs for *in vitro* neurosphere generation, impractical and dangerous. We believe that MSCs will be more practical for generating neurospheres with the long term goal of generating functional neurons. Previous data has shown that MSCs can present a neural phenotype when stimulated in a specific manner (Heo *et al* 2013, Sasaki *et al* 2008). For these reasons, we believe that MSCs will be an efficient source of NSCs and could be used for *in vitro* preparation to treat neuronal loss disorders. It has not been addressed which of these cell sources most reliably and readily converts into NSCs. We hypothesise that as dental pulp stem cells have a closer lineage to NSCs and present neural stem cell or progenitor markers *in vivo*, the cell line will more readily convert down a neural lineage than other MSC sources.

ADSC, BMSC and DPSCs spheres were grown to produce spheres and analysed for the expression of neuronal markers by semi-quantitative PCR analysis and immunostaining. It is believed that the spheroids produced from the neurosphere production protocol with dental pulp stem cells will be more similar to those of endogenous neuronal stem cells and as such, will present a higher concentration and quantity of neuronal markers than other MSCs treated in the same manner.

1.7 Aims

The aims of this investigation were as follows:

- To culture and characterise spheroids which have been induced from DPSCs and determine whether they express a neural phenotype by analysing the expression of neural markers; nestin and CD133, mesenchymal markers; CD146, STRO-1, vimentin and CD105 and the neural crest marker P75.
- To compare DPSCs, BMSCs and ADSCs to determine whether the neural crest lineage primes DPSCs for a neural induction. This will be achieved by comparing the expression profiles of the previous markers on the MSCs cells before and after inducing sphere formation.

2 *Materials and Methods*

2.1 **Animals and solutions**

Primary mesenchymal stem cells were obtained from Male Wistar rats (120-180g). All animals were sacrificed and then obtained from Aston University following the UK Home Office Animals (Scientific Procedures) Act (ASPA). Sterile conditions were maintained by ensuring all treatment of the cells occurred within a laminar flow culture hood (Gelaire, Sydney, Australia) after extraction. Primary cells were used as previous evidence suggests that cryopreservation induces permanent phenotypical changes (Tan *et al* 2007, Milosevic *et al* 2005). Cells were grown in either growth media (GM) , made up of α -MEM media (Biosera, Sussex, UK) containing 1% penicillin/streptomycin (P/S) (Sigma-Aldrich, Dorset, UK) and foetal bovine serum (FBS) (Sigma-Aldrich, Dorset, UK), 20% for passage 0 (P0), 10% FBS for P1-2, or in neuronal induction media , made up of DMEM with 50% F12 media (Sigma-Aldrich, Dorset, UK) containing 20ng/ml epidermal growth factor (EGF) (Peprotech, London, UK), 20ng/ml fibroblast growth factor 2 (FGF-2) (Peprotech, London, UK), 2% B27 supplement (Gibco Life technologies, Paisley, UK) and 1% P/S.

2.2 **Cell Lines and isolation**

2.2.1 **Adipose stem cell isolation**

Adipose tissue was dissected from the rats' hip/abdomen and transported to sterile conditions in α -MEM/1% P/S. The tissue was finely minced using a sterile scalpel blade (Swann-Morton, Sheffield, UK) and trypsinised in 4ml of trypsin EDTA solution (Sigma-Aldrich, Dorset, UK) within a MACSmix tube rotator (Miltenyi Biotec, Surrey, UK) for 30

minutes. The trypsinisation was quenched with equal volumes of GM. The tissue was then filtered through a 70µm nylon mesh filter (Fisher Scientific, Loughborough, UK) and the filtrate of extracted cells was centrifuged at 150 xg for 4 minutes. The cell pellet was resuspended in 1ml GM and seeded into a T25 flask (Fisher Scientific, Loughborough, UK) containing 4ml GM.

2.2.2 Bone Marrow stem cell isolation

Femurs were extracted and transported to sterile conditions in α-MEM containing 1% P/S media. The condyle ends of the bone were removed and a hole was made through the bone using a BD microlance-3 23 gauge needle (BD Biosciences, Oxford, UK). 5ml of α-MEM with 1% P/S was passed through using a 10ml syringe to dissociate the cells. The cellular suspension was then centrifuged at 150 xg for 5 minutes. The resultant pellet was resuspended in 2ml of GM and seeded into a T75 flask (Fisher Scientific, Loughborough, UK) containing 8ml of GM.

2.2.3 Dental pulp stem cell isolation

Rat incisors were transferred to sterile conditions in α-MEM containing 1% P/S. The posterior end of the incisors was removed using a sterile scalpel blade and the dental pulp was extracted. The dental pulp was minced using a sterile scalpel blade. Subsequently, 2 methods were used to extract the stem cells from the DP. The first method involved trypsinising, filtering and seeding the cells as for the adipose stem cell isolation. Alternatively, the minced DP tissue was trypsinised following the same protocol as described previously, however the whole sample was seeded directly into a T25 flask.

2.3 Cell culturing

2.3.1 Mesenchymal stem cell culturing

Mesenchymal cells were grown in T25/T75 flasks as and incubated in sterile conditions at 37°C in 5% CO₂ in a RS Biotech CO₂ chamber (CM Scientific, West Lothian, UK). Previous work in this lab has shown that these conditions are able to encourage stem cell proliferation. A mild hypoxic condition would properly mimic the conditions observed *in vivo* and previous data has shown that this encourages the proliferation of neural stem cells (De Filippis & Delia, 2011) however this was not possible so normoxic conditions were used. Previous studies have shown that these conditions are still viable for the upregulation of mesenchymal stem cells (Gil-Perotin *et al* 2013). Cells were cultured in GM, which was replaced every 2-4 days. At ~70% confluency, cells were passaged, split into thirds, each of which was resuspended into a new flask. Cells were cultured until ~70% confluency at P2 and then taken for analysis (figure 2).

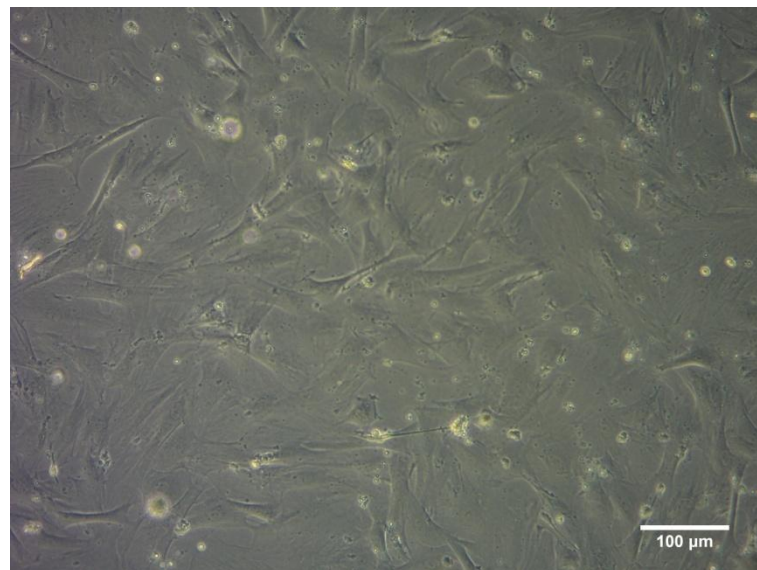


Figure 2: An example of mesenchymal stem cells at 70% confluency. When 70% confluency was met, cells were trypsinised and either reseeded at one third of the density or taken for analysis. Scale bars represent 100μm

2.3.2 Induction to neural stem cells and subsequent culturing

Cells were trypsinised, centrifuged and resuspended in the neural induction media at a defined cell concentration. The cells were seeded into a HydroCell, low adherence plate (Thermo Scientific Nunc, Loughborough, UK) or 60mm bacterial grade plates (Fisher Scientific, Loughborough, UK). At day 4, a volume equal to half the original seeding volume of neural induction media was added. At day 7-10, optical microscopy images were taken with Zeiss Primovert microscope (Zeiss AxioCam, Cambridge, UK). Between day 7-10, the cells were taken for imaging.

2.4 Polymerase chain reaction (PCR)

2.4.2 Primers

A list of the primers used in this study is shown below:

Gene	Relevance	Sequence	Source	Accession no. (product size, base pairs)
CD105	Mesenchymal marker	F-TTC AGC TTT CTC CTC CGT GT R-TGT GGT TGG TAC TGC TGC TC	Invitrogen	NM_001010968.2 (324)
CD146	Mesenchymal marker	F- CAACTCATTTCAGGGCCTCAT R- AAGCACCATTCTCCCACTTG	Invitrogen	NM_023983.3 (309)
GAPDH (glyceraldehyde-3-phosphate dehydrogenase)	Housekeeper gene	F- CGA TCC CGC TAA CAT CAA AT R-GGA TGC AGG GAT GAT GTT CT	Invitrogen	(391)
Vimentin	Possible neural/mesenchymal marker	F-AGATCGATGTGGACGTTTCC R- GCAGGTCCTGGTATTACAG	Invitrogen	NM_031140.1 (395)
Nestin	Neural marker	F-CAT TTA GAT GCT CCC CAG GA R-AAT CCC CAT CTA CCC CAC TC	Thermo Scientific	NM_012987.1 (285)
P75	Neural crest lineage marker	F- CCTCTGGAGGTGCCAAGGAG R- TTGGATCCTGCTGGGCGCTGTGCTGTC	Invitrogen	(275)

Table 1: PCR primers list and their sources (Invitrogen, Paisley, UK; Thermo Scientific, Loughborough, UK)

2.4.3 PCR procedure

Cells were centrifuged at 150 xg for 4 minutes. The pellet was lysed using 350µl RLT buffer (Qiagen, Manchester, UK) containing 0.1% mercaptoethanol. RNA was extracted following

the manufacturer's instructions in the RNeasy mini kit (Qiagen, Manchester, UK). Samples were treated with 350µl of 70% ethanol and spun once at 9000 xg for 30 seconds. This was then repeated with RW1 buffer then RPE buffer and then 500µl RPE buffer at 9000 xg for 2 minutes. RNA was collected by centrifugation with 50µl of RNase free water for 1 minute at 9000 xg. cDNA was created from the samples using a thermal cycling block (Eppendorf, Stevenage, UK) using the Bioline Tetro Kit (Bioline, London, UK).

cDNA was incubated with REDTaq, forward and reverse primers and RNase free water, within a thermal cycling block and run for a maximum of 36 cycles. Cycles included denaturing at 94°C, followed by annealing at 55°C and finally allowing extension at 72°C. cDNA samples were then loaded onto a 1.5% (w/v) agarose (Sigma-Aldrich, Dorset, UK) gel in 60ml of Tris-acetate-EDTA (TAE) buffer (Severn Biotech Ltd, Worcestershire, UK) containing 3µl ethidium bromide (Sigma-Aldrich, Dorset, UK) and run at 110 volts for 30 minutes. The PCR products were visualised as bands on the gel under UV and photographed using a G-Box gene analyser and the GeneSnap software (Syngene, Cambridge, UK). Traditionally, a ladder is used with each investigation to determine that correct bands were made. However, time and resource limitations mean that this was not possible in the present study so results have to be taken with caution.

2.5 Immunofluorescence

2.5.1 Antibodies

A list of the antibodies used to stain and visualise the cells, is shown below:

Antibody specificity	Stain	Working dilution	Species source	Source
CD133	Neural	1:300	rabbit	abcam
CD146	MSC	1:250	rabbit	abcam
Nestin	Neural	1:250	mouse	BD Biosciences
P75	Neural crest	1:250	Rabbit/mouse	Sigma-Aldrich /Novocastra
Stro-1	MSC	1:200	mouse	R&D Biosciences
Rabbit IgG, Alexafluor 488	-	1:500	goat	Molecular Probes
Mouse IgG, Alexafluor 594	-	1:500	goat	Invitrogen

Table 2: List of antibodies used and their sources (abcam, Cambridge, UK; Sigma-Aldrich, Dorset, UK; BD Biosciences, Oxford, UK; Novocastra, Leica Biosystems, Milton Keynes, UK; R&D Biosciences, Cambridge, UK; Molecular Probes; Invitrogen). Concentrations were not supplied of the primary products from the sources so working dilutions of their products have been stated instead.

2.5.2 Immunohistochemistry

Sagittal sections from decalcified Sprague Dawley rat teeth (supplied by Dr Leadbeater) were stained and visualised. 10µm sections were taken using a cryostat microtome (Bright, Huntingdon, UK) and mounted onto polarised microscope slides (Thermo Scientific, Loughborough, UK). Slides were washed in 10mM Phosphate buffered saline (PBS) containing 0.1% Triton-X (Sigma-Aldrich, Dorset, UK). Slides were dried and a hydrophobic marker (Vector Laboratories Inc., Peterborough, UK) was drawn around the tissue. 100µl of blocker solution: containing PBS/Triton-X solution (PBS-T) with 10% normal goat serum (NGS) (Biosera, Sussex, UK) and 3% bovine serum albumin (BSA) (Sigma-Aldrich, Dorset, UK) was added to each tissue sample. Slides were incubated for 1 hour in a humidified chamber at room temperature before replacing the blocker solution with 100µl of primary antibody

solution, made of PBS-T, 3% BSA and the appropriate dilution of primary antibody. Slides were incubated in a humidified chamber for 16-18 hours at 4°C before washing in PBS-T for 3x5 minutes. 100µl of secondary antibody solutions were added and incubated for 1 hour at room temperature before washing in PBS for 3x5 minutes. Coverslips were mounted onto the slides using Vectashield mounting media containing DAPI (Vector Laboratories Inc., Peterborough, UK). Slides were then incubated at -4°C until analysed by fluorescence microscopy.

2.5.3 Immunocytochemistry

2.5.3.1 *Immunocytochemistry of mesenchymal stem cells*

Mesenchymal stem cells were reseeded after P2 onto a 0.17mm thick coverslip (Smith Scientific Limited, Kent, UK) within a cell culture at its previous concentration and left for 1 day to adhere. Coverslips were fixed in formalin (Sigma-Aldrich, Dorset, UK) for 10 minutes at room temperature before washing in PBS for 3x5 minutes, followed by washing in PBS with 3% BSA for 3x5 minutes. Parafilm (Sigma-Aldrich, Dorset, UK) was laid onto a large petri dish and 50µl of primary antibody solution was pipetted onto the film. A coverslip was laid cell side down onto the drop and then left to incubate at 4°C for 16-18 hours within the petridish in a humidified chamber. The coverslip was washed 3x5 minutes in PBS before incubation with the secondary antibody for one hour in a darkened humidified chamber at room temperature, following the same protocol. Coverslips were washed 3x5 minutes in PBS and excess fluid removed. Coverslips were then mounted onto a slide (Menzel-Glaser, Braunschweig, Germany) using Fluoroshield mounting medium containing DAPI (Sigma-Aldrich, Dorset, UK) and stored at 4°C.

2.5.3.2 Immunocytochemistry of, 'neurospheres'

Spheroids were imaged as described by Sasaki *et al* 2010 to avoid seeding and differentiation (Deleyrolle & Reynolds 2009). Spheroids were transported to a 12 well plate using a wide gauge blunt ended needle to prevent damage. The cells were then left for 5 minutes to settle. Media was aspirated whilst viewing under an inverted, phase contrast microscope (Zeiss AxioCam, Cambridge, UK) to minimise loss of spheres.

The spheres were fixed to base of the wells with 4% formaldehyde (Sigma-Aldrich, Dorset, UK) for 20 minutes before washing in 400µl PBS for 3x5minutes. Spheres were incubated in PBS-T for 5 minutes before 3x5minute washes in PBS. 400µl of PBS/3% NGS was added for 30 minutes. After a subsequent wash, cells were incubated with PBS containing 3% BSA for 15 minutes. Another wash was performed and 200µl of primary antibody was added and left overnight in a humidified chamber at 4⁰C. Spheres were washed in PBS before adding 200µl of secondary antibody solution and incubating at room temperature in a darkened humidified chamber. A final wash with PBS was performed before addition of DAPI with Prolong anti-fade reagent (Life technologies, Paisley, UK). Cells were then stored at 4⁰C before imaging.

2.6 Analysis

2.6.1 PCR

PCR Band intensities were measured with GeneTools software (Syngene, Cambridge, UK) and compared to GAPDH bands as described by Shi *et al* (2001) (figure 3). Where possible intensities were compared using a paired or unpaired t-test. Data were checked for normality using a Shapiro-Wilk test, however the low sample size meant that non-parametric

tests would not have been appropriate. Post-hoc tests and non-parametric tests were not used as the low sample size would have meant that no significance could have been found. All statistical tests were performed using SPSS statistics version 21 (IBM Corp, New York, USA). Graphs were generated of the data using Sigmaplot (Systat Software Inc, London, UK).

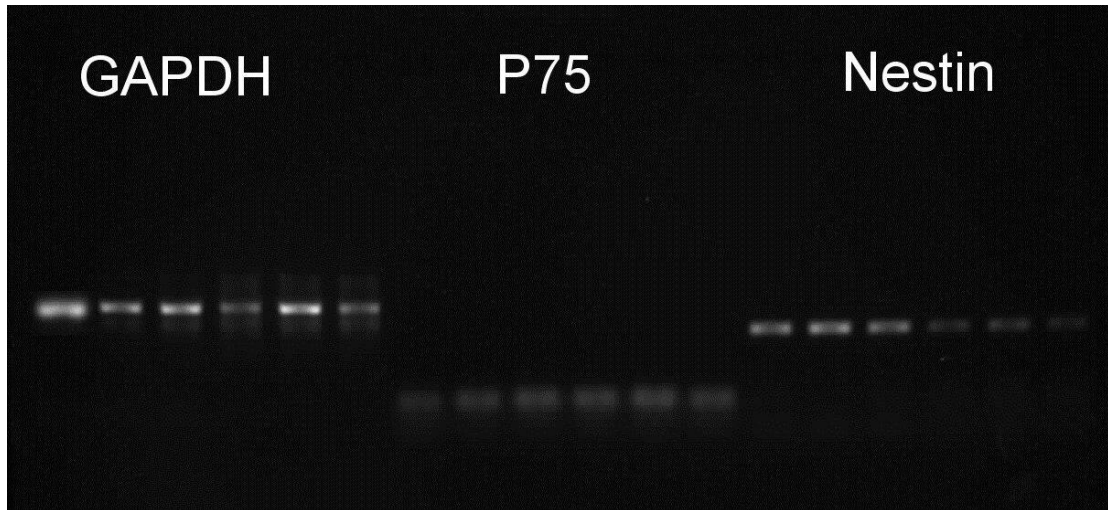


Figure 3: An example of the PCR data bands. Specified cDNA bands were compared to their corresponding GAPDH band intensity to determine a relative level of expression.

2.6.2 Microscopy

Bright-field microscopy images were taken of sphere and mesenchymal cultures using an inverted bright-field microscope. Fluorescent microscopy images of the dental pulp tissue and cell cultures were obtained using a Zeiss Axioplan-2 fluorescent microscope (Carl Zeiss Ltd, Herfordshire, UK). Images were taken from within the tissue site and analysed. Images of the spheres and mesenchymal stem cells were obtained using a fluorescent inverted microscope. Compared images were modified equally to remove background on ImageJ (National Department of Health, Maryland, USA) before qualitative analysis.

3 Results

3.1 Seeding density of spheroids

Prior to the main investigations, a preliminary study was performed to examine the effects of different seeding concentrations using bone marrow mesenchymal stem cells.

Concentrations above 5×10^4 cells/ml showed extensive clustering of cells, which were much larger than the expected neurospheres (figure 4). It is likely that due to the high concentrations, cells were in such close proximity that they adhered to create a large, densely packed cluster of cells. Sufficiently high concentrations were needed to be detectable through the cell counting technique and so that sufficient samples could be obtained for PCR analysis. Therefore the highest cell concentration where the dense and possibly harmful structures did not develop, was used for all following experiments. The optimum concentration based on these preliminary observations was 5×10^4 cells/ml.

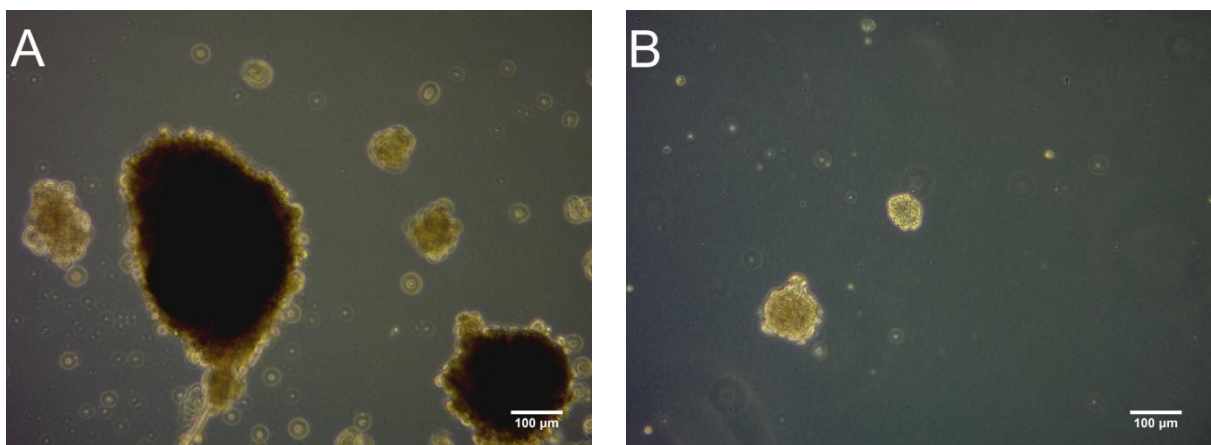


Figure 4: A bright-field microscopy images showing an example of different cell densities. (A) cells seeded at 10^6 cells/ml developed large clustering cell structures which were extremely dark in the centre. Small possible neurosphere like cultures can be observed however much larger and darker structures indicate improper growth of the cells. Scale bars represent $100\mu\text{m}$.

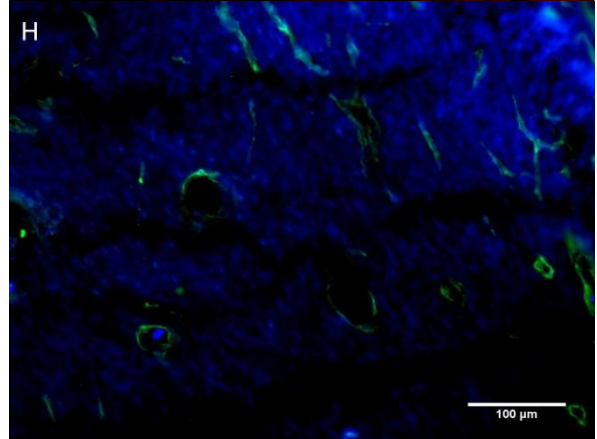
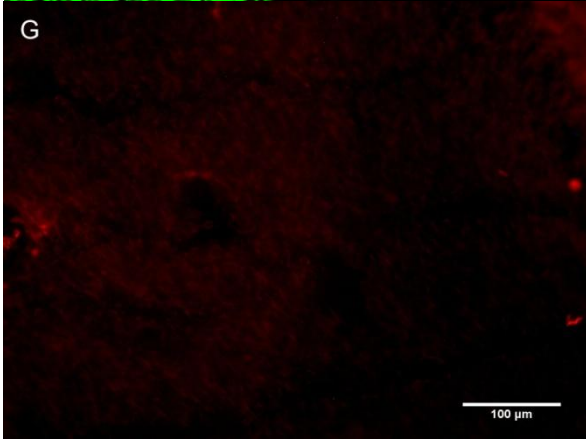
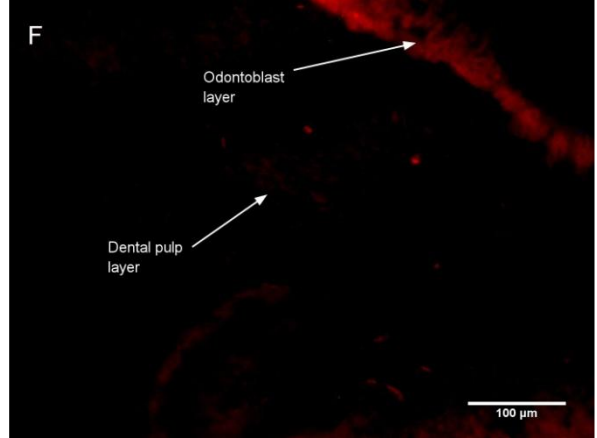
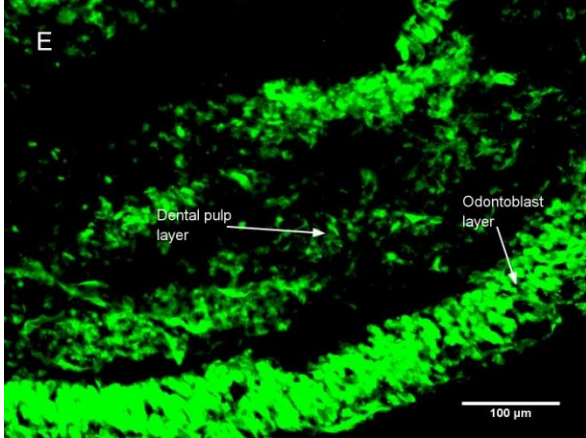
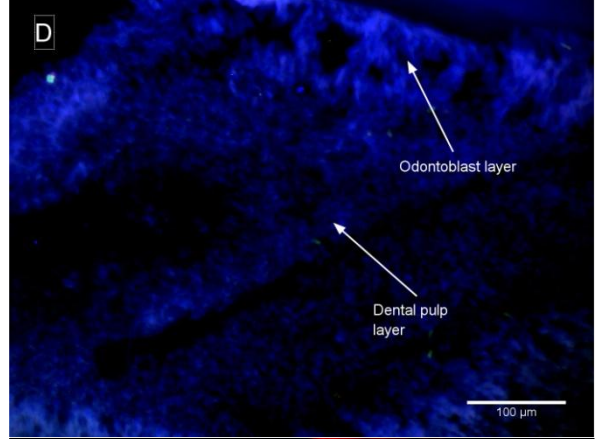
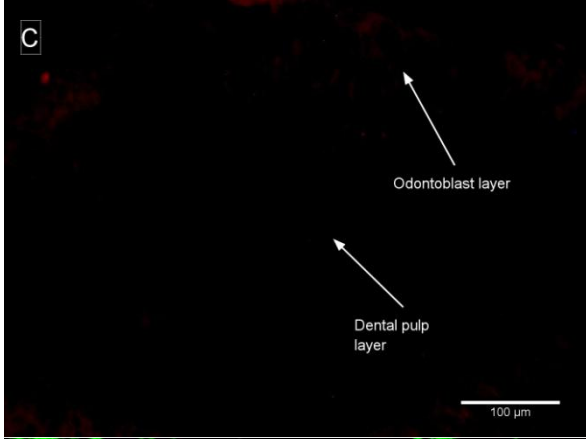
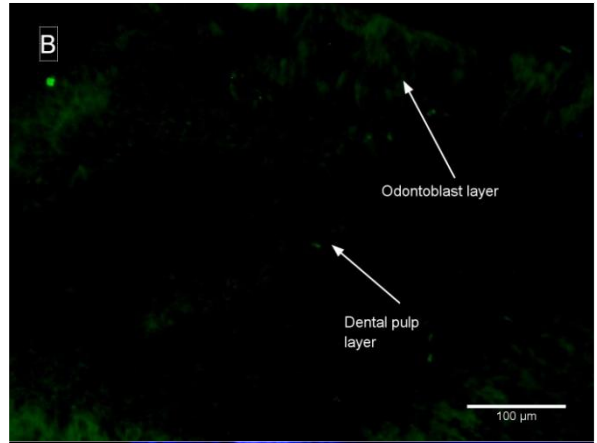
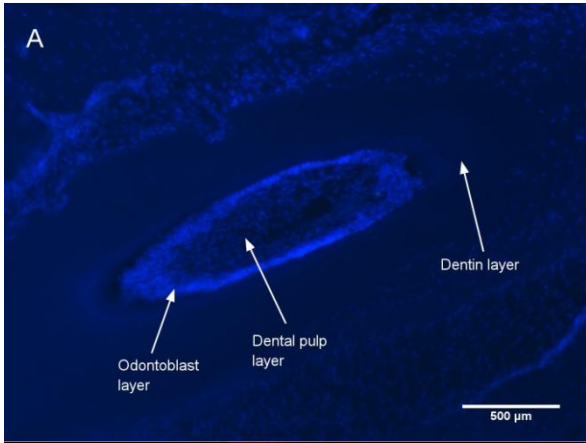
3.2 Neural/mesenchymal marker expression in murine teeth

Images were obtained from within the dental pulp from the rat teeth incisors slices (figure 5A). Control images showed a higher fluorescence intensity on areas of the odontoblast layer suggesting a significant amount of background staining within this region (figures 4.2 B-D). It can be observed that there was relatively strong staining of P75 within the dental pulp layer. The staining can also be seen to be extremely strong on the odontoblast layer as shown by the bright non-specific staining occurring on the edges of control images (figure 5E).

The intensity of nestin staining appears to be quite variable. When co-stained with either CD146 or CD133, some images show only faint staining, and is potentially background (figure 5F). Other images however show an increased level of nestin staining, which is clearly greater than that seen in the control groups (figure 5G). Artefacts appear to be causing the increased signal in some samples which could be creating glare across the observed tissue. Because of the variability, it is difficult to determine the nestin staining from the data.

CD146 staining, like P75 can be found at high levels in the odontoblast layer, however very little signal can be observed in the dental pulp layer. Most images show CD146 expression surrounding areas which lack DAPI staining suggesting CD146 surrounds nerve tracts or blood vessels (figure 5H). CD146 co-staining with nestin showed no co-localisation.

CD133 staining showed very little staining, however it was more apparent than nestin stains (figure 5I). Some co-localisation between nestin and CD133 can be observed (figure 5J).



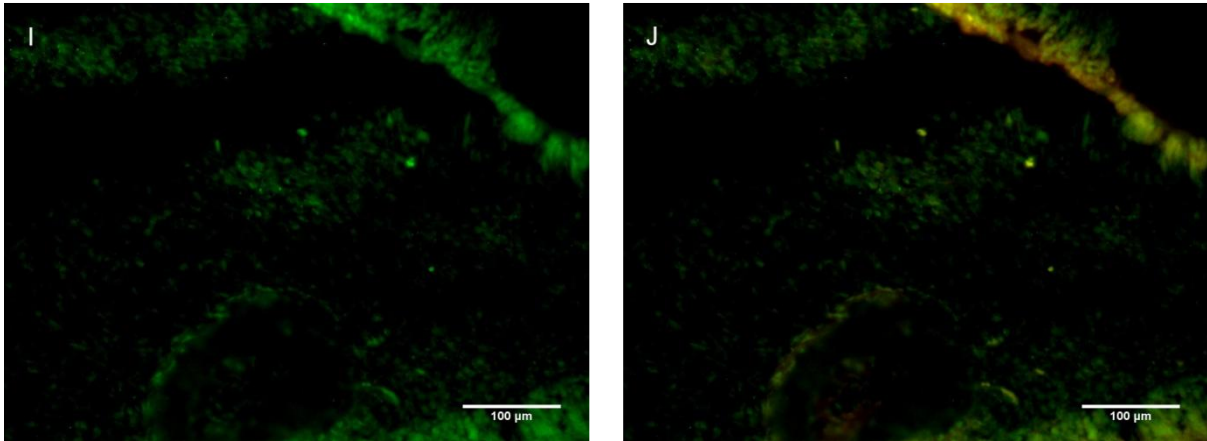


Figure 5: Representative images of the stained dental pulp sections are displayed. (A) A larger image showing the anatomy of slices which were imaged. Images were taken within the dental pulp layer, with occasional odontoblast layers appearing in shot. (B-D) Control images taken of the dental pulp sections. (B) Staining with just the Alexafluor 488 secondary antibody, (C) just the Alexafluor 594 secondary antibody and (D) a merged image of the two secondary antibodies with DAPI staining. Note how the brighter DAPI staining occurs on the edges of the image, where the odontoblast layer resided. This represented much larger background staining, hence slight corresponding green and red stains can be observed on the single control images. (E) An example of the P75 stained tissue. (F-G) Nestin staining from the section, note how although the staining is fairly low in both samples, the variation between the absence of staining in sample in F and amount in G is quite striking. (H) CD146 staining (green) with DAPI (blue). Note how the green staining appears to surround areas where there is a lack of DAPI staining. CD133 images in the dental pulp are shown, (I) CD133 independently, (J) CD133 with nestin stains. Although CD133 appears more apparent, sections of nestin and CD133 can be seen to co-localise at some sites within the tissue. Scale bars represent 100µm.

3.3 Growth patterns of mesenchymal stem cell populations and spheres

It was observed that the growth pattern for the trypsinised dental pulp tissue was very slow and regularly stalled at P2 meaning that insufficient cells were collected (figure 6A). All other tissue samples were observed to grow relatively well and reached high levels of confluency within one week of seeding (figures 6B-D).

Figure 7 shows a clear example of the growth of spheres in the neural induction media. It has to be noted however that due to availability of the HydroCell plates, different sized wells were used. Both 12 well plates and large individual wells showed similar results (figure 7). Spheres were developed from all cell types, however DPSC spheres were characteristically smaller, rarely exceeding 100µm in diameter, than their ADSC and BMSC counterparts which averaged around 150-170µm but could reach 200µm.

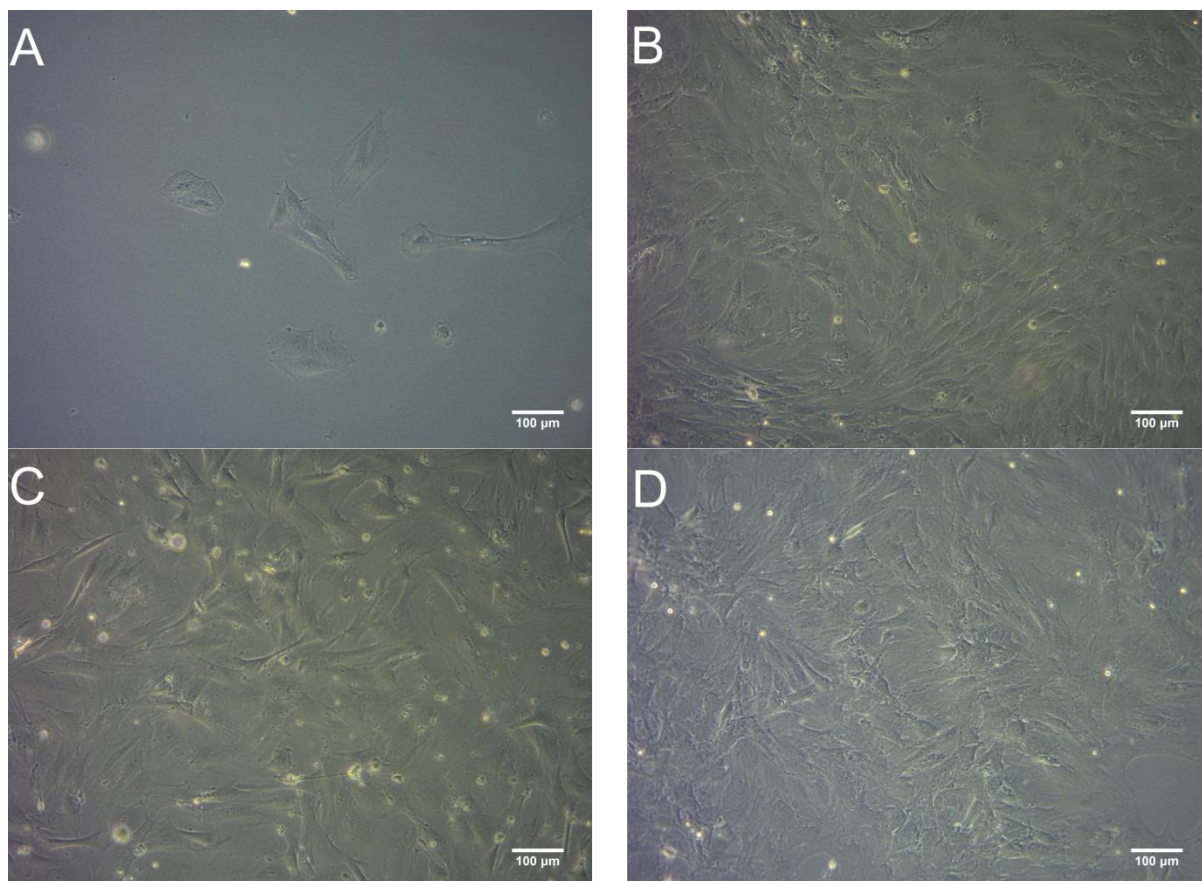


Figure 6: Light microscopy images of the mesenchymal stem cells one week after reaching P2. (A-B) Images of the different dental pulp stem cell treatments. Stem cells which were trypsinised (A) showed low growth rates and did not reach confluency at P2, whereas those treated by directly seeding the minced tissue (B) were observed to grow at much faster and more reliable rates. (C) ADSCs and (D) BMSCs all both showed rapid growth rates and reached 70% confluency within a week of seeding. Scale bars represent 100µm.

Both Adipose and dental pulp tissue grew into spheroids, however adipose spheres appear much larger (figure 7A and B). In BMSC samples there was frequent cell adhesion to the HydroCell plates (figure 7C).

Large clusters of cells with dark, dense centres were observed with the spheres grown in the 96 well plates (figure 8), similar to those seen when seeding at high densities (figure 4A), however there was also signs of smaller, less dense and brighter spheres growing as well (figure 8B).

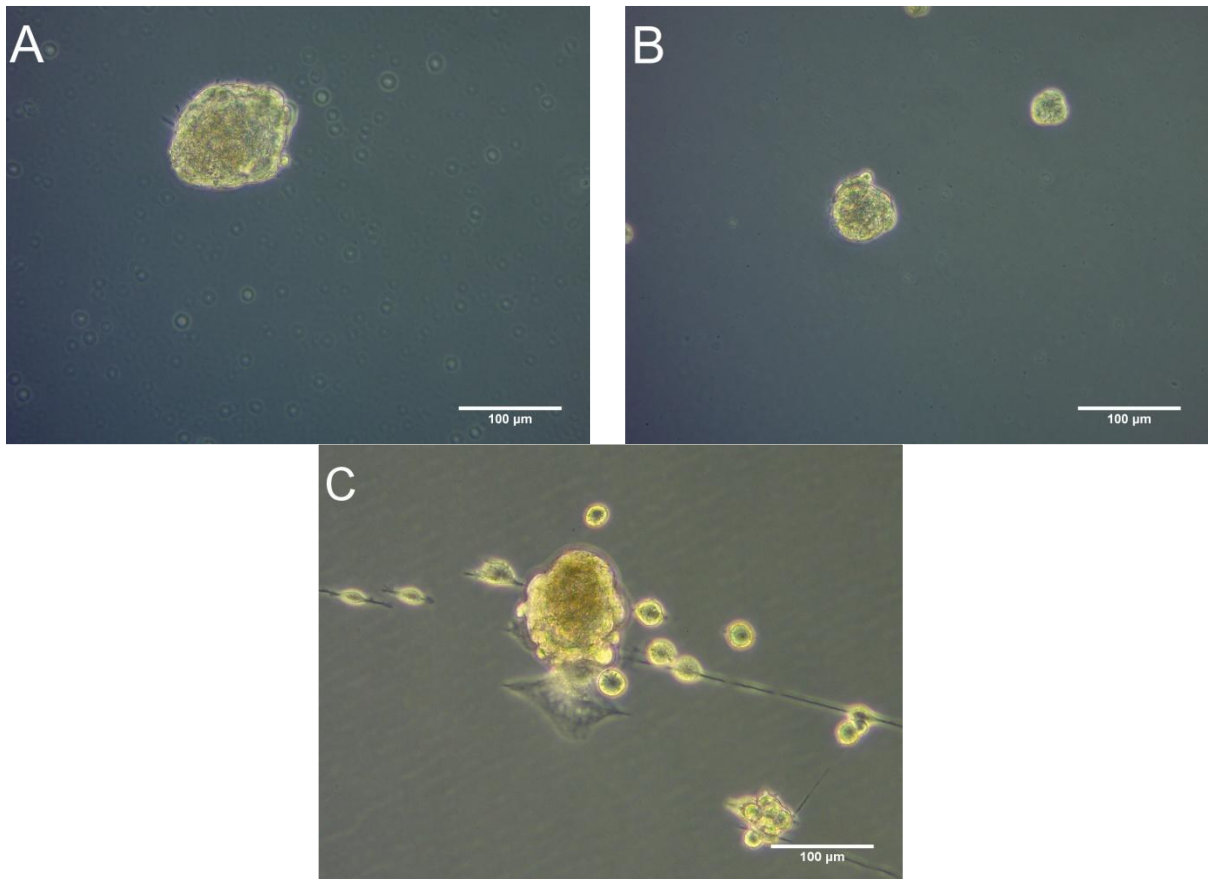


Figure 7: Representative images of the spheres generated by the three stem cell types in large HydroCell plates. (A) Adipose spheres which have managed to grow relatively large in the treatment period, (B) dental pulp derived spheres and (C) bone marrow derived spheres. Some bone marrow stem cells can be seen to have long processes extending from their somas indicating that they have adhered and are gaining a fibroblast like expression. Scale bars represent 100µm.

Latter samples were grown on bacterial grade plates which lacked the anti-adhesive properties of HydroCell plates. In these samples, there was a significant increase in the number of cells adhering to the plates and presenting fibroblast-like morphologies, with finger like extensions from the soma (figure 9). This was most notable in the bone marrow stem cell sample, as visible by the large and flat appearing cells which did not show any spheroid characteristics. Spheroids that did develop appeared much smaller and less frequent (figure 9D). The adipose tissue did not even grow into spheres, however the cells were seeded a few days after reaching confluency, so it possible that the cells were damaged prior to neural induction (figure 9B).

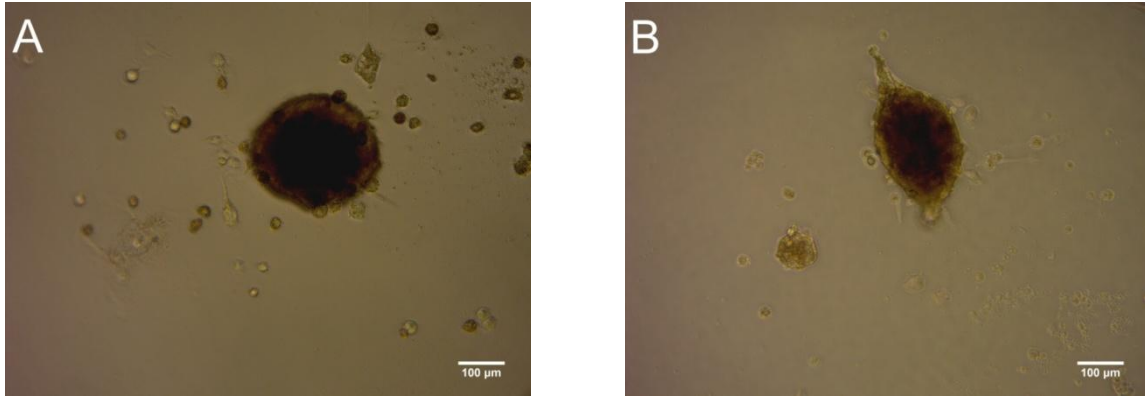


Figure 8: Representative optical microscopy images of spheroids formed by the (A) adipose stem cells and (B) dental pulp stem cells within the 96 well plates. Large clusters are seen with dark centres. (B) A, 'normal,' sphere can be observed adjacent, clearly indicating the variation in the density of the structures.

Due to the low sample size, all of the data were used in subsequent analysis despite variability in the morphology of the spheres within groups.

3.4 Immunocytochemistry of mesenchymal cells

It can be observed that there is strong staining for CD146 for the adipose and bone marrow samples (figures 10A and C). Staining appears to surround DAPI nuclear stain (not shown) so does not locate to the nucleus. There was some correlation between the CD146 staining and the nestin staining for both adipose and bone marrow samples, although this is not exclusive (figures 10A-D). The nestin staining was quite variable within sample groups, with both high levels and low levels being observed. Very low levels of CD146 could be seen on some of the cells in the dental pulp group, whereas no nestin staining was observed (figure 10E-F).

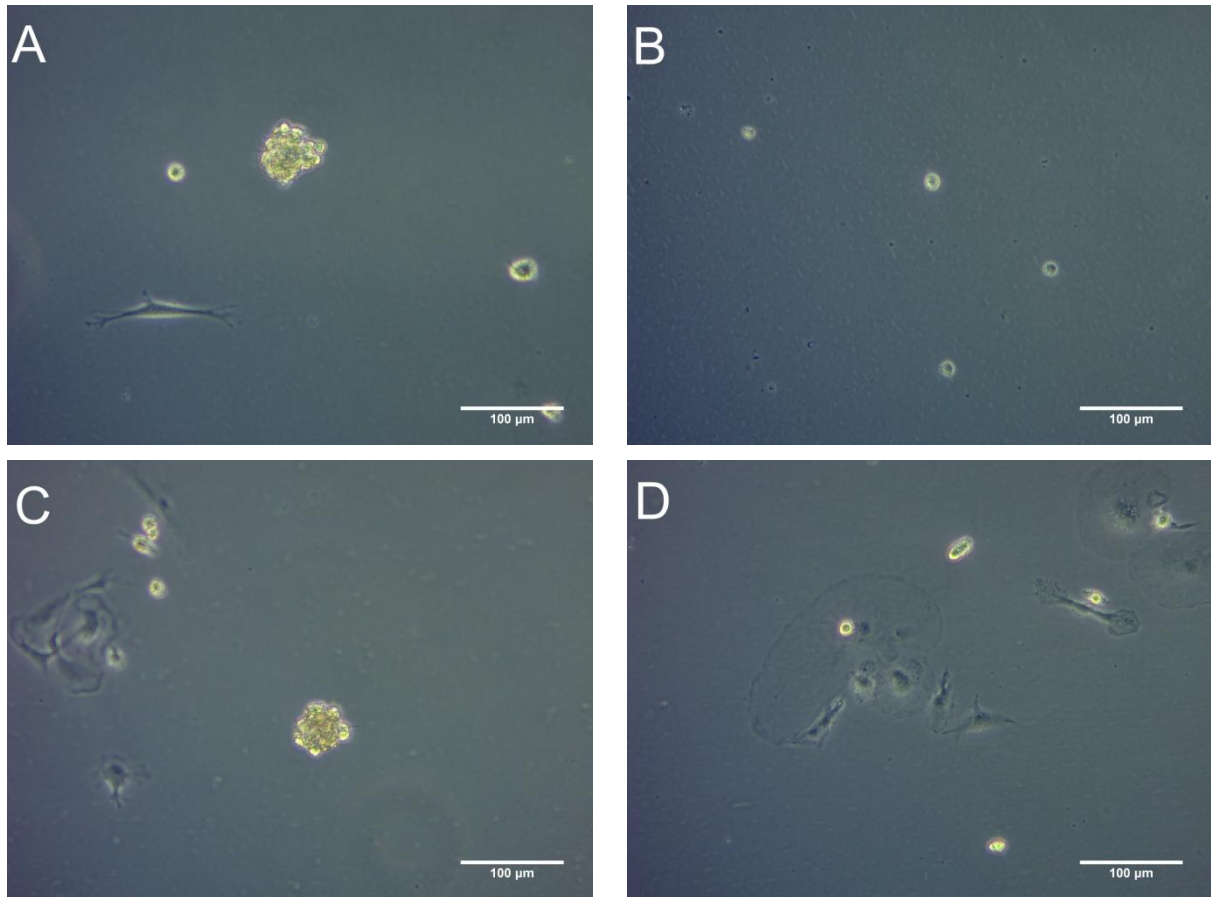


Figure 9: Light microscopy images showing the spheres formed in the bacterial grade plates. (A) Dental pulp stem cell derived sphere with an adhered cell in the background. (B) Adipose stem cells did not form spheroids in the bacterial grade plates and instead appeared to dissociate and die. (C) Bone marrow derived spheres as well as (D) large adhering cells forming fibroblast-like colonies.

Low levels of CD133 and Stro-1 are seen consistently throughout the 3 samples prior to neural induction (figure 11). The adipose and dental pulp data should be taken with caution as only one image was obtained. For the adipose sample, CD133 staining tended to coincide with areas where air bubbles could be seen which may have accentuated any signal (figure 11A). The data suggests a strong co-localisation between the samples, with Stro-1 only appearing at sites of high intensity CD133 staining. CD133 staining in the dental pulp seemed to correlate almost precisely with the Stro-1 (figure 11E-F).

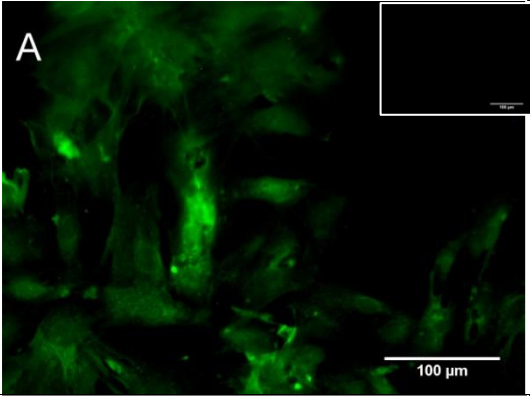
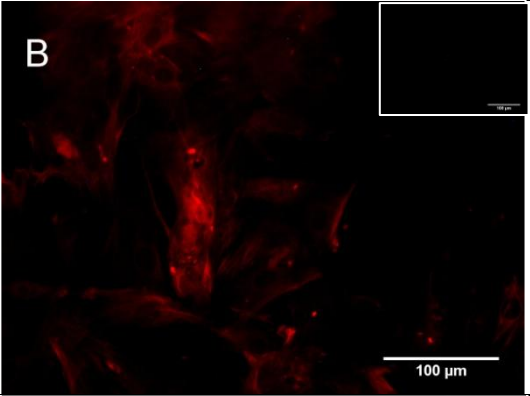
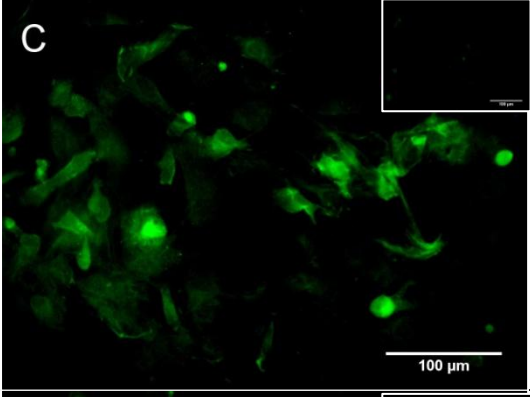
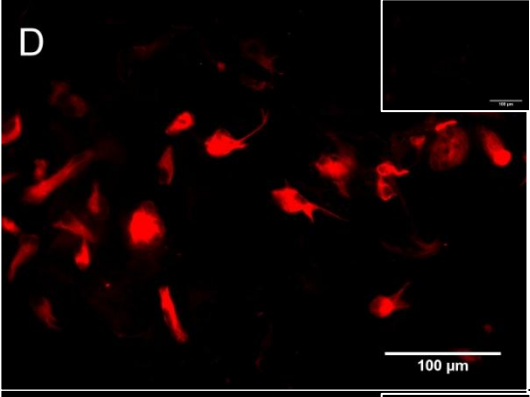
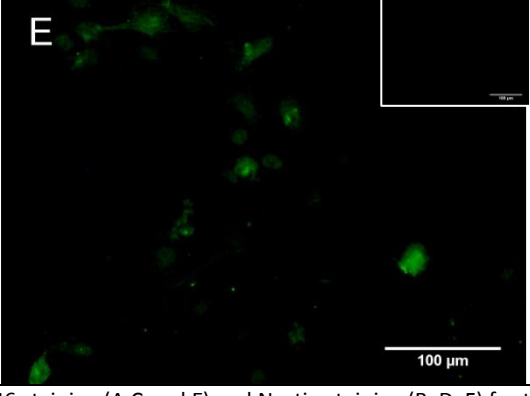
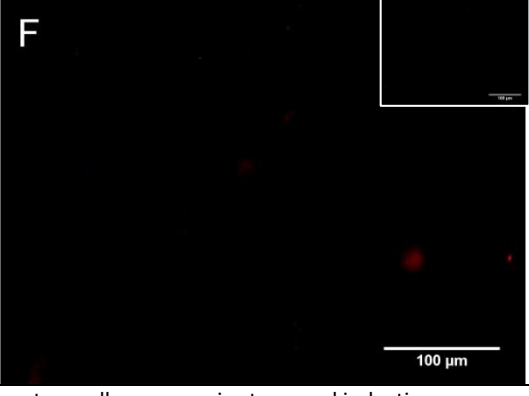
Stem cell source	Stain	
	CD146	Nestin
Adipose		
Bone Marrow		
Dental pulp		

Figure 10: CD146 staining (A,C and E) and Nestin staining (B, D, F) for the stem cell sources prior to neural induction treatment. Scale bars represent 100µm. (Insets) Control images for the respective images.

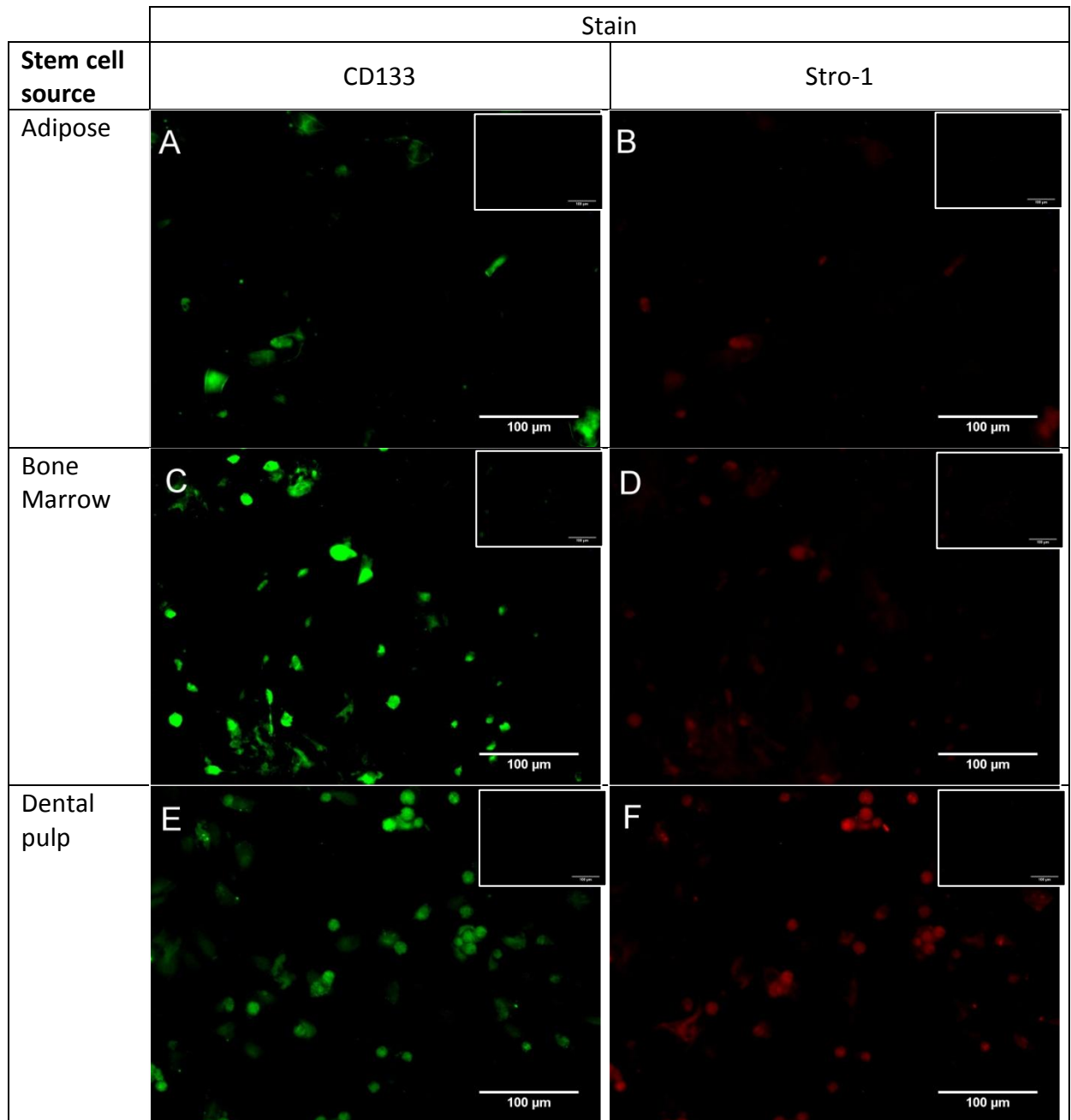


Figure 11: CD133 staining (A,C and E) and Stro-1 staining (B, D, F) for the stem cell sources prior to neural induction treatment. Scale bars represent 100µm. (Insets) Control images for the respective images.

Only one sample was obtained for the P75 stains for each MSC source. No P75 staining was observed in the ADSCs (figure 12A). Bone marrow showed a low level of staining, however the stain co-localised perfectly with CD133 staining, possibly indicating a region of excess non-specific staining (figures 12B and C). This unfortunately cannot be confirmed from the

data. DPSCs seem to express high levels of filamentous projections surrounding DAPI stained nuclei, however only in a certain subpopulation of the cells (figure 12D).

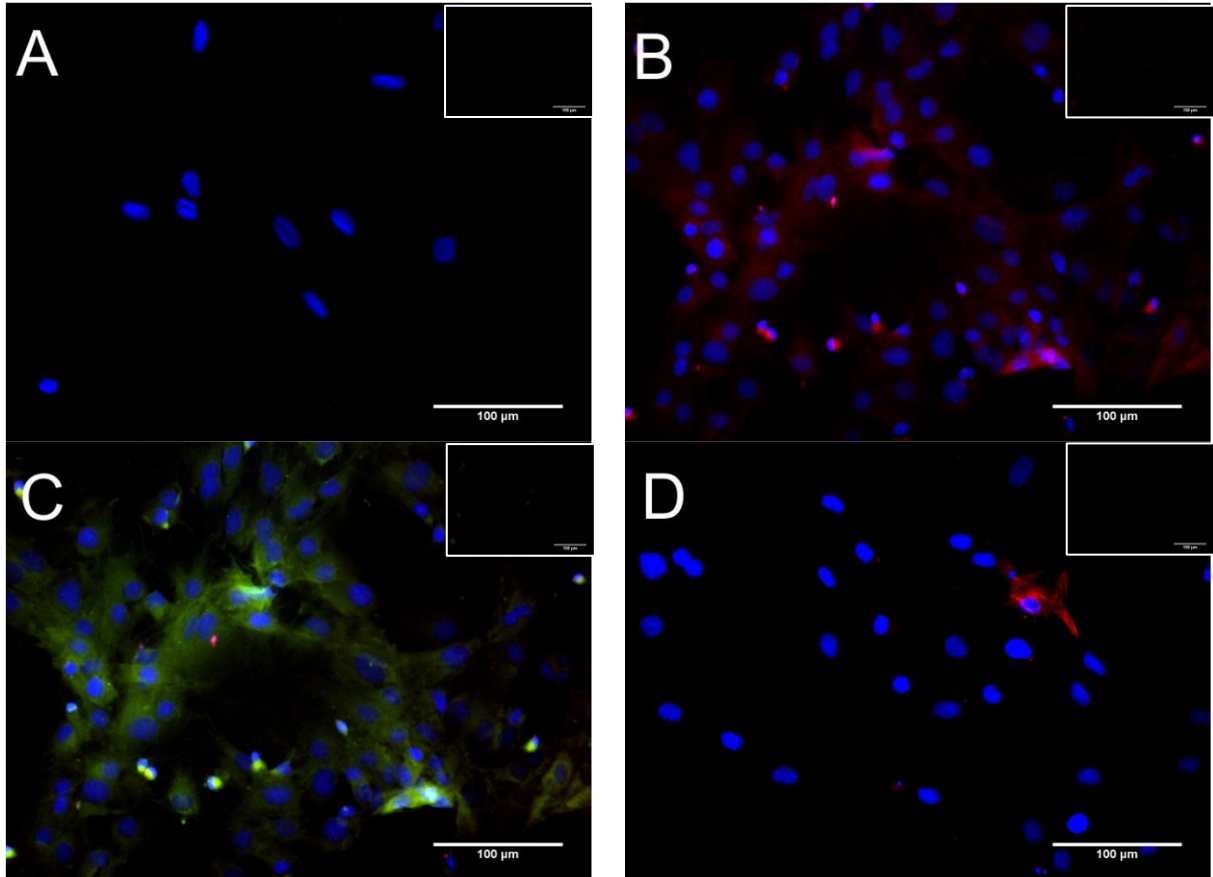
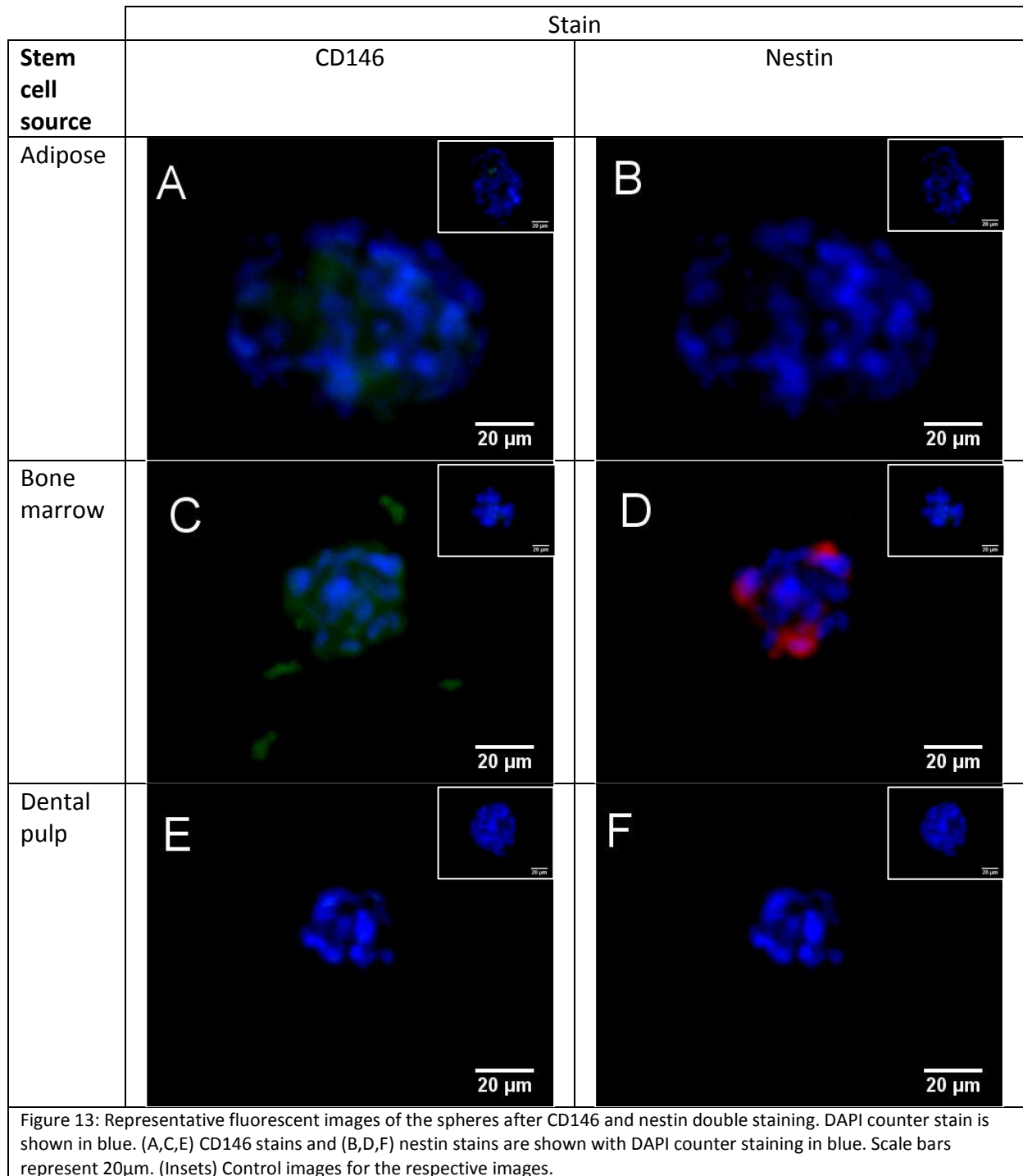


Figure 12: P75 images taken of the MSCs prior to neural induction. Blue staining shows DAPI, red shows P75 and stained nuclei with (A) ADSCs, (B-C) BMSCs and (D) DPSCs. Green staining in (C) shows the CD133 staining from one example which appears to correspond with the P75 stain. Scale bars represent 100µm. (Insets) Control images for the respective images.

3.5 Immunocytochemistry of neurosphere cultures

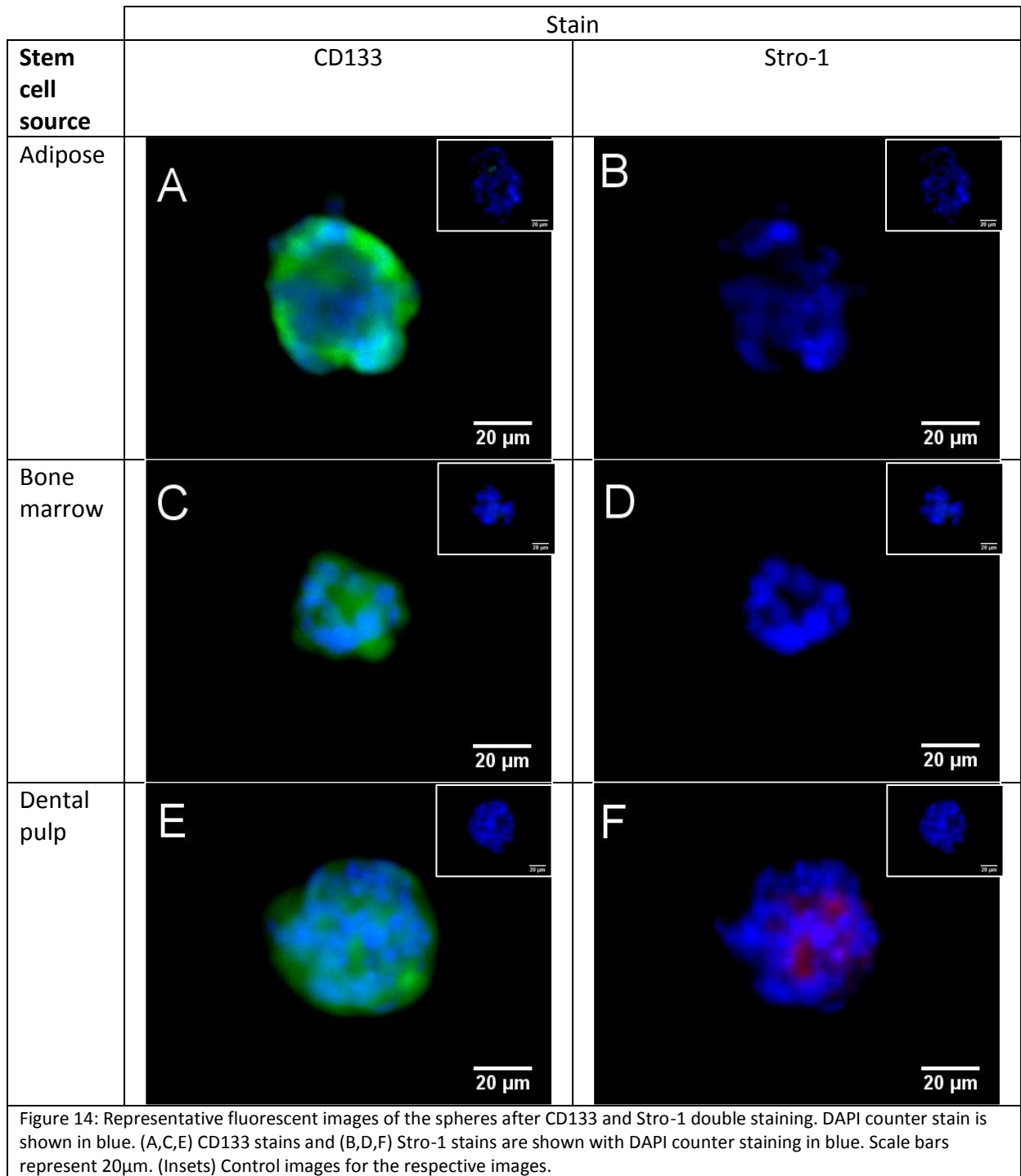
Despite checking the size of spheres prior to imaging, sphere size was not were not always consistent after collecting by the method proposed by Sasaki *et al* (2008), which may have affected the expression profile. P75 staining was not successful so has not been included.



CD146 was observed on both the ADSC and BMSC derived spheres, however the distribution was not the same (figures 13A, C and E). ADSC spheres expressed more CD146 in the centre whereas BMSC derived spheres expressed CD146 uniformly across the structure (figures 13A and C). No expression was observed for the DPSC derived spheres (figure 13E). Only the

BMSC derived spheres showed any nestin staining (figure 13B, D and E). Nestin was only found in subpopulation of BMSC spheres and was only found in small collections on edges of spheres, surrounding DAPI nuclear staining (figure 13D).

CD133 was found in all MSC derived sphere populations, however ADSC spheres only showed a subpopulation which expressed the protein (figures 14A, C, and E). When CD133 was present on ADSC spheres, it tended to show the strongest signal on the outer layer of the spheres, although low levels were still observed within the core (figure 14A). CD133 varied in intensity on BMSC spheres but always was observed uniformly across the structure (figure 14C). A similar observation was found with DPSC spheres, however some did show a higher intensity stain on the periphery. Again all stains appeared to surround DAPI nuclear staining. Stro-1 staining was not observed on either ADSC or BMSC spheres (figure 14B and D). Most DPSC spheres did not show Stro-1 staining however a subpopulation showed low levels in the core of the spheres. Weak, possibly background staining showed some co-localisation between CD133 and Stro-1 in DPSC derived spheres (figure 14E-F).



3.6 Semi-quantitative polymerase chain reaction analysis

From the semi-quantitative analysis of PCR band intensities, Shapiro-Wilk tests were performed to test normality. There was no evidence ($p > 0.05$) that any samples showed a normal distribution, however the low count restricts the reliability of this test. Some samples did not have a sufficient count ($n < 3$) to test normality. Levels of nestin compared to the GAPDH do not appear to change after neural induction for all three cell types and no significant differences could be observed ($P > 0.05$). All cell types show low levels of nestin expression, with the dental pulp stem cells showing the lowest levels of expression, although this has not been shown statistically ($P > 0.05$). Vimentin levels appear to drop after neural induction, although again this was not shown significantly. A relatively large change was observed for both the bone marrow and adipose stem cells (over tenfold for the bone marrow) (figures 15, 16 and 17).

Very low CD105 expression was recorded in all samples (figures 15, 16 and 17). CD146 levels also appear very low in both the BMSCs and DPSCs and no change in expression was observed between the mesenchymal and neural induction treated cells (figures 16 and 17). Qualitatively, there was a reduction in the CD146 expression in the adipose stem cells after neural induction however this was not statistically significant ($P > 0.05$) (figure 15).

Similar to the other markers, no significant change in the mean ratio of P75 against GAPDH expression was identified ($P > 0.05$), therefore the data suggests that no changes occur in the P75 expression after neural induction. However the mean expression of P75 increases by over threefold in the dental pulp stem cell (figure 17) suggesting a potential, statistically unrecognised increase.

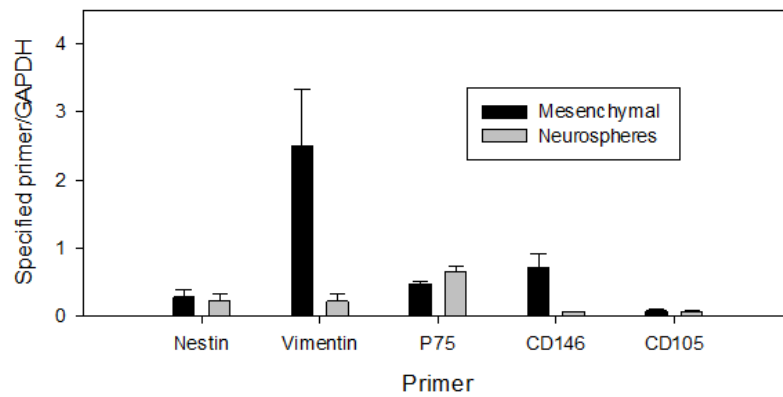


Figure 15: Semi-quantitative PCR analysis for the adipose stems both before and after neural induction treatment. No statistical difference was found between the groups. Error bars represent one SEM.

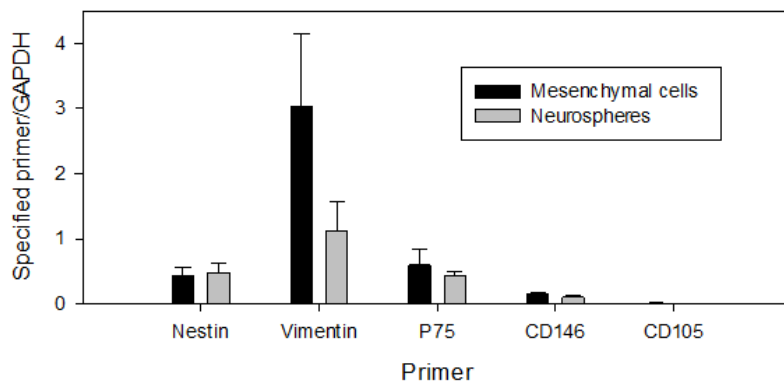


Figure 16: Semi-quantitative PCR analysis for the bone marrow stems both before and after neural induction treatment. No statistical difference was found between the groups. Error bars represent one SEM.

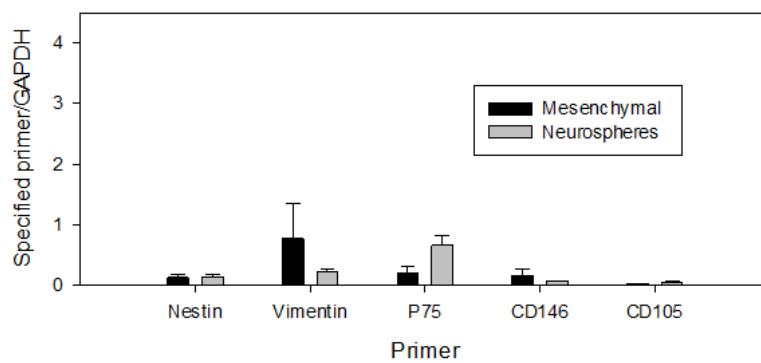


Figure 17: Semi-quantitative PCR analysis for the dental pulp stems both before and after neural induction treatment. No statistical difference was found between the groups. Error bars represent one SEM.

ANOVA tests were used to determine if there was a difference in the means of the primer band intensities/GAPDH band intensities for the spheres, between the three stem cell sources (figure 18). Statistical analysis could not be performed for the CD105 analysis as the count was too low. Significance was not found between any of the groups ($P > 0.05$, nestin $P = 0.47$, vimentin $P = 0.35$, P75 $P = 0.64$, CD146 $P = 0.55$), so no evidence was obtained to suggest a change in mean expression after neural induction treatment. Despite the lack of significance, there appears to be a decrease in the vimentin expression levels for the three groups, with bone marrow maintaining the highest level of expression. Nestin levels appear slightly higher in the BMSC spheres but then also correspond to a reduced level of P75 compared to the other stem cell types. The large range in band intensities that was visible qualitatively makes these results questionable.

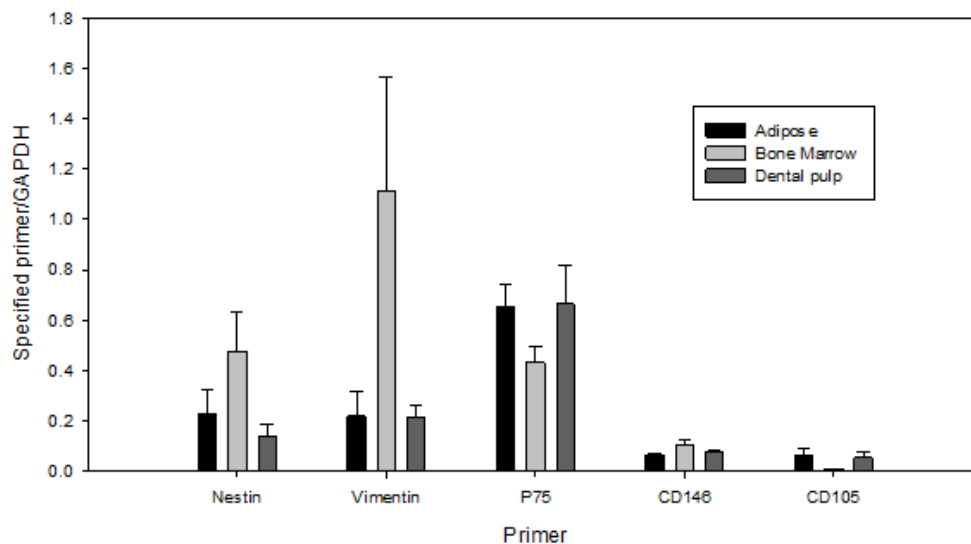


Figure 18: Semi-quantitative PCR analysis of the, 'neurospheres,' between the three stem cell sources. No statistical difference was found between the groups. Error bars represent one SEM.

4 *Discussion*

The purpose of this investigation was to characterise the neural potential of spheres produced from different mesenchymal stem cells sources. This should provide an indication of which source will most readily convert down a neural lineage when stimulated.

4.1 **Sphere formation capabilities**

On a procedural point of view, it appears that the spheres need a large area to expand properly. The clustering of cells in small wells of the 96 well plates demonstrates a limitation with this method. MSCs appear to require a certain volume, probably so that they can maintain a certain distance from surfaces and stay free in solution. The number of spheres obtained is significantly lower than the number of cells which were seeded. Either the cells must have conjoined, raising the question over whether spheres can form from single cells, or extensive cell death occurred after seeding in the HydroCell plates. If there has been cell death, it would be interesting to examine which cells are able to form spheres. It is likely that a pluripotent subpopulation exists within MSC populations, which has a specific phenotype allowing for neural induction. We tried to examine this by comparing the distribution and prevalence of certain markers within the population of cells before and after neuronal induction treatment.

BMSCs showed a tendency to adhere to the surface of the plates. It has previously been reported that adherence of neural stem cells causes them to differentiate (Deleyrolle and Reynolds 2009), thus MSC adherence is likely to interrupt the conversion to NSCs. BMSCS

however showed the greatest growth rate prior to neural induction treatment. A higher cell population could be created before neuronal induction.

4.2 Neural phenotypes of MSC derived spheres

Immunostaining for P75 was not observed in ADSC samples and arguably BMSCs, in agreement to previous reports (Caddick *et al* 2006, Radtke *et al* 2009). A few of the DPSCs appeared to show strong P75 stain prior to neural induction, indicating that a heterogenous population must have grown from the original samples. This also raises the question about the relative proportion of the DPSCs which possess the neural-crest lineage and thus the hypothesised ease of neural induction. P75 staining was not examined in spheres due to availability of the antibody.

Although not shown statistically, it was interesting to observe that DPSCs had lower or equal levels of expression of P75 to the ADSC and BMSC populations. It is difficult to explain why this may have occurred. Another possibility is that only a subpopulation of DPSCs maintain P75 expression after extraction and growth as observed in our immunocytochemistry results. P75 levels appear to increase in the DPSC derived spheres. Considering no sources indicate that P75 expression is upregulated during neural induction of DPSCs, one could argue that P75 expressing DPSCs are preferentially upregulated by the neural induction treatment.

All stem cells sources showed CD133 staining of spheres. Uniformly, the expression was highest on the outer layers of the spheres, indicating that a neural stem phenotype is found mostly on the surrounding cells. This could possibly be due to cells in the centre of the

sphere being starved of nutrients and dying (Gil-Perotin *et al* 2013). This however goes directly against the observations of Xiao *et al* (2013) and Ilieva & Dufva (2013) who saw signs of proliferation, through immunostaining for the cell proliferation markers Ki67/Oct4/Nurr1 (Scholzen and Gerdes 2000, Zeng *et al* 2004), only within the core of the spheres. It would be interesting to examine if co-staining is observed with CD133 and markers of proliferation. The high intensity staining in the spheres shows CD133 to be a promising marker of a neural converted MSC, however this observation must be taken with caution due to the lack of quantitative data. It would have been useful to examine the mRNA levels of CD133 to back up this observation.

Nestin expression profiles showed further difficult results. Variable nestin staining was observed within the ADSC and BMSC populations but not the DPSC population, contradictory to previous reports (Farahani *et al* 2011, Young *et al* 2013). There was no evidence to suggest any change in the nestin expression after neural induction treatment in any of the cell types possibly suggesting that the procedure does not induce conversion down a neural line.

4.3 Mesenchymal characteristics of MSC derived spheres

Both the ADSCs and BMSCs showed strong CD146 staining as would be expected of a mesenchymal cell population. Oddly the dental pulp only expresses a subpopulation with CD146. This again indicates that there is a heterogenous population of stem cells within the dental pulp.

The huge, although not significant, reduction in the mean vimentin expression levels for all MSC sources suggests that the treatment has converted all the cell types away from a MSC phenotype. Although all samples show a loss of the mesenchymal markers, it could be argued that the lower levels seen in DPSCs prior to neural induction indicate that they are not as far differentiated. It could be argued that the massive downregulation of vimentin could make vimentin a viable candidate for a FACS marker. It would be interesting to examine the cells through flow cytometry to examine the expression profile of individual cells within the populations.

Stro-1 staining appears to be quite questionable as it appears to co-localise perfectly with CD133 in the MSC populations. Sample sizes of 1 make the data very questionable and it is possible that the strong co-localisation could just be a result of excess background staining. Previous unpublished data in this lab suggest that the Stro-1 antibody that was used was unreliable. The lack of CD105 expression indicates that too few cycles were used in this study, which may have affected results of other markers as well.

4.4 Limitations

There were a number of limitations observed within this study. Availability of growth plates was a major limitation as we observed different morphologies which likely altered the phenotypes of cells. Another concern is the use of serum to quench the trypsin. As serum has been shown to prevent the generation of neurospheres (Gil-Perotin *et al* 2013), it is possible that the short term contact may prevented neural conversion. Additionally, we used a single protocol to upregulate all MSC types, which may not be appropriate.

The immunocytochemistry data from the spheroid was extremely difficult to analyse. This is because the sphere diameters, around 150µm, were extremely large compared to the structures that are normally examined by conventional fluorescence microscopy (usually between 10-20µm in this lab). This would have been improved if sections could have been taken, however due to the fragility of the spheres this was not possible (Sasaki *et al.* 2010). It would have been preferable to use a confocal microscope as this would have allowed higher resolution images to be obtained, however technical difficulties meant that this was not available. A major limitation was availability of certain rat specific antibodies and primers. This meant that a number of valid markers of neuronal/mesenchymal stem cells had to be excluded. Other markers which have been used include Neurod1 as well as K⁺ channels, however it still needs to be determined which are only found in NSC, not neural progenitors. A major concern with the immunofluorescence was the tendency for variable results. This indicates that it may be worth trying to develop the protocol to include a more efficient blocker, or incubate with blocker solutions for an extended treatment time. Lack of ladders meant that it was not possible to be confident with the data.

A major limitation is that a positive control was not available. To do this would have meant developing a technique to extract neural stem cells which was not realistic in the available time. Alternatively neurospheres could be derived from a commercially available cell line. One such source would be the tumourigenic, neuroendocrine PC12 cells (Tyson *et al.* 2003). These cells have been shown to upregulate when treated with EGF, as used in the neural induction protocol for this investigation and so could easily model NSC growth. Additionally, they have been shown to readily convert to neurons or neuron-like cells when stimulated in

a specific manner (Kimmelman *et al* 2002). Although PC12 cells have been shown to express these characteristics, they have not been shown to form neurospheres.

4.5 Future directions and implications

It is well known that the cells within these samples are heterogenous which limits the characterisation of the cells within this study. We planned from this study to identify a definitive marker which indicates that the cells have entered a neural line, however the results are questionable. A specific NSC marker would allow FACS analysis to examine the heterogeneity of the spheres. Considering that the conversion between MSC to NSC phenotypes will not be instant, flow cytometry would be more appropriate to examine changes. Chronological studies would also be useful to compare as this will be a way of evaluating the therapeutic benefit.

Considering the lack of NSC marker upregulation, it would be beneficial to examine other growth protocols that may further encourage a NSC induction. Previous studies have shown that the use of Noggin has aided conversion of both embryonic and adult fibroblasts to NSC-like spheres (Wada *et al.* 2009) (Shofuda *et al.* 2013) as well as hypoxia being beneficial for neural conversion (De Filippis and Delia 2011). It would be interesting to examine the effects of these treatments on the ability of the MSCs to convert to NSCs so that a definitive single method can be created. Furthermore, it would be beneficial to examine which proteins are directly involved in the conversion process. This, as well as markers of NSCs, could be looked into by performing a microarray on NSCs. Knockout cell lines could then be developed to examine if the cells respond differently to neural induction without certain proteins. This

information could allow the development of a more efficient protocol which can directly stimulate neural induction of the MSCs.

It is not clear how translational rat dental pulp will be with human DPSCs. We have observed in this lab that human dental grows far more readily than rat dental pulp, which may be due to a procedural approach but could indicate that human DPSCs are more pluripotent than their rat counterparts. This would be surprising considering that rats have one set of teeth which constantly grow throughout their life, whereas humans have a deciduous set and adult set of teeth (Kerkis and Caplan 2012). It would be interesting to know whether there is a difference between murine teeth and human deciduous/adult teeth to determine which would be the optimum source for neural induction. Finally, the integrative capacity of the cells still needs to be evaluated due to previous difficulties with NSCs (Young *et al.* 2000). There is no point in developing novel neurons for therapeutic treatments if they cannot be integrated into the developed system.

5. *Conclusions*

It can be concluded that all stem cell types appeared to develop into spheres and lose some markers of MSCs. Although the data suggests that DPSCs express the least mesenchymal phenotype of the studied MSCs after neural induction, insufficient data was collected to confirm that they appeared more like NSC than the other MSC sources. We have indicated that vimentin and CD133 are useful markers to detect MSCs or neural converted MSCs however limitations such as the time required to grow the cells, infections and possible protocol errors resulted in insufficient and questionable data. Further studies need to be completed to gain extra data to address the hypotheses as well as addressing the translatability of the results.

6. Bibliography

- Abraham, A. *et al.* "Members of the high mobility group B protein family are dynamically expressed in embryonic neural stem cells." *Proteome Science* 11 (2013).
- Abranches, E. *et al.* "Neural Differentiation of Embryonic Stem Cells In Vitro: A Road Map to Neurogenesis in the Embryo." *PLoS ONE* 4 (2009): p. e6286.
- Altman, J. "Are new neurons formed in the brains of adult mammals." *Science*, 1962: 1127-28.
- Alvarez-Buylla, A., and J. Garcia-Verdugo. "Neurogenesis in Adult Subventricular Zone." *The Journal of Neuroscience*, 2002: 629-34.
- Anderlini, P., J. Rizzo, M. Nugent, N. Schmitz, R. Champlin, and M. Horowitz. "Peripheral blood stem cell donation: an analysis from the international bone marrow transplant registry (IBMTR) and European group for blood and marrow transplant (EBMT) databases." *Bone Marrow Transplant* 7 (2001): 689-92.
- Brewer, G., J. Torricelli, E. Evege, and P. Price. "Neurobasal Medium/B27 supplement: A new serum-free medium combination for survival of neurons." *Focus* 16 (1994): 6-9.
- Caddick, J., P. Kingham, N. Gardiner, M. Wiberg, and G. Terenghi. "Phenotypic and functional characteristics of mesenchymal stem cells differentiated along a schwann cell lineage." *Glia* 54 (2006): 840-9.
- Caplan, A. "Mesenchymal stem cells." *Journal of Orthopaedic Research* 9 (2005): 641-50.
- Cave, J., M. Wang, and H. Baker. "Adult subventricular zone neural stem cells as a potential source of dopaminergic replacement neurons." *Frontiers in Neuroscience* 8 (2014).
- Chaichana, K., G. Zamora-Berridi, J. Camara-Quintara, and A. Quinones-Hinjosa. "Neurosphere Assays: Growth Factors and Hormone Differences." *Stem Cells*, 2006: 2851-7.
- Cho, T. *et al.* "Human neural stem cells: electrophysiological properties of voltage-gated ion channels." *Neuroreport* 13 (2002): 1447-52.
- Covas, D. *et al.* "Multipotent mesenchymal stromal cells obtained from diverse human tissues share functional properties and gene-expression profile with CD146+ perivascular cells and fibroblasts." *ISEH Experimental Hematology* 36 (2008): 642-54.
- Crisan, M. *et al.* "A perivascular origin for mesenchymal stem cells in multiple human organs." *Cell Stem Cell* 3 (2008): 301-13.
- Darabi, S., T. Tiraihi, A. Ruintan, H. Abbaszadeh, A. Delshad, and T. Thaeri. "Polarized neural stem cells derived from adult bone marrow stromal cells develop a rosette-like structure." *In vitro cellular & developmental biology. Animals*, 2013: 638-52.
- De Filippis, L., and D. Delia. "Hypoxia in the regulation of neural stem cells." *Cellular and Molecular Life Sciences* 68 (2011): 2831-2844.
- Deleyrolle, L., and B. Reynolds. "Isolation, expansion, and differentiation of adult mammalian neural stem and progenitor cells using the neurosphere assay." *Methods in Molecular Biology* 549 (2009): 91-101.
- Ellis, K., D. O'Carroll, M. Lewis, G. Rychkov, and S. Koblar. "Neurogenic potential of dental pulp stem cells." *Stem Cell Research & Therapy* 5 (2014).

Ethics Committee of the American Society for Reproductive Medicine. "Donating embryos for human embryonic stem cell (hESC) research: a committee opinion." *Fertility and Sterility* 100 (2013): 935-9.

Farahani, R., M. Simonian, and N. Hunter. "Blueprint of an ancestral neurosensory organ revealed in glial networks in human dental pulp." *The Journal of Comparative Neurology*, 2011: 3306-26.

Forostyak, S., P. Jendelova, and E. Sykova. "The role of mesenchymal stromal cells in spinal cord injury, regenerative medicine and possible clinical applications." *Biochimie*, 2013: 2257-70.

Fox, L. *et al.* "Membrane properties of neuron-like cells generated from adult human bone-marrow-derived mesenchymal stem cells." *Stem Cells and Development* 19 (2010): 1831-41.

Geuna, S., P. Borriero, M. Fornaro, and M. Giacobini-Robecchi. "Adult stem cells and neurogenesis: Historical roots and state of the art." *The Anatomical Record*, 2001: 132-41.

Gil-Perotin, S., M. Duran-Moreno, A. Cebrian-Silla, M. Ramirez, P. Garcia-Belda, and J. Garcia-Verdugo. "Adult neural stem cells from the subventricular zone: A review of the neurosphere assay." *The Anatomical Record* 296 (2013): 1435-1452.

Heo, J., S. Choi, H. Kim, E. Kim, J. Park, T. Kim, E. You, and H. Kim. "Neural transdifferentiation of human bone marrow mesenchymal stem cells on hydrophobic polymer-modified surface and therapeutic effects in an animal model of ischemic stroke." *Neuroscience* 238 (2013): 305-18.

Janebodin, K. *et al.* "Isolation and characterization of neural crest-derived stem cells from the dental pulp of neonatal mice." *PLoSOne* 6 (2011): e27526.

Jin, K. *et al.* "Neurogenesis in dentate subgranular zone and rostral subventricular zone after focal cerebral ischemia in the rat." *Proceedings of the National Academy of Sciences of the United States of America* 98 (2001): 4710-5.

Kempermann, G., L. Wiskott, and F. Gage. "Functional significance of adult neurogenesis." *Current Opinion in Neurobiology* 14 (2004): 186-91.

Kerkis, I., and A. Caplan. "Stem cells in dental pulp of deciduous teeth." *Tissue Engineering* 18 (2012): 129-38.

Kimmelman, A., N. Nunez, and A. Chan. "R-Ras3/M-Ras induces neuronal differentiation of PC12 cells through cell-type-specific activation of the mitogen-activated protein kinase cascade." *Molecular Cell Biology* 22 (2002): 5946-61.

Krystkowiak, P. *et al.* "Alloimmunisation to Donor Antigens and Immune Rejection Following Foetal Neural Grafts to the Brain in Patients with Huntington's Disease." *PLoS ONE* 2 (2007): e166.

Kulbatski, I., A. Mothe, H. Nomura, and C. Tator. "Endogenous and exogenous CNS derived stem/progenitor cell approaches for neurotrauma." *Current Drug Targets* 6 (2005): 111-26.

Laywell, E., P. Rakic, V. Kukekov, E. Holland, and D. Steindler. "Identification of a multipotent astrocytic stem cell in the immature and adult mouse brain." *Proceedings of the National Academy of Sciences of the United States of America*, 2000: 13883-8.

Lemasson, M., A. Saghatelian, J. Olivo-Marin, and P. Lledo. "Neonatal and adult neurogenesis provide two distinct populations of newborn neurons to the mouse olfactory bulb." *The Journal of Neuroscience*, 2005: 6816-25.

Li, J., N. Christophersen, V. Hall, D. Soulet, and P. Brundin. "Critical issues of clinical human embryonic stem cell therapy for brain repair." *Cell Press* 3 (2008): 146-53.

Li, P. *et al.* "Adult rat hippocampus soluble factors: a novel transplantation model mimicking intracranial microenvironment for tracing the induction and differentiation of adipose-derived stromal cell in vitro." *Neuroscience Letters* 542 (2013): 5-11.

- Lin, T., O. Islam, and K. Heese. "ABC transporters, neural stem cells and neurogenesis – a different perspective." *Cell Research* 16 (2006): 857-71.
- Mani, S. *et al.* "The epithelial-mesenchymal transition generates cells with properties of stem cells." *Cell* 133 (2008): 704-15.
- Mead, B., A. Logan, M. Berry, W. Leadbeater, and B. Scheven. "Intravitreally transplanted dental pulp stem cells promote neuroprotection and axon regeneration of retinal ganglion cells after optic nerve injury." *Investigative Ophthalmology & Visual Science* 54 (2013): 7544-56.
- Milosevic, J., A. Storch, and J. Schwarz. "Cryopreservation does not affect proliferation and multipotency of murine neural precursor cells." *Stem Cells* 23 (2005): 681-8.
- Monje, M., S. Mizumatsu, J. Fike, and T. Palmer. "Irradiation induces neural precursor-cell dysfunction." *Nature Medicine* 8 (2002): 955-62.
- Ninagawa, N., R. Murakami, E. Isobe, Y. Tanaka, H. Nakagawa, and S. Torihashi. "mesenchymal stem cells originating from ES cells show high telomerase activity and therapeutic benefits." *Differentiation; research in biological diversity* 82 (2011): 153-64.
- Nussbaum, R., and C. Ellis. "Alzheimer's Disease and Parkinson's Disease." *The New England Journal of Medicine*, 2003: 1356-64.
- Phillips, W., A. Michell, H. Pruess, and R. Barker. "Animal models of neurodegenerative diseases." *Methods in Molecular Biology* 549 (2009): 137-55.
- Priebe, M., A. Chiodo, W. Sclza, S. Kirshblum, L. Wuermsler, and C. Ho. "Spinal Cord Injury Medicine. 6. Economic and Societal Issues." *Spinal Cord Injury Medicine*, 2007: S84-88.
- Radtke, C., B. Schitnz, M. Spies, J. Kocsis, and P. Vogt. "Peripheral glial cell differentiation from neurospheres derived from adipose mesenchymal stem cells." *International Journal of Developmental Neuroscience* 27 (2009): 817-23.
- Reynolds, B., and S. Weiss. "Generation of Neurons and Astrocytes from Isolated Cells of the Adult Mammalian Central Nervous System." *Science*, 1992: 1707-10.
- Safford, K. *et al.* "Neurogenic differentiation of murine and human adipose-derived stromal cells." *Biochemical and Biophysical Research Communications* 294 (2002): 371-9.
- Sasaki, R. Aoki, S., M. Yamato, H. Uchiyama, K. Wada, T. Okano, and H. Ogiuchi. "Neurosphere generation from dental pulp of adult rat incisor." *European Journal of Neuroscience* 27 (2008): 538-548.
- Sasaki, R. *et al.* "A protocol for immunofluorescence staining of floating neurospheres." *Neuroscience Letters* 479 (2010): 126-7.
- Satelli, A., and S. Li. "Vimentin in cancer and its potential as a molecular target for cancer therapy." *Cellular and Molecular Life Sciences* 68 (2011): 3033-46.
- Scholzen, T., and J. Gerdes. "The Ki-67 protein: from the known and the unknown." *Journal of Cell Physiology* 182 (2000): 311-22.
- Scuteri, A., M. Miloso, D. Foudah, M. Orciani, G. Cavaletti, and G. Tredici. "Mesenchymal stem cells neuronal differentiation ability: a real perspective for nervous system repair?" *Current Stem Cell Research and Therapy* 6 (2011): 82-92.
- Shi, S., P. Robey, and S. Gronthos. "Comparison of human dental pulp and bone marrow stromal cells by cDNA microarray analysis." *Bone* 29 (2001): 532-9.

Shofuda, T. *et al.* "A method for efficiently generating neurospheres from human-induced pluripotent stem cells using microsphere arrays." *Neuropharmacology and Neurotoxicology* 24 (2013): 84-90.

Stoica, B. *et al.* "PARP-1 Inhibition Attenuates Neuronal Loss, Microglia Activation and Neurological Deficits after Traumatic Brain Injury." *Journal of Neurotrauma*, 2014: ahead of print.

Tan, F., K. Lee, S. Gouk, R. Magalhaes, A. Poonepali, and M. Hande. "Optimization of cryopreservation of stem cells cultured as neurospheres: Comparison between vitrification, slow-cooling and rapid cooling "freezing" protocols." *Cryoletters* 6 (2007): 445-60.

Thies, W., and L. Bleiler. "2013 Alzheimer's disease facts and figures." *Alzheimer's and Dementia*, 2013: 208-45.

Tyson, D., S. Larkin, Y. Hamai, and R. Bradshaw. "PC12 cell activation by epidermal growth factor receptor: role of autophosphorylation sites." *International Journal of Developmental Neuroscience* 21 (2003): 63-74.

Vogel, W., F. Grunebach, C. Messam, L. Kanz, W. Brugger, and H. Buhning. "Heterogeneity among human bone marrow-derived mesenchymal stem cells and neural progenitor cells." *Hematopoietic Stem Cells* 88 (2003): 126-33.

Wada, T. *et al.* "Highly efficient differentiation and enrichment of spinal motor neurons derived from human and monkey embryonic stem cells." *PLoS One* 4 (2009): e6722.

Xu, Y. *et al.* "Neurospheres from rat adipose-derived stem cells could be induced into functional Schwann cell-like cells in vitro." *BMC Neuroscience* 9 (2008).

Yang, H. *et al.* "Sonic hedgehog released from scratch-injured astrocytes is a key signal necessary but not sufficient for the astrocyte de-differentiation." *Stem Cell Research* 9 (2012): 156-66.

Young, F., A. Sloan, and B. Song. "Dental pulp stem cells and their potential roles in central nervous system regeneration and repair." *Journal of Neuroscience Research* 91 (2013): 1383-93.

Young, M., J. Ray, S. Whiteley, H. Klassen, and F. Gage. "Neuronal differentiation and morphological integration of hippocampal progenitor cells transplanted to the retina of immature and mature dystrophic rats." *Molecular and Cellular Neuroscience* 16 (2000): 197-295.

Zeng, X. *et al.* "Dopaminergic differentiation of human embryonic stem cells." *Stem Cells* 22 (2004): 925-40.

Zhang, S., M. Wernig, I. Duncan, O. Brustle, and J. Thomson. "In Vitro differentiation of transplantable neural precursors from human embryonic stem cells." *Nature Biotechnology* 19 (2001): 1129-33.

Zwart, I. *et al.* "Analysis of neural potential of human umbilical cord blood-derived multipotent mesenchymal stem cells in response to a range of neurogenic stimuli." *Journal of Neuroscience research* 86 (2008): 1902-15.



UNIVERSITY OF
BIRMINGHAM



*Investigating the role of the
dynamic synaptic cleft size and
its role in plastic processes*

Simon Foale

1005702

This project is submitted in partial fulfilment of the requirements for the award of the MRes

Neuropharmacology and Neurobiology

School of Clinical and Experimental Medicine

Supervisor: Professor Attila Sik

Contents

1 Introduction	3
1.1 Long-term potentiation (LTP)	4
1.2 Synaptic cleft size	6
1.3 Effect of tissue preparation on cleft size	11
1.4 Study rationale and Hypothesis	13
1.5 Aims.....	14
2 Materials and Methods	14
2.1 Animals and Experimental design.....	15
2.2 Solutions.....	15
2.3 Cell extraction and growth.....	16
2.3.1 Isolation neocortical cell procedure.....	16
2.3.2 Cell counting procedure	17
2.3.3 Poly-d-lysine pre-treatment.....	17
2.3.4 Microfluidic devices.....	18
2.3.5 Neuron culturing	20
2.3.6 Cell staining	20
2.3.7 Arabinofuranosyl (Ara-C) treatment.....	22
2.4 Cell imaging.....	22

2.4.1 Principles of FRET microscopy.....	22
2.4.2 FRET microscopy procedure.....	24
2.5 Analysis.....	25
3 Results	26
3.1 DiO staining protocols.....	26
3.2 Imaging protocol and configurations.....	28
3.3 Detection of FRET signals.....	29
3.4 The effects of fixation on FRET signals.....	30
3.5 FRET microscopy analysis of neurons with LTP induction	30
4 Discussion	37
4.1 Synapses can exhibit variable FRET signal with Dil/DiO staining.....	37
4.2 Limitations and future implications	38
5 Conclusion	42
6 Bibliography.....	43

List of figures

1. Evidence of forskolin inducing long term potentiation..... page 4
2. Relationships between synaptic cleft size and postsynaptic response..... page 5
3. Fixatives effects on synapses..... page 10
4. Axonal growth with microfluidic devices..... page 16
5. Staining procedure within microfluidic devices..... page18
6. Principles of fluorescence resonance energy transfer..... page20
7. Varying DiO staining procedures.....page 24
8. DiO labelled axons extension through microgrooves..... page 25
9. Control FRET images..... page 26
10. Surface plot diagram of high FRET signals..... page 27
11. Effects of aldehyde fixation on FRET signals at synapses..... page 28
12. Effects of forskolin on FRET signals at synapses..... page 29
13. Appearance of novel FRET signal after fixing..... page 32
14. Sham treatment effects on FRET signal..... page 33

Tables

1. Configurations of laser gains and powers trialled..... page 25
2. Synaptic FRET signals before and after-forskolin treatment.....page 30
3. Comparative changes in synaptic FRET signals before and after forskolin... page 31

Acknowledgements

I would like to express my greatest appreciation to the members of the Cellular Neuroscience group. Professor Sik's guidance and motivation was inspiration throughout the project. I am hugely indebted to him for his input during the project. Special thanks must also be made to Sahar Avazzadeh for her help and guidance with the day to day lab work. Thanks also must be made to the many students and supervisors who provided assistance and support with the work.

Abstract

Synaptic plasticity is an extremely important neurophysiological process that is essential for proper development and learning. It is believed that the synaptic cleft size will have a major role in determining the synaptic efficacy and thus could play a role in endogenous long-term potentiation (LTP) processes. Smaller synaptic clefts will allow a more efficient transfer of neurotransmitters causing a larger post-synaptic response. Previous investigations into the synaptic cleft size have relied on electron microscopy, however this method requires the neurons to be fixed. The fixation process alters the synaptic structure creating inaccurate and possibly disproportionate results. We used fluorescence resonance energy transfer (FRET) microscopy with the lipophilic dyes, DiI and DiO, to indirectly measure synaptic cleft size *in vitro* and examine the changes observed after fixing of the neurons and inducing LTP. We have shown that it is possible to use FRET microscopy to examine dynamic changes in neuronal populations. Our data suggests that there is enlargement of the synaptic cleft following aldehyde fixation. Unexpectedly, the synaptic cleft also appears to enlarge after forskolin induced LTP, possibly indicating an enlargement of small synaptic clefts upon LTP induction. Limitations mean that further experiments are required to confirm these findings.

1 *Introduction*

Synaptic plasticity is an important biological process which is essential both during development, to create the proper connections in the neural circuits, and in adulthood. In the adult mammal, synaptic plasticity is known to be vital for both learning and memory and is arguably the most important process involved in how we understand the world around us (Lynch 2004, Malenka and Nicoll 1999).

Although a significant amount of research has been focussed on understanding the mechanisms behind long term potentiation (LTP), gaining a better understanding of the mechanism behind synaptic plasticity could have huge ramifications. This will lead to the discovery of what can go wrong during development, in neurodegenerative disease or simply during ageing. This could allow for the development of therapies to help treat abnormal conditions and maintain proper neuronal function.

1.1 Long-term potentiation (LTP)

Hebb (1949) originally proposed the concept that neurons are able to strengthen their connections when they are repeatedly firing together, whether causal or coincidental. This theory has led to the discovery of two methods of altering synapses; LTP, increasing synaptic efficacy, and long term depression (LTD), decreasing synaptic efficacy (not to be confused with the reversal of LTP). Much research has been put into how LTP is able to strengthen synapses and the role that this has in neurological processes such as learning and memory. LTP is the process where the synapses of two neurons are able to produce stronger connections as a result of synchronised firing. This results in the postsynaptic neuron

membrane generating an action potential more readily than previous responses (Malenka and Nicoll 1999, Moore and Baleja 2012).

To look into the physiology of LTP, it is important to reliably and reproducibly induce LTP into a neuronal sample. Ever since Lomo (1966) showed that providing a test shock could result in strengthening of the hippocampal dentate gyrus' response, indicating the possibility of externally induced LTP, multiple methods to bring LTP about have been developed.

Morgan & Teyler (2000) originally showed that by stimulating a population of *ex vivo* hippocampal neurons with a short-theta burst stimulus, a reproducible LTP response could be produced which appears to work through both the N-methyl-D-aspartate receptor (NMDA) and voltage dependent calcium channel (VDCC) pathways. This was shown by an increased field excitatory postsynaptic potential (fEPSP) being observed in control groups compared to the amino-5-phosphonovaleric (APV) and nifedipine, blockers of NMDA and VDCC receptors respectively. Numerous studies have since shown that this method can be used reproducibly *in vivo* and *in vitro* (Grover *et al* 2009). There are disadvantages with this method however, as the electrodes have to be placed directly at the site of interest, which is not always possible due to the expense and difficulty of setting up of the equipment. Additionally, although an overall tissue LTP is observed, not every neuron is affected. It can then be very difficult to locate the precise synapses which have been affected (Otmakhov *et al* 2004).

Due to difficulties with using electrodes, methods have also been developed to induce LTP chemically. High concentration potassium solutions have been shown to induce LTP in rat hippocampal slices, again with data suggesting that it works in a calcium and glutamate

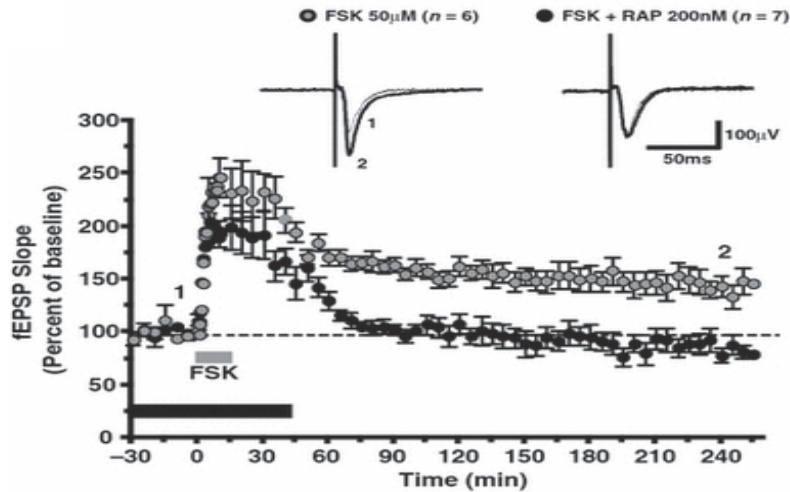
dependent manner (Fleck *et al* 1992). Interestingly though, this data is not universal and other reports have actually shown that high potassium concentrations can result in a significant reduction in the fEPSP, however this was also with a raised glutamate concentration (Harrison and Alger 1993).

Another promising method is through the use of the compound forskolin. Forskolin is an adenylate cyclase (AC) activator. increased AC activation leads to an increase in the cyclic adenosine monophosphate (cAMP) which can in turn lead to a raised level of active cAMP response element binding protein (CREB)/mammalian target of rapamycin (mTOR) which are believed to have a role in the transcription and maintenance of proteins involved in maintaining LTP, thus producing an observable increase in fEPSP (figure 1) (Otmakhov *et al* 2004, Fortin *et al* 2010, Gobert *et al* 2008). There is some debate as to how effective forskolin is independently, with some reports indicating that it can only induce LTP when in a magnesium free solution, however most reports seem to indicate forskolin as a reliable tool for chemically inducing LTP. Another advantage of forskolin induced LTP is that data suggests that it can be relatively easily reversed. Fortin *et al* (2010) showed that rapamycin addition was able to revert the fEPSP slope produced with forskolin alone, without causing a reduction below baseline, which could indicate LTD induction rather than LTP prevention (figure 1A).

1.2 Synaptic cleft size

Synaptic cleft size is likely to have a role in the amount of activity induced at the postsynaptic receptor. This is because a reduced distance between the two membranes will

A)



B)

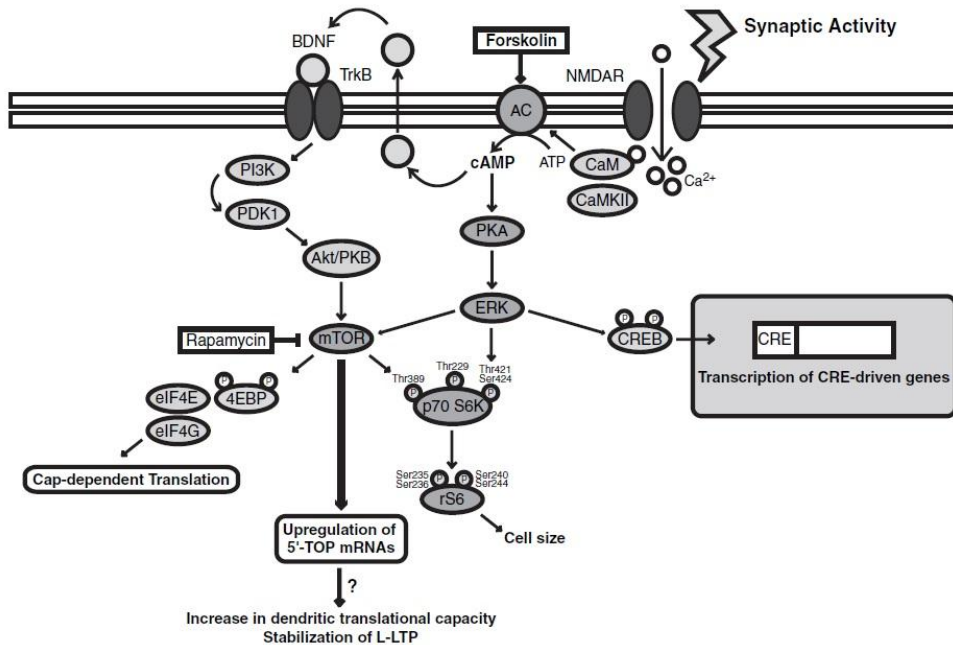


Figure 1: (A) Data showing forskolin treatment causing an increase in the fEPSP of cultured rat hippocampal slices. After application of 50mM forskolin for 15 minutes (grey bar), a maintained increase in fEPSP is observed for a 2 hour period. Co-treatment with rapamycin is shown to prevent the fEPSP being maintained long term and thus prevent LTP. (B) The model indicating the methods by which forskolin can induce LTP. Forskolin appears to activate AC leading to an upregulation in phosphorylated cAMP. Multiple pathways lead to the activation of mTOR and CREB pathways which causes the upregulation of mRNAs involved with dendritic structure. Rapamycin is also believed to inhibit the activity of mTOR, leading to reversal of the induced LTP. Both figures were used with permission from (Goibert *et al.* 2008).

mean that the neurotransmitters will not have to migrate as far. The concentration of the neurotransmitter which reaches the postsynaptic membrane will be increased due to decreased diffusion and clearance. This allows more neurotransmitters to bind to the postsynaptic membrane, increasing post-synaptic receptor occupancy and eliciting a

stronger response (Savtchenko and Rusakov 2007, Wahl *et al* 1996). There is however no direct data to back up this theory. Computer models from this lab and others have been developed to analyse this relationship. Following the expected relationship and dynamics of the synaptic cleft, significant changes can be observed from subtle changes in the synaptic cleft size (figure 2A and B) (Sik, unpublished data, Wahl *et al* 1996). Based on these data, it is expected that *in vivo*, there is likely to be a method to utilise the synaptic cleft size to control signal strengths between neurons.

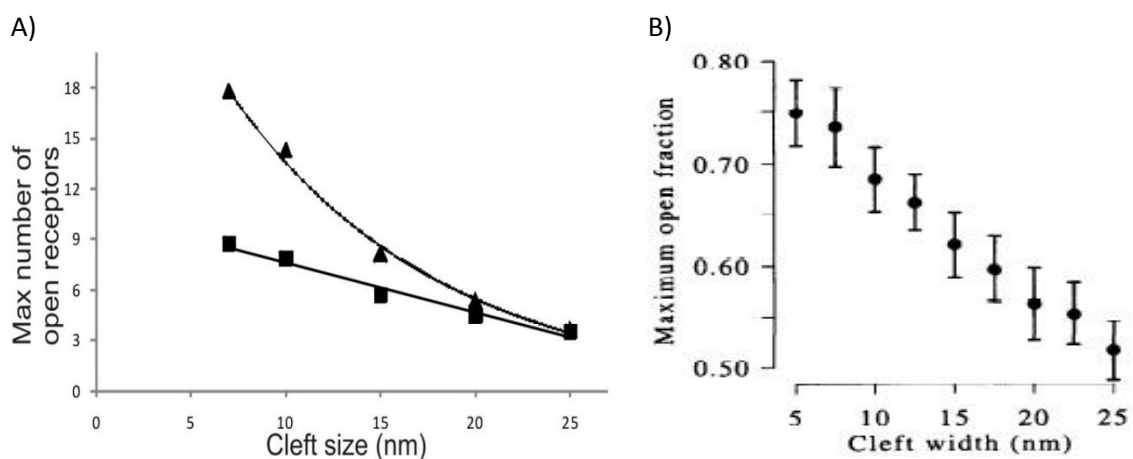


Figure 2: Models showing the effect of varying cleft sizes on the amount of open receptors on the postsynaptic membrane. A) showing a count whilst (Sik unpublished data) B) shows the proportion that are open (used with permission from Wahl *et al* 1996), with both models indicating that smaller cleft sizes, below 25nm, will cause an increase in the open receptors, allowing a greater EPSC to be induced.

It has long been theorised that the dendritic spines, one of the structures which contain the synaptic membranes, react during synaptic plasticity (Ramon y Cajal 1911). Since then multiple studies have demonstrated that there is a link between dendritic spine structure and LTP (Fortin *et al* 2010). Bourne *et al* (2008) reviewed a number of changes in dendritic spines, namely that spine enlargement is observed after LTP induction and a corresponding shrinkage can be observed during LTD. This has been further shown by an increase in rhodamine-phalloidin staining, a specific binder of polymerised actin, in spines which had received theta burst stimulation to induce LTP (Lin *et al* 2005). Additionally LTP in the form

of theta bursts causes the phosphorylation of cofilin through p21-activated kinase, resulting in inactivation of the cofilin. Cofilin normally functions to depolymerise actin filaments, thus LTP should help to maintain the spine structure (Fedulov *et al* 2007).

Varying the actin filament build up has been shown synaptic responses after LTP through the trafficking of receptors, however it has also been shown that there is an alteration the synaptic structure following LTP (Schwechter and Tolia 2013). Synapses going through LTP have been shown to develop a perforated structure. A perforated synapse occurs when small areas of the postsynaptic membrane receive reduced postsynaptic densities, that is a loss of electron dense regions. This corresponds with a loss of receptors and creates a doughnut shape, which Geinisman (1993) has shown is able to envelop the presynaptic membrane. As a result a greater contact area can be created between the synaptic membranes, allowing for an increased response.

As well as this, LTP can cause a concave synapse to develop (Weeks *et al* 2003), that is a enlarging of the presynaptic membrane. This could aid the enveloping described by Geinisman (1993). Concave synapses have been shown to have a build up in calcium binding proteins compared to other synapses, indicating a higher calcium concentration and likely to lead to an increase in calcium induced vesicle release (Buchs and Muller 1996). Additionally computer models suggest that the concave structure is able to draw cause a greater diffusion of calcium to the outer membranes on the synapse, which would theoretically increase the influx of calcium following activation (Weeks *et al* 2003). The bulging is also likely to cause shrinkage in the synaptic cleft size, supporting the hypothesis that a reduced cleft size is induced by LTP. Weeks *et al* 2003 demonstrated that the structural changes

observed through LTP were not observed with ketamine treatment, indicating that a more regulated process must be occurring than just over stimulation.

These data indicate that the synapse actually is able to go through drastic remodelling following LTP. Although these mechanisms have not been directly linked to the size of the synaptic cleft, it is very likely that the increase in actin filaments and the remodelling of the synaptic elements could allow the presynaptic and postsynaptic membranes to grow towards each other. The maintenance of these filaments should also be able to prevent the membranes from retreating and help maintain the reduced distance between the membranes.

Furthermore, an increase in cell-cell adhesion molecules has been observed after LTP induction in hippocampal slices (Calabrese *et al* 2006). N-cadherins have been shown to be able to stabilise the structure of the synapse. After NMDA receptor activation, β -catenin phosphorylation has been shown to occur, which prevents the endocytosis of N-cadherins, allowing them to maintain connections across the synapse and hold the structure together (Tai *et al* 2007). There is also a link between the ephrin receptors, which hold cell surfaces together closely and NMDA receptors at the synapse. Increased NMDA receptor concentrations, (seen after LTP) correlate with increased ephrin receptors concentrations, leading to stronger cell-cell adhesions. Again, these data have not been directly linked to synaptic cleft size, however it is very likely that increased cell-cell adhesions will result in a reduced manoeuvrability of the synaptic membranes and help to hold the membranes together between nanometre junctions. It should also be noted that all of these previous

studies were performed using rat hippocampal neurons, thus it is not clear how translatable the results are.

Active synapses do not tend to be larger than 20nm (Savtchenko and Rusakov 2007), and as such are far too small for any changes in the synaptic cleft size to be detected by conventional microscopy methods. Electron microscopy can be used to overcome this barrier, gaining resolution below the nanometre scale (Erni *et al* 2009). However using electron microscopy has its limitations as cells have to be prepared before they can be visualised, which is likely to result in alterations to the microstructure.

1.3 Effect of tissue preparation on cleft size

A number of studies have looked at the relationship of the synaptic cleft size, however to examine the synaptic cleft, electron microscopy has to be performed. This requires preparation of the samples being used. A number of methods have been developed to fix the tissue however they all contain flaws. The traditional approach is through fixation with aldehyde. Aldehyde works by encouraging cross-linking between proteins via covalent bonds. This method however has been shown to dehydrate the cells and lead to tissue shrinkage (Hayat 1989). This remodelling and dehydration which will likely pull the synaptic cleft open. Experiments using other fixation procedures show a marked difference in the aggregation of synaptic components. Furthermore, this method takes around 30 minutes to properly fix cell samples, and longer for tissue samples. During this time biological processes, especially enzymatic reactions, are still active, and it is very likely that there will be some response to the fixation procedure. It is unknown whether this will have a significant effect on the synapse morphology (Rostaing *et al* 2006, Leunissen and Yi 2009).

Rostaing *et al* (2006) showed that rapid freezing procedures appear to maintain a more endogenous morphology than aldehyde fixation. The conventional cold metal freezing procedure can only achieve proper fixation at around 10 μ m from the surface, which is likely to miss a lot of the important elements of the synapse. The high pressure freezing (HPF) technique, using between 200-210 MPa, has been far more effective and can achieve fixation of depths up to 300 μ m (Leunissen and Yi 2009). Additionally, this method prevents the formation of ice crystals due to the way that the water freezes at the high pressures, helping to maintain the original structure (Rostaing *et al* 2006, Leunissen and Yi 2009).

Rostaing *et al* (2006) further showed that presynaptic morphology was altered differently in aldehyde fixation compared to HPF. Presynaptic terminals appeared to shrink following aldehyde preparation, when compared to the HPF method (figure 3). They also observed a change in the vesicle localisation, with aldehyde fixation observing homogenous distributions rather than clustering in HPF (figure 3). It is not clear which method is more similar to live samples, however these results indicate that the preparation alters the synapse irreversibly.

Because of these complications, it is unlikely that synapses will be equally affected by the current preparation methods. As a result, the size of the synaptic clefts will not stay in proportion to their original sizes and it is impossible to reliably examine synaptic cleft sizes. It is for this reason that a different method needs to be utilised to examine cleft size and functions. It would be advantageous to use other methods which allow live cells to be analysed. Fluorescence resonance energy transfer (FRET) microscopy is an indirect method

to measure the co-localisation between molecules which can achieve signals at extremely small resolutions (between 0.1-10nm) (Herman *et al* 2012).

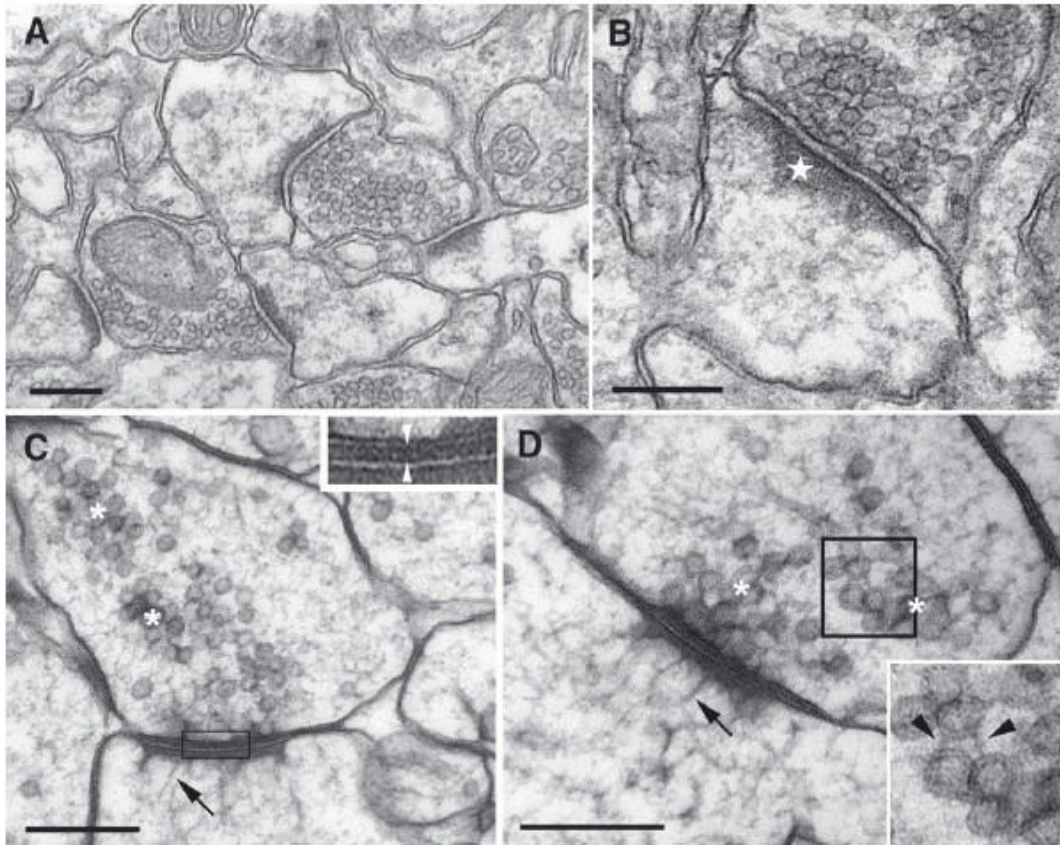


Figure 3: synapses of neurons in the Stratum radiatum. (A and B) treatment with aldehyde compared to (C and D) HPF treatment. A much denser area can be seen on the postsynaptic membrane, the white star (B) of the aldehyde treated neurons compared to that of the HPF treated postsynaptic membrane, as seen in the arrows (C and D). Vesicles in the terminals of HPF treated appear to be clustered, white asterisk (C and D) compared to the even distribution of aldehyde treated vesicles, indicating a difference in response to the fixation treatment. A clear difference can also be observed in the synaptic cleft size, however it can be ascertained whether this is due to the treatment or due to natural variation. Used with permission from (Rostaing *et al* 2006).

1.4 Study rationale and Hypothesis

It is hypothesised that there will be a simple morphological change in the structure of the synapse following LTP, which will lead to the presynaptic and postsynaptic membranes becoming physically closer. Treating the neurons with forskolin will cause LTP to be induced which will cause an observable shrinkage of the synaptic cleft compared to untreated samples. Fixation of the tissue will then result in a reduced signal due to shrinkage pulling

the synaptic membranes apart. If the hypothesis is observed, this could add data to support that altering synaptic cleft size is in fact a utilised *in vivo* method of synaptic plasticity.

1.5 Aims

The aims of this investigation were as follows:

- To develop a protocol for investigating the dynamic change of synaptic cleft *in vitro*.
- To examine whether aldehyde fixation artificially causes enlargement of the synaptic cleft.
- To examine whether the size of synaptic cleft changes after LTP induction.

2 *Materials and Methods*

2.1 **Animals and Experimental design**

Male BALB/c were used in this investigation, and collected from the Biomedical Services Unit (BMSU) at the University of Birmingham between P0-5. 5 animals were used per batch and then reduced to 4 once the procedure had been optimised. Once taken, mice were sacrificed by decapitation under the Home Office project licences of Professor Attila Sik and Dr Caroline Chadwick following the guidelines set by the UK Home Office Animals (Scientific Procedures) Act (ASPA) 1986. Before extraction the animals were kept in the BMSU in a 12 hour light-dark cycle with access to food and water *ad libitum*.

2.2 **Solutions**

All solutions were sterilised either by autoclaving or passing the ingredients through a 0.22µm pore (Millipore Ltd, Watford, UK). They are as follows:

- 40x solution: 10ml double distilled water (ddH₂O), 10ml 20% w/v glucose (Gibco-Life Technologies, Paisley, UK), 20ml 100mM sodium pyruvate (Gibco-Life Technologies, Paisley, UK) and 10ml penicillin/streptomycin (P/S) (Gibco-Life Technologies, Paisley, UK).
- Dissection solution: 27ml ddH₂O, 300µl 1M HEPES (4-(2-hydroxyethyl)-1-piperazineethanesulphonic acid) (Gibco-Life Technologies, Paisley, UK), 3ml Hank's Balanced Salt Solution (HBSS) 6.67X (Gibco-Life Technologies, Paisley, UK) and 750µl 40X solution.

- Growth media: 10ml Neurobasal media (Gibco-Life Technologies, Paisley, UK), 220µl B27 growth supplement (Gibco-Life Technologies, Paisley, UK), 50µl P/S and 25µl glutamax solution (Gibco-Life Technologies, Paisley, UK).
- Trituration media: 19ml Neurobasal media, 130µl 30% (w/v) bovine serum albumen (BSA) (Sigma-Aldrich, Dorset, UK), 1ml 40X solution and 270µl 0.15M deoxyribonuclease (DNAse) I (Sigma-Aldrich, Dorset, UK).
- BSA column media: 5ml trituration media, 200µl BSA and 150µl 0.1M sodium hydroxide (Sigma-Aldrich, Dorset, UK).
- Papain solution: 4ml ddH₂O, 750µl HBSS 6.67X, 125µl 40x solution, 50µl 50mg/ml L-cysteine hydrochloride (Sigma-Aldrich, Dorset, UK) and 66µl DNaseI. When used, 90µl of 12U/ml papain (Worthington Biochemical Corporation, Berkshire, UK) was added to 2ml of the solution.

2.3 Cell extraction and growth

2.3.1 Isolation of neocortical cells

All tools were autoclaved prior to use. Dissected heads were stored on ice. The entire procedure was carried out within a class II laminar flow hood (Camlab Ltd, Cambridge, UK).

The skin on the top of the head and the skull were dissected along the midline to expose the brain. The brain was then removed and stored in dissection solution on ice. Each brain was then dissected individually whilst viewing under a dissection microscope (Leica, London, UK).

The cerebellum was removed using a sterile scalpel blade (World Precision Instruments, Hertfordshire, UK). Dura mater was removed. The ventral surface of the brain was exposed

and the brainstem was extracted. The remaining neocortex was resuspended in dissection media. Neocortices were finely minced using a sterile scalpel blade and separated into two falcon tubes (BD Biosciences, Oxford, UK) containing the papain solution. Solutions were incubated at 37°C with 5% CO₂ in an incubator (RS biotech, West Lothian, UK). After 15 minutes, solutions were centrifuged at 400 xg for 15 minutes at 21°C (Beckmann Coulter Ltd, High Wycombe, UK). The digestion solution was aspirated and replaced with 2mls of trituration solution. Both solutions were then homogenised by triturating through 3 glass pipettes with successively smaller tips (Fisher Scientific Ltd, Loughborough, UK). This mechanically disrupted the adhering of the cells so that a homogenous solution was made. The solutions were passed through a 70µm pore (BD Biosciences, Oxford, UK) before centrifugation at 400 xg for 5 minutes at 21°C. Trituration solution was aspirated from both solutions and the two solutions were homogenised in 1ml of growth media.

2.3.2 Cell counting procedure

30µl of the cell solution was removed and suspended with 30µl of trypan blue (Sigma-Aldrich, Dorset, UK). The solution was triturated and 10µl of the solution was pipetted onto each side of a Burker Chamber (Assistent, Rhön, Germany). Counts were performed in the 4 corner squares of the device and averaged to obtain a mean cell count, used to calculate the overall cell concentration.

2.3.3 Poly-d-lysine pre-treatment

Microfluidic devices (MFDs) (Xona Microfluidics LLC, Temecula, U.S.A) adhered onto MatTek glass bottom dishes (MatTek corporation, Bratislava, Slovak Republic) or coverslips (VWR international, Lutterworth, UK) suspended in 24 well plates (SPL life sciences, Korea) were

used for cell suspension. The MFDs or coverslips were coated in poly-d-lysine (PdL) (BD Biosciences, Oxford, UK) to aid neuron adhesion. Coverslips were used as a control for proof of principle and to determine the effects of culturing in the MFDs.

Glass coverslips were washed in ddH₂O three times, followed by washing three times in 70% ethanol (VWR international, Lutterworth, UK) and three times again in ddH₂O. The coverslips were incubated in 10% nitric acid, overnight at room temperature. Coverslips were washed in ddH₂O three times and either washed in 70% ethanol. The coverslips were allowed to air dry within the fume hood. Once dry, they were washed in 50mg/ml of PdL within a borate buffer pH8.5 (Sigma-Aldrich, Dorset, UK) and incubated at 37°C overnight, before being washed in ddH₂O three times and allowed to air dry within the fume hood.

MatTek devices were coated in 2ml of the aforementioned PdL solution and incubated at 37°C overnight. Devices were washed three times in ddH₂O and three times in ethanol before air drying before use.

2.3.4 Microfluidic devices

MFDs were used to separate the neurons into 2 subpopulations which can extend axons between each other. The MFDs are made using poly(dimethylsiloxane), a non-toxic and transparent polymer. Previous studies have shown the devices to be suitable for neuron growth as well as confocal microscopy, making them suitable for high resolution live imaging (Park *et al* 2006, Millet *et al* 2007, Taylor *et al* 2005, Taylor and Jeon 2011).

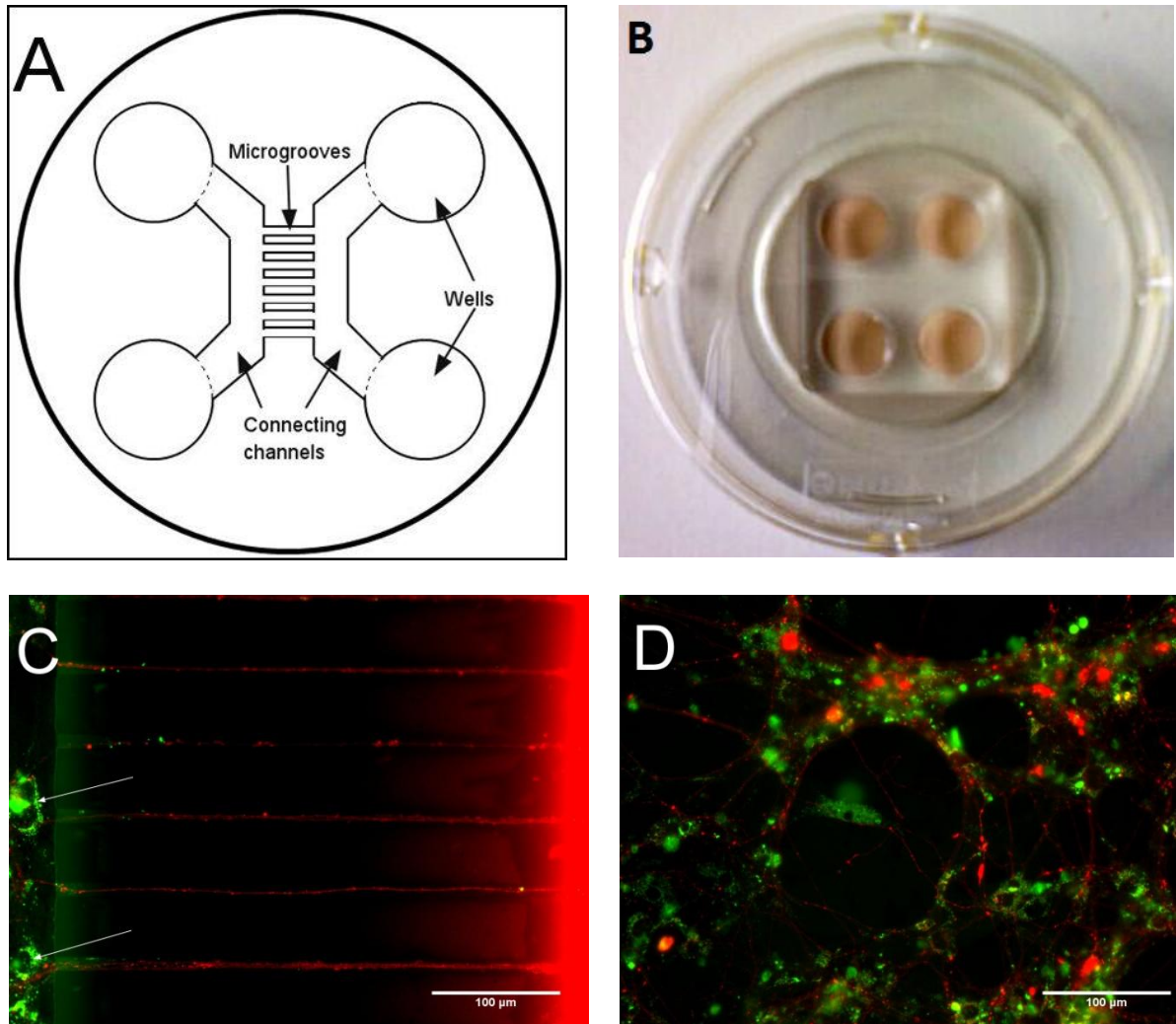


Figure 4: (A) A disproportionate representation of the MFDs. Solutions were pipetted into the circular wells where they could freely enter the connecting channels and the cells could adhere. The microgrooves between the channels allowed the growth of axons but prevented the passage of cell somas. (B) An image of a MFD with media assembled onto the MatTek glass bottom dish. (C and D) Fluorescence microscopy image showing two neuron populations stained with different dyes and separated by the MFD chambers. (C) Axons can be seen extending between the two subpopulations of neurons. Arrows show somas which can be seen to be too large to pass through the channels. (D) Image of two differently stained axons dispersing after entering the adjacent channel and appearing to synapse to neurons. Arrows show what appears to be boutons on the structures. Scale bars represent, 100 μm for C and D. Images (C) and (D) were adjusted to accent staining using ImageJ (National Department of Health, Maryland, USA).

4 wells are present on the devices. 2 pairs of 2 wells are separated by microgrooves (figure 4A and B). These grooves then connect to larger channels which pass between the two wells (figure 4A and C). Larger channels allow neurons to enter and seed within. Microgrooves only allow minute structures to enter, preventing entry of neuron somas, however axons are able to extend freely through the grooves (figure 4C) (Park *et al* 2006).

2.3.5 Neuron culturing

Cells were seeded at 16×10^6 cells/ml following previous unpublished work from this lab showing efficient growth and maintenance of BALB/c mice neocortex neurons. 15 μ l of cell solution was used per well pair in the MFDs and 30 μ l for the coverslips. The suspended cells were incubated at 37°C, 5%CO₂ for 45 minutes to promote cell adhesion before addition of growth media. Small MFDs received 100 μ l, large MFDs received 130 μ l and coverslips received 1ml of growth media. Excluding during the staining procedure (days 1-4), the cells were fed every 2-3 days by aspirating half the overall media per well and replacing with equal volumes of fresh growth media.

2.3.6 Cell staining

Neurons were labelled with the lipophilic dyes, DiO or/and DiI. The dyes were previously dissolved in dimethyl sulphoxide at a concentration of 40mg/ml and 2mg/ml respectively. Dyes were diluted to 10 μ M in growth media for use. Neurons were stained such that one subpopulation was stained with the DiI dye and one subpopulation was stained with the DiO dye (figure 5A). To optimise the staining procedure, neurons were stained at different time points after seeding and the time period of the DiO incubation was varied. An overview is presented below.

A)

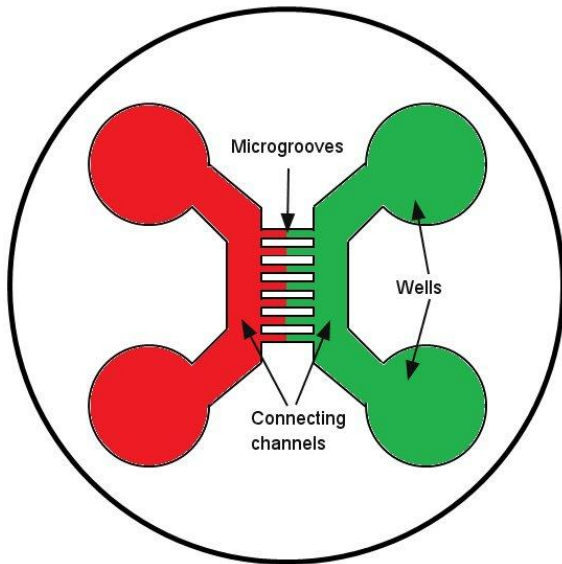
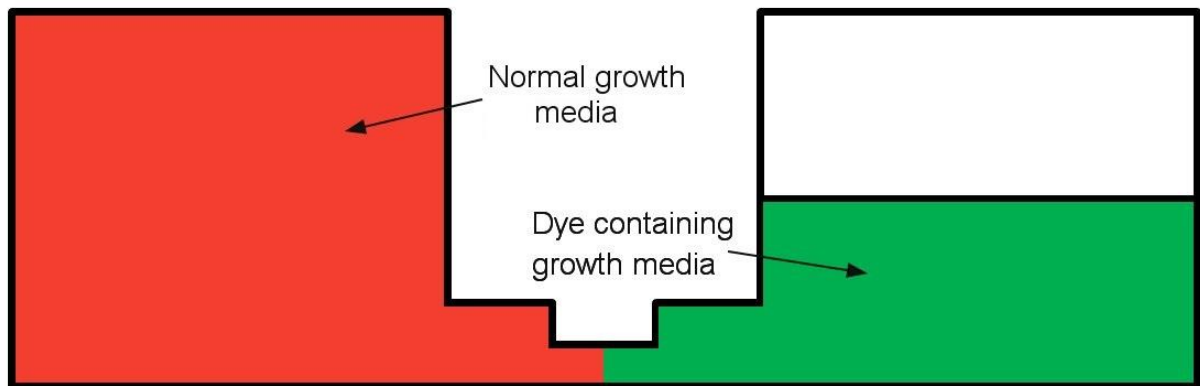


Figure 5: (A) A disproportionate representation of the MFD set up, indicating the separate dyes. Dyes were separated into the neuron subpopulations by the microgrooves as represented by the different colours. (B) Hydrostatic pressures prevented the dye from crossing over. Note the reduced level of media in the well containing the growth media supplemented with dye.

B)



Growth media was aspirated from one of the subpopulations of cells. One well from that subpopulation was then refilled with the dye solution. The dye solution could freely flow to the empty well, passing through the channel and displacing the growth media. The volume of dye solution was half the volume of growth media in the neighbouring neuron subpopulation (figure 5B). Hydrostatic pressures prevented the dye from passing between the two subpopulations (Taylor *et al* 2005). After a predetermined period of time, the dye solution was aspirated and replaced with the original volume of growth media. The procedure was then repeated for the neighbouring subpopulation of neurons with the other dye.

2.3.7 Arabinofuranosyl cytidine (Ara-C) treatment

To prevent the upregulation of glial and stem cell populations, Arabinofuranosyl cytidine (Ara-C) (Sigma-Aldrich, Dorset, UK) was added on D2 and removed on D4/5 after suspension. This is because previous studies in this lab have shown that excessive upregulation of non-neuronal cells can block the extension of axons between the neuron populations or outcompete the neurons. 5 μ M Ara-C was added within the DiO solution or within the growth media. Ara-C is a DNA synthesis inhibitor, which is believed to incorporate onto the primers of DNA strands and prevent the binding of DNA polymerase, stalling the upregulation of cells. The cells are still left viable so axonal growth is unaffected (Major *et al* 1982).

2.4 Cell imaging

Cells were imaged between D7-14 to allow sufficient growth of the axons. Previous studies have shown that central nervous system neurons are likely to become unviable if left for longer (Taylor *et al* 2005). Fluorescence imaging was used to examine axonal growth through the microgrooves as well as to examine the efficacy of the dyes. This was performed using a BX61 automated upright microscope (Olympus, Southend-on-sea, UK).

2.4.1 Principles of FRET microscopy

FRET microscopy is able to examine nanometre interactions between proteins (Herman *et al* 2012). Two fluorophores are required for this technique, a specific donor and acceptor. The donor fluorophore, when excited, loses its excitation through two methods. Firstly, emission is observed through conventional fluorescence emission. Alternatively, if the acceptor fluorophore is sufficiently close, signal can be passed between the dyes by long range dipole-

dipole interactions (Padilla-Parra and Tramier 2012, Herman *et al* 2012). The acceptor fluorophore becomes excited and emits fluorescence. Following this theory, the amount of emission observed from the acceptor is inversely proportional to the distance between the two fluorophores. FRET is dependent on the sixth power of the separation distance, and thus is very sensitive to small changes (Sekar and Periasamy 2003). This means that a minute dynamic change in the synaptic cleft size will result in an observable change in the intensity of the FRET signal.

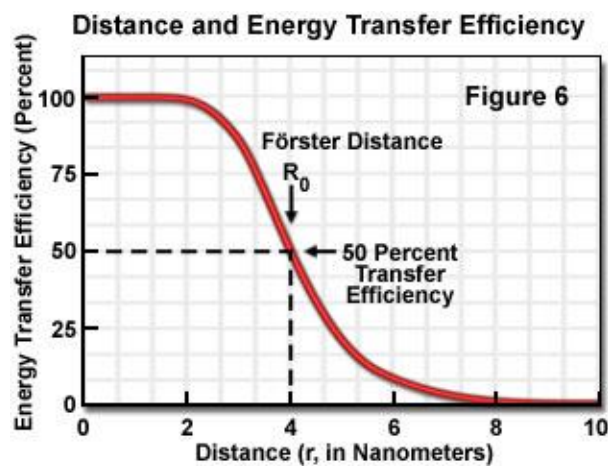


Figure 6: Graph showing the efficiency of energy transfer between FRET probes. The closer the probes are, the more efficient the transfer of energy, resulting in increased fluorescence by the acceptor probe. Beyond 10nm, the signal becomes negligible (taken with permission from (Herman *et al* 2012))

For this investigation, the FRET pair dyes Dil and DiO were used. This is because the dyes are lipophilic so will localise to the membrane of the cells (ABD Bioquest Inc 2008, Sengupta *et al* 2007) and are non-toxic (Honig and Hume 1986). The dyes also fluoresce significantly more when in a lipid environment, so there should be a reduction in background staining. The DiO dye is excited by a laser of 484nm. DiO is then able to transfer its energy to the Dil dye up to a distance of around 10nm (figure 6), allowing a signal to be observed in the Dil channel. The wavelengths of the lasers were chosen to allow a spectral overlap that is required for the long range dipole-dipole interaction to occur, but reduce the amount of co-excitation, to prevent excessive background signal.

2.4.2 FRET microscopy procedure

Labelled coverslips and MFDs with clear axonal processes extending between the neuron subpopulations, as shown through fluorescence microscopy (figure 4C), were taken for FRET analysis using Nikon A1R confocal microscope and software (Nikon, Surrey, UK). Samples were originally used to develop an efficient calibration procedure which could be used to image the cells and limit the amount of spectral bleed through signal.

Once the procedure had been finalised, cultured neurons were imaged at three time points. The media was then aspirated and replaced with growth media containing 50 μ M forskolin (abcam, Cambridge, UK) to induce LTP. Previous investigations have only incubated with forskolin for around 20 minutes and then examined after one hour, however these investigations use a run through system, so there is a consistent source of forskolin for this time (Otmakhov *et al* 2004, Gobert *et al* 2008). Because it was not possible to replicate this within the incubating chamber of the confocal microscope and the forskolin will take time to diffuse within the channels, neurons were incubated with forskolin for 40 minutes. After this time, the forskolin was removed and replaced with growth media. One hour after forskolin addition, allowing for LTP induction (Gobert *et al* 2008, Otmakhov *et al* 2004, Fortin *et al* 2010), images were taken. Neurons were then fixed in 4% formaldehyde for 30 minutes for a negative control. The formaldehyde was then aspirated and replaced with growth media for imaging.

Images were taken at multiple depths, 200 μ m apart, for each time point and examined qualitatively to ensure that images at around the same depth were used for comparisons. A maximum of 6 images were taken at each time point to minimise the risk of photobleaching.

2.5 Analysis

Surface plots were generated of the high FRET signal to identify sites of synapses using the Image-Pro analyzer 3D software (Media cybernetics, Maryland, U.S.A.). Red and green channels were examined to identify high (>75%) and medium (25-75%) FRET signals. Graphs showing the strength of FRET signal were generated with the data from the Nikon A1R software, using Sigmaplot (Systat Software Inc, London, UK). To avoid, bias, areas of FRET measurements were examined on all depths and the depth with the greatest signal was analysed. Due to limitations and sample loss, insufficient data was acquired to perform a statistical analysis.

3 *Results*

3.1 **DiO staining protocols**

Fluorescent images of the stained neurons showed a striking difference between Dil and DiO staining characteristics despite both being lipophilic dyes (figure 7). It was observed that Dil staining was very prominent and axons were easily visible, however DiO staining only showed intracellular vesicles. To overcome this, DiO staining was trialled for different time periods. Dil co-staining was trialled alongside to act as a control for the DiO stains. It was observed that increasing the staining duration led to an increase in the intensity of staining within axons. This was apparent as early as 1 day (figure 7A and C), however a three day staining period showed extensive axon staining that was still clear over the background stains (figure 7E). As a three day treatment appeared to make the axons of DiO labelled axons as apparent as Dil labelled axons, it was decided that a three day staining procedure will be used for the remaining experiments.

The three day treatment was further analysed to examine the visibility of the axons in the MFDs. In 30 minute samples, DiO stained axons were not seen passing through the microgrooves (data not shown). In the 3 day treated sample, weak DiO positive stains could be observed passing into the Dil labelled subpopulations' channel (figure 8).

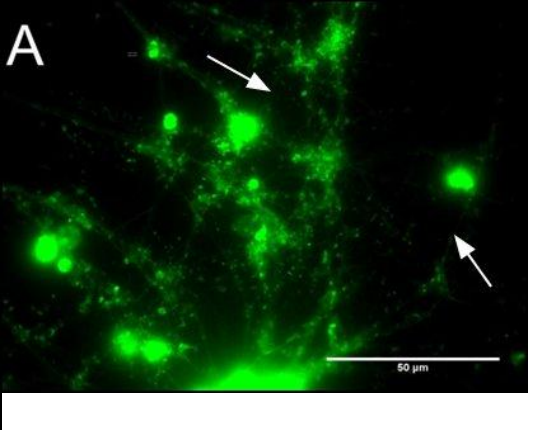
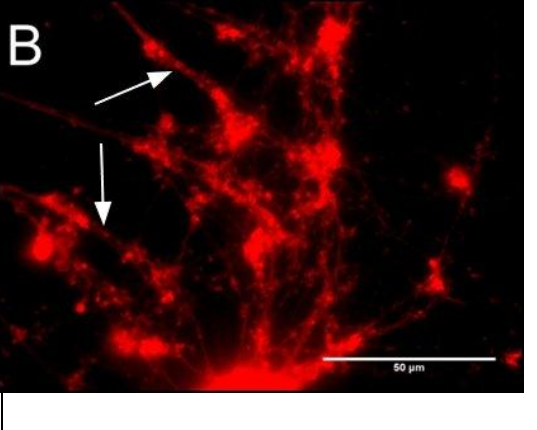
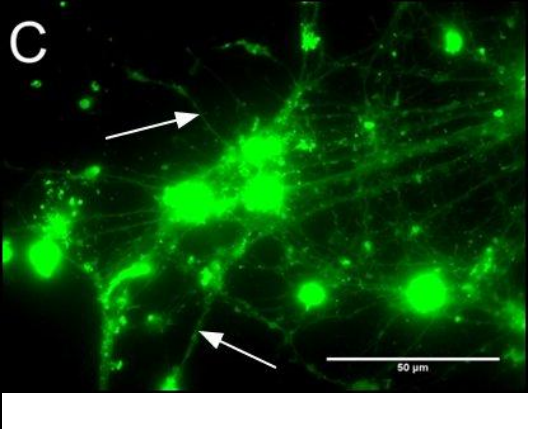
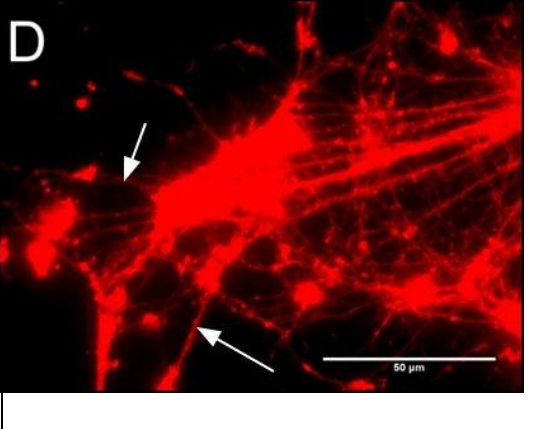
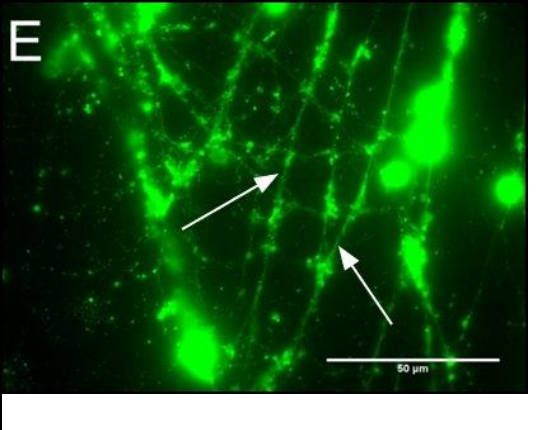
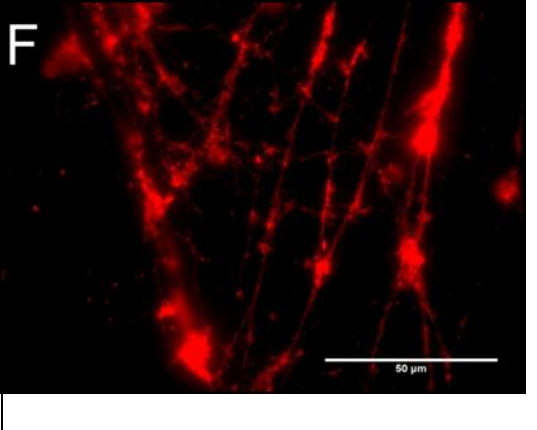
DiO staining duration	DiO stain	Dil stain
1 hour		
1 day		
3 day		

Figure 7: Representative images showing the varied duration of DiO stains. Dil staining (B, D and F) can be observed to be fairly consistent, whereas DiO staining (A, C, E) appears to become more defined over longer treatment periods, with axons becoming clearer. Scale bars represent 50µm. Arrows show axonal staining.

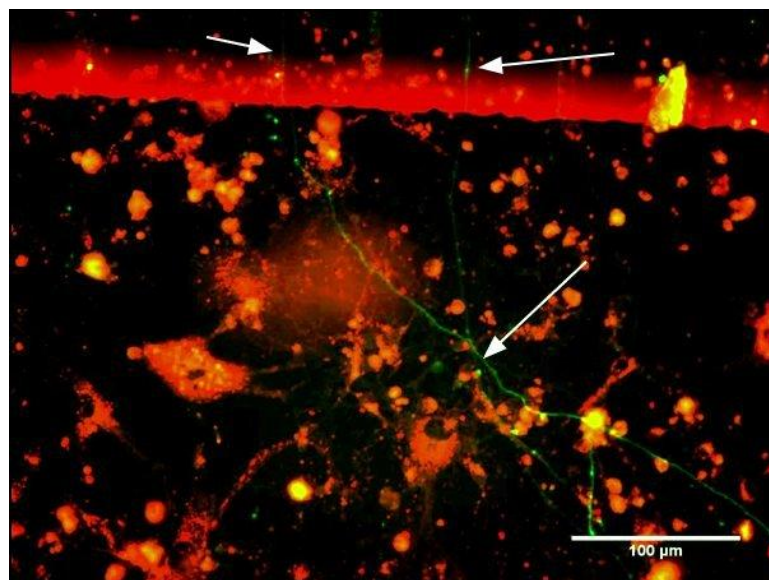


Figure 8: Arrows show green axons extending from the DiO subpopulation through microgrooves to the DiI stained side of the MFDs. Images were adjusted using Image-Pro analyzer 3D software to remove background.

3.2 Imaging protocol and configurations

Multiple configurations were trialled on the A1R software to develop the optimum conditions for FRET analysis. Earlier trials had a number of issues with observing the stains as well receiving an appropriate FRET signal. Details of the settings can be seen in table 1.

Configuration	Wavelength			
	488		561	
	Gain	Power	Gain	Power
1	75	100	57	100
2	100	3	92	100
3	100	10	84	100

Table 1: Details of the laser gains and powers used in the optimisation of FRET images.

It was observed that the low gain used for configuration 1 meant that DiI staining was difficult to observe. Two alternatives were trialled which both showed clear DiI staining however the latter configuration was chosen because a clearer signal was observed when viewed in the FRET channel (data not shown).

Extensive trials were performed to determine an appropriate setting for the FRET method analysis on the Nikon A1R software. A method was eventually determined which was able to induce a strong FRET signal in positive controls yet not cause any signal to be observed in negative control images (figure 9).

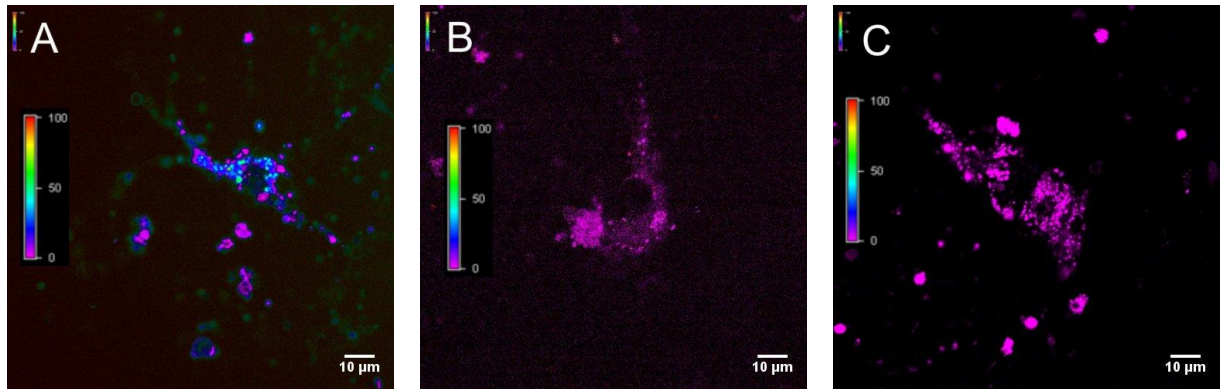


Figure 9: FRET signal intensity images of control MFD seeded neurons. (A) + control with both stains, although not extensive, signal was observed. Negative stains were also taken with (C) Dil only and (D) DiO only to show FRET signals were not generated by incorrect procedures. FRET scales on the images indicate the intensity of FRET signal recorded.

It should be noted that in subsequent data, it was observed that DiO stained axons were still difficult to observe within the Dil stained subpopulation when viewed under the confocal microscope. To overcome this issue, synapses were only examined between Dil stained axons in the DiO stained subpopulation.

3.3 Detection of FRET signals

Surface plot analysis showed that by using the optimum configuration, there was no high intensity FRET signal recorded in any images (figures 10A). This is shown by a lack of any peaks on the red light surface plot, which represents around 70-100% FRET signal strength. Medium FRET signal was observed in a number of images, as shown by green peaks which represent 25-75% FRET signal.

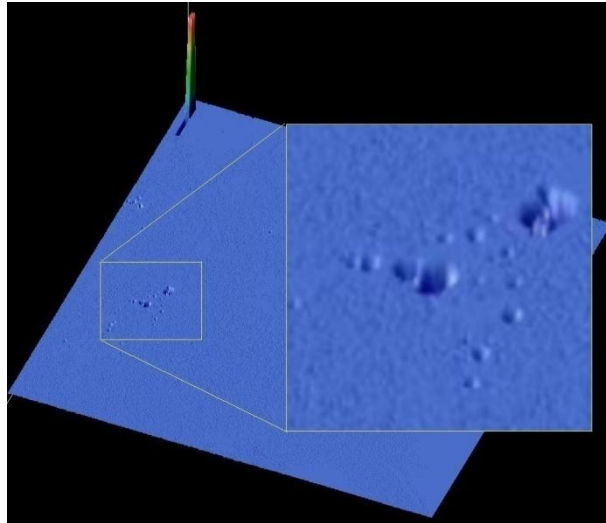


Figure 10: An example of a surface plot focussing on the red channel. Blue channel was subtracted from the red channel to remove any areas of pink signal, which represented a 0% FRET signal intensity. This resulted in some areas dropping below the lowest recorded red signal and may have hidden some weak red signals (around the 75% FRET signal area). This can be seen from enlarged section. Signal in the top corner is from the scale bar being incorporated into the image.

3.4 The effects of fixation on FRET signals

The effects of fixation treatment alone were examined (figure 11). Areas of FRET signal intensity were identified by examining surface plot diagrams. Medium FRET signal was observed at two sites on the pre-treated image (figure 11A). A reduction in the actual maximum FRET signal percentage of around 7% was observed (figure 11C).

3.5 FRET microscopy analysis of neurons with LTP induction

Subsequent analysis was focussed on examining the effects of forskolin followed by fixation on the FRET signal. Unfortunately, there were extensive issues with infections and MFD adherence leading to sample loss. Results were only obtained from one treatment group unless stated, giving a count of 1 for the data. Statistical analysis could not be performed because of the low sample size so the results need to be viewed with caution.

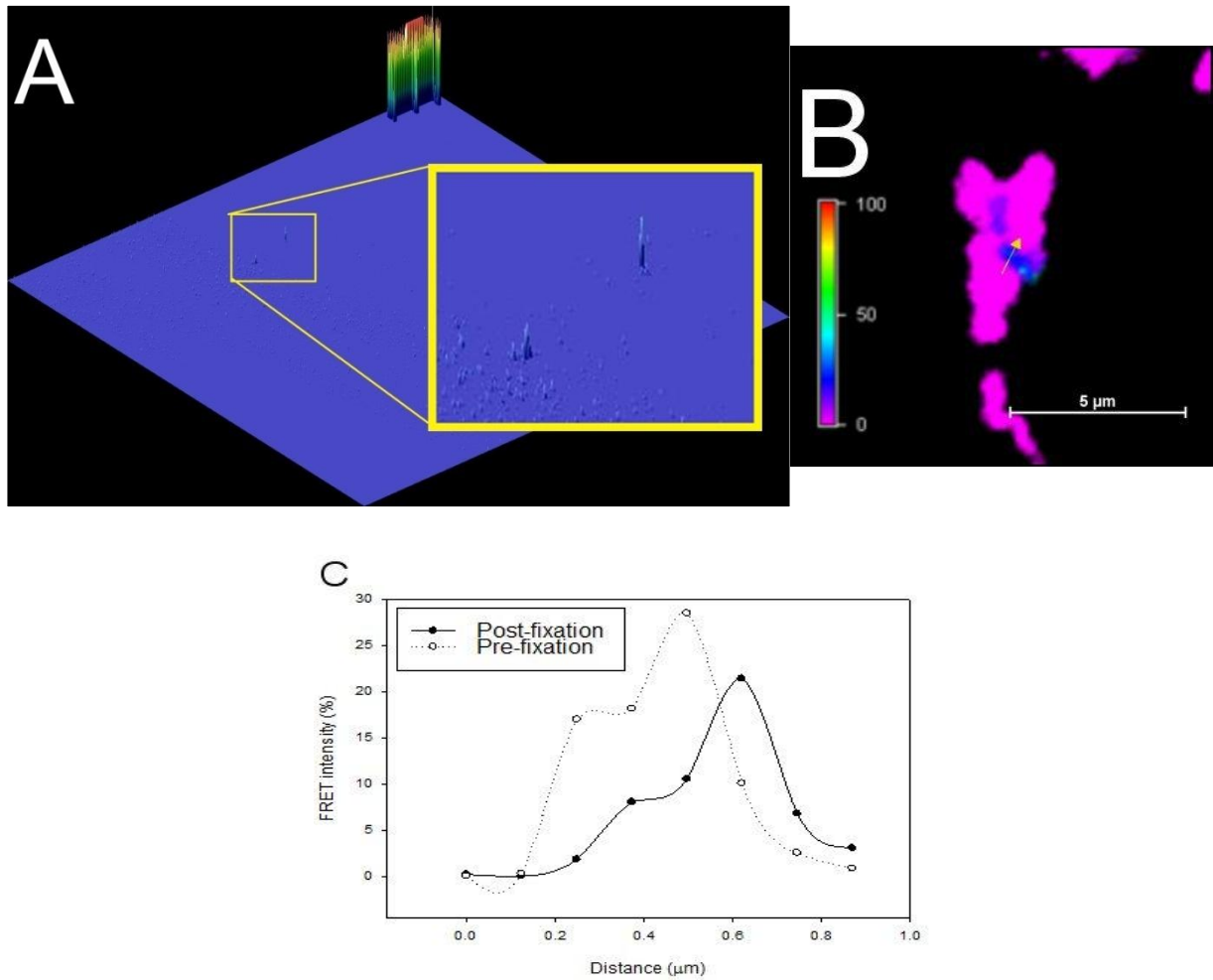


Figure 11: Analysis of the sample which was only fixed. (A) surface plot of the signal intensity of the pre-treated image. Two small sites of signal were observed. (B) Site of medium FRET signal intensity in the pre-treated sample. The arrow correlates with the region which was analysed quantitatively to create graphs. Scale bar represents 5µm. FRET scales on the images indicate the intensity of FRET signal recorded. (C) Graph showing the changing FRET signal intensity corresponding to the arrow.

Qualitatively, it is clear that the FRET signal reduces with treatment as the images lose

blue/green signal for pink signal (figure 12). Medium signal was observed in surface plots

(data not shown), corresponding with blue/green stains on the FRET signal intensity images

(figures 12A,D,G,J).

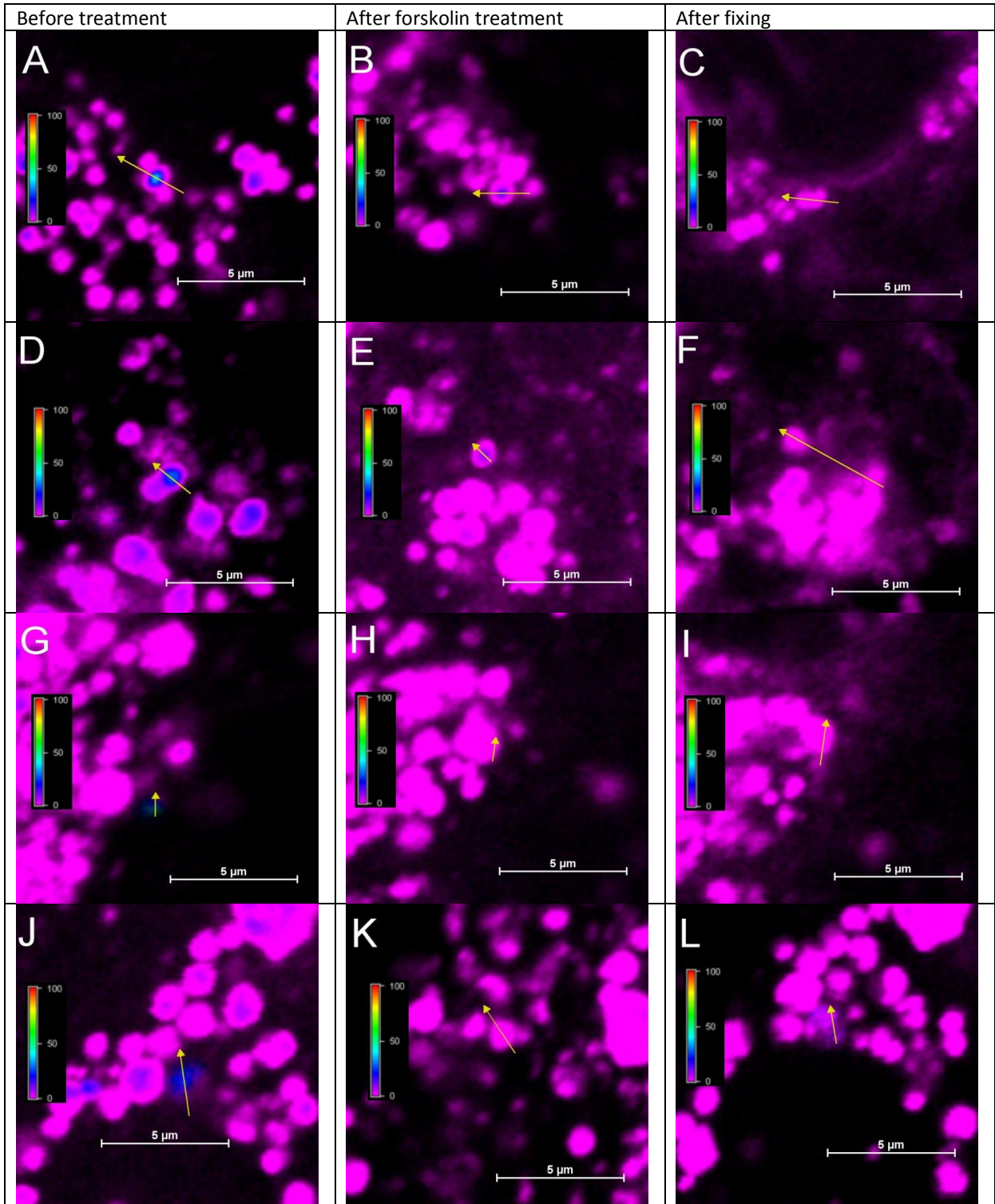


Figure 12: FRET signal intensity images at the site of signal for obtained samples at the three treatment stages. (A-I) show 3 synapses from sample 1, (A-C) synapse 1, (D-F) synapse 2, (G-I) synapse 3. (J-L) shows the synapse from sample 2. Arrows show the area measured for quantitative analysis. Scale bars represent 5 μ m. FRET scales on the images indicate the FRET signal recorded.

This was observed with all samples. Despite a clear reduction in signal intensity, it is difficult to be confident that analysis was taken at the same synapse as the staining appeared to adjust over time (figure 12). The intensity of FRET signals at the different treatments stages has been summarised in table 2. It could be observed that the highest signals were seen in untreated synapses. After the addition of forskolin, a huge drop in FRET signal intensity was observed, which in some examples led to a complete loss of signal. The mean signal intensity suggests that results after forskolin treatment are arguably negligibly small, with a maximum signal of 13%. After fixation the results do not appear to change by any identifiable amount.

Synapse analysed (sample-synapse number)	Pre-treatment maximum FRET signal (%)	Post-forskolin treatment maximum FRET signal (%)	Post-fixation maximum FRET signal (%)
1-1	43.9	13.0	3.1
1-2	27.6	0	0
1-3	55.7	0	0
2-1	25.8	5.8	9.8
Mean	38.3	4.7	3.2

Table 2: FRET intensity signals recorded at the synapses of samples. Signals were recorded at sites before treatment, after forskolin treatment and after fixing with formaldehyde. FRET signals reduced after forskolin treatment in all groups, whereas variable results were seen after fixing of the cells.

Percentage changes in the raw FRET signal percentage were calculated to try and overcome the differences brought in by the different size synapses prior to any LTP induction or fixing.

There is a consistent observation that FRET signals decreased substantially from any treatment, unless all FRET signal has been previously extinguished (table 3).

Interestingly, there was an area which managed to gain a strong signal after fixation where signal had not previously been observed (figure 13A) as indicated by the clear peak in the surface plot as well as being clear qualitatively (figure 13A and B). Whereas FRET intensity

signal was at 0 at this point before and during the treatment periods, after fixation, the signal increased to over 50% (figure 13C).

Synapse analysed (sample-synapse number)	Actual change in the maximum % FRET signal between pre and post-forskolin treatments [percentage change in percentage signals]	Actual change in the maximum % FRET signal between post-forskolin treatments and post-fixation [percentage change in percentage signals]
1-1	-30.9 [-70.4]	-9.9 [-76.4]
1-2	-27.6 [-100]	0 [0]
1-3	-55.7 [-100]	0 [0]
2-1	-20 [-77.5]	4.0 [68.1]
Mean	-33.6 [-87.0]	-1.5 [-2.1]

Table 3: Changes in FRET intensities were examined between the different treatment stages. Actual reductions in the raw FRET signal percentage, as produced by the A1R graphs, as well as a percentage change in the raw FRET signal percentages are presented.

To further analyse the effects of forskolin, images were taken before and after sham treatment in one sample (figure 14). Qualitatively, it can be observed that there was a reduction in the signal, which could also be observed from qualitative analysis of the surface plot data. The data showed a drop of about 20% in the raw FRET signal intensity, although this cannot be shown statistically (figure 14D). It could be argued that the reduction in signal intensity is reduced in sham treatment, only a 46.8% drop compared to the average 87% reduction seen in forskolin treated groups. Only one observation was made for the sham group so this statement must be viewed with some scepticism.

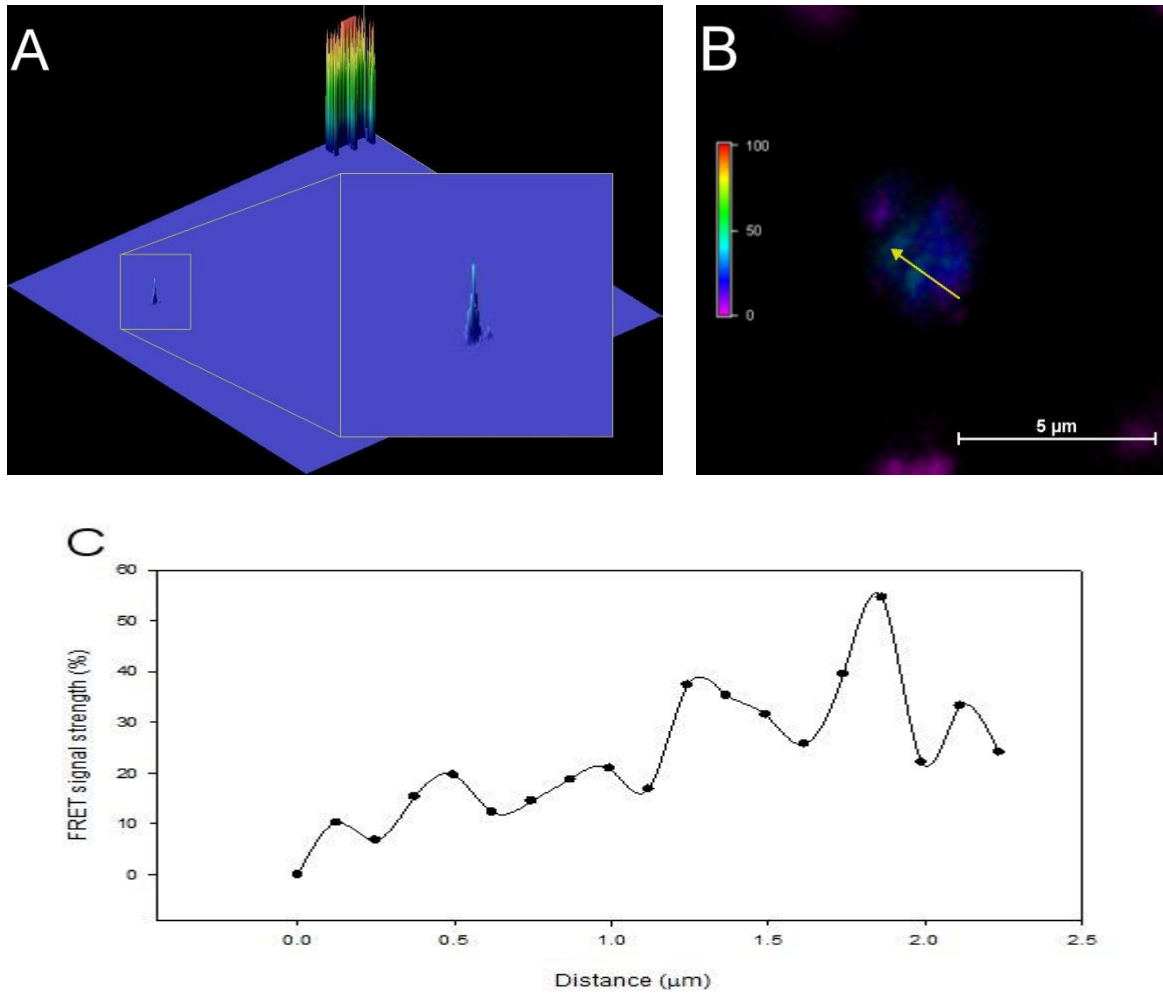


Figure 13: Evidence of an extra FRET signal appearing after fixation in one sample. (A) A medium FRET signal surface plot. The area highlighted by the red circle shows a peak which was not observed in the untreated and forskolin treated images. (B) The FRET intensity signal can be observed when focussed on qualitatively as well as (C) quantitatively along the arrow in (B). The data shows a very strong signal reaching over 50% FRET signal intensity. (B) FRET scales on the images indicate the FRET signal recorded.

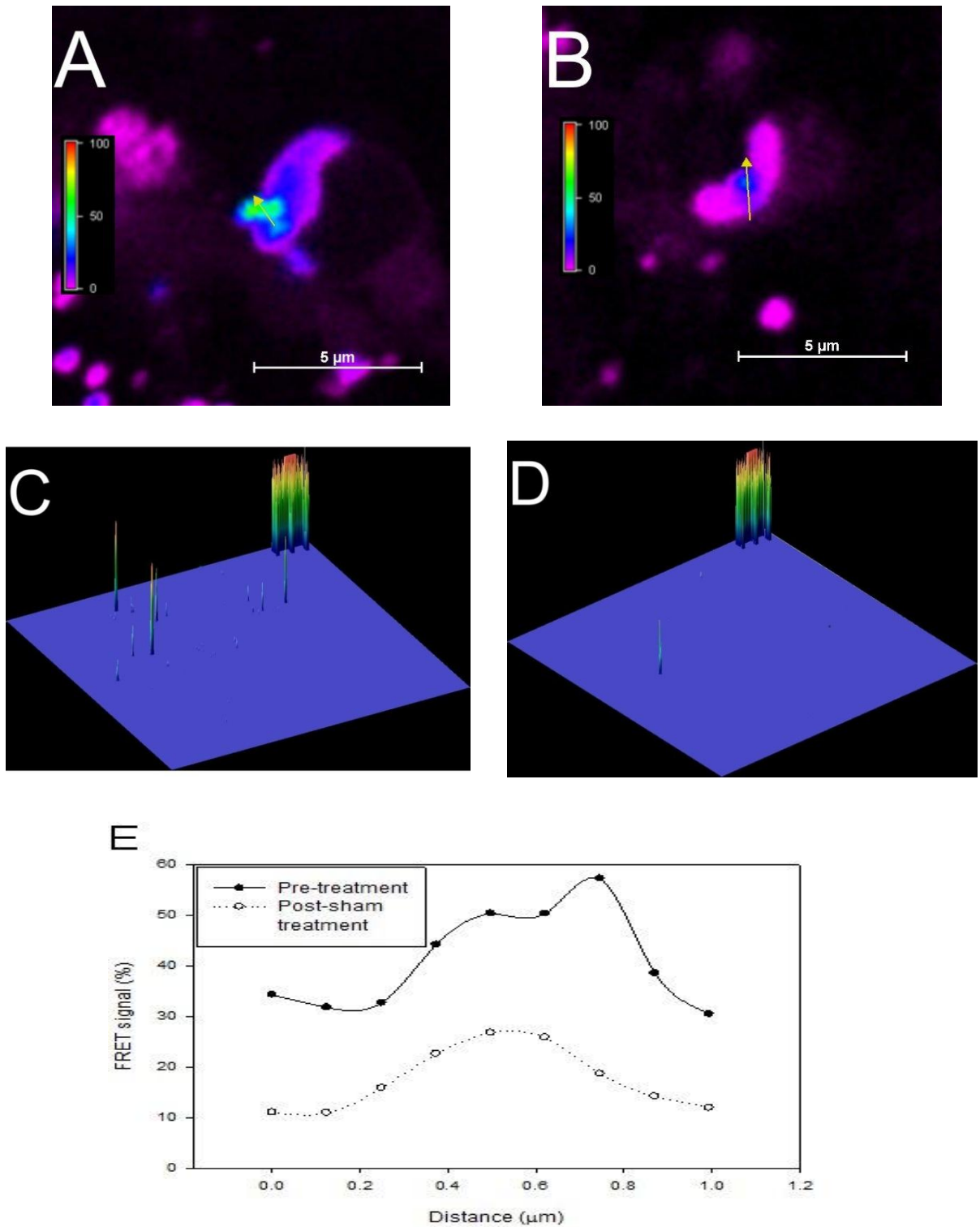


Figure 14: Data showing the effects of sham treatment on FRET signals produced by neuron samples in MFD cultures. FRET signals can be observed of the pre-treated (A) and post-sham treated (B) at the same synapse. Scale bars represent 5μm. FRET scales on the images indicate the FRET signal recorded. A clear reduction in the signal can be seen which is backed up by a drop in the intensity and frequency of peaks on a medium FRET signal (green channel) surface plot of the pre-treatment (C) and sham treated (D) samples. Quantitative analysis of the data from the FRET image, taken at the position of the arrows (A and B) show that a clear reduction in signal is observed after sham treatment.

4 Discussion

4.1 Synapses can exhibit variable FRET signal with DiI/DiO staining

Due to a number of limitations, results collected in this study are inconclusive for addressing the hypothesis. The low sample size also means that it is difficult to feel too confident with any results obtained. From the results it is possible to show that FRET signal can be created at the synapses between DiI and DiO stained neurons. This gives a strong indication that the synapses can be smaller than 10nm, opposing electron microscopy data stating synapses suggesting synapses tend to be within 15-25nm range (Savtchenko and Rusakov 2007). It was also possible to observe a decrease in the FRET signal after fixation, agreeing with previous reports (Hayat 1989, Leunissen and Yi 2009, Rostaing *et al* 2006). It is unlikely that fixation will induce proportional changes in the synaptic cleft size, thus invalidating the data on synaptic cleft sizes from these previous investigations.

One interesting explanation is that there was a decrease in the FRET signal after LTP induction with forskolin, which is debatably larger than the change induced in sham treatments. This was unexpected as it was hypothesised that by inducing LTP, the synaptic cleft will shrink, aiding neurotransmitter delivery and transmission (Gobert *et al* 2008, Wahl *et al* 1996). This result may simply be due to loss of fluorescence due to photobleaching, however it could be a sign that sufficiently small synaptic clefts actually increase in size upon LTP induction. Savtchenko *et al* (2007) argued that decreasing the cleft size below 12nm increases the electrical resistance, causing a decrease in the excitability of the synapse. The loss of signal could be a sign that the synapses are enlarging to overcome this electrical

resistance. Despite this idea, the limitations in this investigation meant that the data does not agree, nor disagree with this hypothesis and further work is required to back up these results.

It is not surprising that there was no sign of high FRET signal in any of the samples. This is because for a high FRET signal, the distance between the probes needs to be less than 4nm, for which there is no data to suggest that this can occur. It is difficult to explain why one sample showed an increase in FRET signal at a lone site after fixation. It could be evidence suggesting that some neurons can be brought closer by fixation, however due to the are of the signal, the more likely explanation is that a contaminant was able to enter during the treatment phases.

4.2 Limitations and future implications

There were a number of limitations encountered when performing this investigation.

Adjustments of the growth, staining and imaging protocols as well as infections, meant that a low number of results were collected.

One of the largest limitations we encountered was with the MFDs. It was observed that after repeated use of the MFDs, a crystal/salt deposition built up which led to a decrease in the ability of the MFDs to adhere as well physically blocking the microgroove so that axons could not extend through. After correspondence with Xona tech support (Xona Microfluidics LLC, Temecula, U.S.A), a number of possible methods to counteract these problems were postulated. These obstructions could be overcome by treating with boiling water, to help the deposits become soluble or by sonication. It has also been reported that hydrochloric acid

can clean the devices however this will likely cause further damage to the devices. The hydrochloric acid could possibly be absorbed into the compound and result in damage to the neurons or alter their behaviour (Toepke and Beebe 2006). The easiest option would be to only use the devices once, however due to time constraints and the expense of the MFDs, this was not an option in the present study.

It was observed that extensive cell death occurred in some samples after MFD seeding. This is most likely to be caused by the crystal/salt deposition, or from abrasion due to detachment of the MFDs, however it is possible that the growth conditions were not optimum. It has been recorded that hypoxic conditions, around 9% O₂, are more suited for neuron survival, as this more closely mimics the conditions found *in vivo* (Brewer and Cotman 1989). Addition of neurotrophic factors may also help to improve the survival rate, however there was only a subset of cells where cell loss was observed, and only after the salt/crystal debris became visible, suggesting that cell death is not a major limitation.

Although there has been extensive work with forskolin, all the data has been collected from samples that are purely from the rat hippocampus (Gobert *et al* 2008, Fortin *et al* 2010, Otmakhov *et al* 2004). It is possible forskolin has no observable effects on the mouse neocortex, or that the cAMP upregulation caused by forskolin may have additional effects in mice neocortical cells which have not been documented, resulting in the observed loss of FRET signal. It would be more likely however that photobleaching has occurred, causing the decrease in signal.

Photobleaching was a significant problem with the data analysis. The results showed a considerable decrease in FRET signal even after sham treatment indicating that signal must

be lost. We tried to account for this by limiting the number of images taken per treatment, thus having larger depth between photos. This increased the chances of taking images at slightly different depths which considering the size of synapses, could have serious implications on the results. Photobleaching is known to be a major issue for FRET studies, especially those involving time lapse images, and thus the, 'donor-recovery after acceptor photobleaching technique has been developed. However, this technique is not suitable for live cell imaging (Zal and Gascoigne 2004). Zal *et al* claim to have developed a technique, deemed E-FRET, which can take the photobleaching into account based on a series of calculations modelling changes over time. They have shown results which back up their claim and theoretically, it could be easy to adjust settings on the previous system to account for the technique, however this would be fully dependent on the facilities available. Additionally, there is the limitation that this method increases noise signal and thus could cause false positive results. Overall, the technique could be beneficial and may be vital to allow for progression in this investigation.

Another approach would be to perform multiple sham tests alongside LTP investigations. Provided that some signal is maintained, errors caused by photobleaching at different stages could be identified and corrected for. Considering we observed total or near total loss of signal in most samples, this approach is likely to be very limited. Additionally, as original synaptic cleft size and other factors will be involved, it is unlikely that this method will be accurate.

Changing the dyes or keeping the cells in hypoxic conditions could help prevent photobleaching. It is not obvious which dyes could be used due to the requirement to enter

the membrane and also be able to work as a FRET pair. One such option would be to genetically incorporate the FRET pairs, CFP and YFP onto proteins found in the synaptic cleft such as ion channels, receptors or transmembrane scaffolds (Shimozono and Miyawaki 2008). This method could help to remove some of the difficulties associated with retrograde transport of markers. For this to be an option there cannot be any interaction between the chosen markers outside of the synaptic cleft, limiting the possible candidate markers. Previous studies have shown that oxygen accelerates photobleaching (Bernas *et al* 2004). Neurons have also been shown to grow preferentially in hypoxic conditions, as this more closely mimics endogenous conditions, so complications are unlikely to occur (Brewer and Cotman 1989). It is unlikely that this method could be implemented though as it would be very expensive.

A major limitation is that FRET microscopy is an extremely sensitive approach. It is possible that most synapses will be larger than 10nm, and thus signal will not be observed. If however, evidence testing the hypothesis is obtained, the model also needs to be tested to prove that LTP induction has actually occurred. It theoretically would be possible to take electrophysiological recordings to examine the fEPSP of the cells (Dichter 1978), however gaining entry to the channels of the MFDs where the examined synapses and neurons reside, would be difficult. Other methods could be to use voltage dependent or calcium dependent dyes. Voltage dependent dyes would clearly indicate a change in the population fEPSP and have been shown to be able to stably examine voltages for up to 8 hours (An *et al* 2012) (Momose-Sato *et al* 1999). This could be utilised to examine the level of fluorescence as an indirect measure of the fEPSP whilst measuring the FRET signal. Calcium sensitive dyes will

also be relevant due to the role that calcium has in the onset and maintenance of LTP through calcium dependent kinases (Wong *et al* 1999, Chen *et al* 2001).

To take this investigation further, studies need to be performed on specific neuron types. It is well documented that different neuronal subclasses use different mechanisms to perform LTP (Bashir 2001). Additionally it would be interesting to examine whether this form of LTP can be observed to change during the natural ageing process, which could link the data to a number of aging or neurodegenerative diseases (Yasuda *et al* 2002). Once an effective procedure has been developed to measure the synaptic cleft size, it would be useful to examine what proteins are involved in the process. This could be done by using microarray data of cells which are shown to be going through LTP. Proteins with altered expression could then be inhibited or knockout models could be used to examine which proteins are involved in the process.

5 *Conclusions*

In conclusion, we have demonstrated that FRET microscopy is a valid technique for examining synaptic cleft size, although further optimisation is required. The data suggests that treatment with aldehyde causes the synaptic cleft to enlarge, however a similar observation was observed after forskolin induced-LTP. Whether this is due to a physiologic function or due to photobleaching has yet to be determined. Further work is required to prove these results as a low sample size may have altered results.

6. Bibliography

- ABD Bioquest, Inc. *DiD, DiI, DiO and DiR for labelling cell membranes*. 2008. tools.lifetechnologies.com/content/sfs/manuals/mp00282.pdf (accessed Feb 4, 2014).
- An, S., J. Yang, H. Sun, W. Kilb, and H. Luhmann. "Long-term potentiation in the neonatal rat barrel cortex in vivo." *The Journal of Neuroscience* 32 (2012): 9511-6.
- Bashir, Z. "Neuronal mechanisms of memory formation: concept of long-term potentiation and beyond." *Brain* 124 (2001): 2335-8.
- Bernas, T., M. Zarebski, J. Bobrucki, and P. Cook. "Minimizing photobleaching during confocal microscopy of fluorescent probes bound to chromatin: role of anoxia and photon flux." *Journal of Microscopy* 215 (2004): 281-96.
- Bourne, J., and K. Harris. "Balancing structure and function at hippocampal dendritic spines." *Annual Review of Neuroscience* 31 (2008): 47-67.
- Brewer, G., and C. Cotman. "Survival and growth of hippocampal neurons in defined medium at low density: advantages of a sandwich culture technique or low oxygen." *Brain Research* 7 (1989): 65-74.
- Buchs, P., and D. Muller. "Induction of long-term potentiation is associated with major ultrastructural changes of activated synapses." *Proceedings of the National Academy of Science of the United States of America* 93 (1996): 8040-5.
- Calabrese, B., M. Wilson, and S. Halpain. "Development and regulation of dendritic spine synapses." *Physiology* 21 (2006): 38-47.
- Chen, H., N. Otmakhov, S. Strack, R. Colbran, and J. Lisman. "Is persistent activity of calcium/calmodulin-dependent kinase required for the maintenance of LTP?" *Journal of Neurophysiology* 85 (2001): 1368-76.
- Dichter, M. "Rat cortical neurons in cell culture: culture methods, cell morphology, electrophysiology, and synapse formation." *Brain Research* 149 (1978): 279-93.
- Erni, R., M. Rossell, C. Kisielowski, and U. Dahmen. "Atomic-Resolution Imaging with a Sub-50-pm Electron Probe." *Physical Review Letters* 102 (2009): e096101.
- Fedulov, V., C. Rex, D. Simmons, L. palmer, C. Gall, and G. Lynch. "Evidence that long-term potentiation occurs within individual hippocampal synapses." *Journal of Neuroscience* 27 (2007): 8031-9.
- Fleck, M., A. Palmer, and G. Barrionuevo. "Potassium-induced long-term potentiation in rat hippocampal slices." *Brain Research* 580 (1992): 100-5.
- Fortin, D., M. Davare, T. Srivastava, J. Brady, S. Derkach, V. Nygaard, and T. Soderling. "Long-term potentiation-dependent spine enlargement required synaptic Ca²⁺-Permeable AMPA receptors recruited by CaM-Kinase I." *The Journal of Neuroscience* 30 (2010): 11565-75.
- Geinisman, Y. "Perforated axospinous synapses with multiple, completely partitioned transmission zones." *Hippocampus* 3 (1993): 417-33.
- Gobert, D., et al. "Forskolin induction of late-LTP and up-regulation of 5' TOP mRNAs translation via mTOR, ERK, and PI3K in the hippocampal pyramidal cells." *Journal of Neurochemistry* 106 (2008): 1160-74.
- Grover, L., E. Kim, J. Cooke, and W. Holmes. "LTP in hippocampal area CA1 is induced by burst stimulation over a broad frequency range centered around delta." *Learning Memory* 16 (2009): 69-81.
- Harrison, C., and B. Alger. "Perfusion with high potassium plus glutamate can cause LTP erasure or persistent loss of neuronal responsiveness in the CA1 region of the hippocampal slice." *Brain Research* 602 (1993): 175-9.
- Hayat, M. *Principles and Techniques of Electron Microscopy*. London: The MacMillan Press, 1989.
- Hebb, D. *The organization of behaviour*. New York: Wiley & Sons, 1949.

- Herman, B., V. Frohlich, J. Lakowicz, T. Fellers, and M. Davidson. *Fluorescence Resonance Energy Transfer (FRET) Microscopy*. 2012. Olympusmicro.com/primer/techniques/fluorescence/fret/fretintro.html (accessed 04 11, 2014).
- Honig, M., and R. Hume. "Fluorescent carbocyanine dyes allow living neurons of identified origin to be studied in long-term cultures." *The Journal of Cell Biology* 103 (1986): 171-87.
- Jones, D. "Synaptic plasticity and perforated synapses: their relevance for an understanding of abnormal synaptic organisation." *APMIS. Supplementum* 40 (1993): 25-34.
- Leunissen, J., and H. Yi. "Self-pressurised rapid freezing (SPRF): a novel cryofixation method for specimen preparation in electron microscopy." *Journal of Microscopy* 235 (2009): 25-35.
- Lin, B., E. Kramar, X. Bi, F. Brucher, C. Gall, and G. Lynch. "Theta stimulation polymerizes actin in dendritic spine of hippocampus." *Journal of Neuroscience* 25 (2005): 2062-9.
- Lomo, T. "Frequency potentiation of excitatory synaptic activity in the dentate area of hippocampal formation." *Acta Physiologica Scandinavica* 277 (1966).
- Lynch, M. "Long-term potentiation and memory." *Physiological Reviews* 84 (2004): 87-136.
- Major, P., E. Egan, D. Herrick, and D. Kufe. "Effect of Ara-c incorporation on deoxyribonucleic acid synthesis in cells." *Biochemical Pharmacology* 31 (1982): 2937-40.
- Malenka, R., and R. Nicoll. "Long-term potentiation: a decade of progress?" *Science* 285 (1999): 1870-4.
- Millet, L., M. Stewart, J. Sweedler, R. Nuzzo, and M. Gillette. "Microfluidic devices for culturing primary mammalian neurons at low densities." *Lab on a Chip* 7 (2007): 987-94.
- Momose-Sato, Y., K. Sato, Y. Arai, I. Yazawa, H. Mochida, and K. Kamino. "Evaluation of voltage-sensitive dyes for long-term recording of neural activity in the hippocampus." *The Journal of Membrane Biology* 172 (1999): 145-57.
- Moore, F., and J. Baleja. "Molecular remodelling mechanisms of the neural somatodendritic compartment." *Biochimica et Biophysica Acta* 1823 (2012): 1720-30.
- Otmakhov, N., et al. "Forskolin-induced LTP in the CA1 hippocampal region is NMDA receptor dependent." *Journal of Neurophysiology* 91 (2004): 1955-62.
- Padilla-Parra, S., and M. Tramier. "FRET microscopy in the living cell: different approaches, strengths and weaknesses." *BioEssays* 34 (2012): 369-76.
- Park, J., B. Vahidi, A. Taylor, S. Rhee, and N. Jeon. "Microfluidic culture platform for neuroscience research." *Nature Protocols* 1 (2006): 2128-36.
- Ramon y Cajal, S. *Histologie du systeme nerveux de l'homme et des vertebres*. Paris, 1911.
- Rostaing, P., et al. "Analysis of synaptic ultrastructure without fixative using high-pressure freezing and tomography." *European Journal of Neuroscience* 24 (2006): 3463-74.
- Savtchenko, L., and D. Rusakov. "The optimal height of the synaptic cleft." *Proceedings of the National Academy of Sciences in the United States of America* 104 (2007): 1823-8.
- Schwechter, B., and K. Tolias. "Cytoskeletal mechanisms for synaptic potentiation." *Communicative and Integrative Biology* 6 (2013): e27343.
- Sekar, R., and A. Periasamy. "Fluorescence resonance energy transfer (FRET) microscopy imaging of live cell protein localizations." *The Journal of General Physiology* 160 (2003): 629-33.
- Sengupta, P., D. Holowka, and B. Baird. "Fluorescence resonance energy transfer between lipid probes detects nanoscopic heterogeneity in the plasma membrane of live cells." *Biophysical Journal* 92 (2007): 3564-74.
- Shimozono, S., and A. Miyawaki. "Engineering FRET constructs using CFP and YFP." *Methods in Cell Biology* 85 (2008): 381-93.
- Tai, C., S. Mysore, S. Chiu, and E. Schuman. "Activity-regulated N-cadherin endocytosis." *Neuron* 54 (2007): 771-85.

Taylor, A., and N. Jeon. "Microfluidic and compartmentalized platforms for neurobiological research." *Critical Reviews in Biomedical Engineering* 39 (2011): 185-200.

Taylor, A., M. Rhee, S. Blurton-Jones, D. Cribbs, C. Cotman, and N. Jeon. "A microfluidic culture platform for CNS axonal injury, regeneration and transport." *Nature Methods* 2 (2005): 599-605.

Toepke, M., and D. Beebe. "PDMS absorption of small molecules and consequences in microfluidic applications." *Lab on a Chip* 6 (2006): 1484-6.

Wahl, L., C. Pouzat, and K. Stratford. "Monte Carlo simulation of fast excitatory synaptic transmission at a hippocampal synapse." *Journal of Neurophysiology* 75 (1996): 597-608.

Weeks, A., T. Ivanco, J. Leboutillier, D. Marrone, R. Racine, and T. Petit. "Unique changes in synaptic morphology following tetanization under pharmacological blockade." *Synapse* 47 (2003): 77-86.

Wong, Scott., et al. "Calcium-stimulated adenylyl cyclase activity is crucial for hippocampus-dependent long-term memory and late phase LTP." *Neuron* 23 (1999): 787-98.

Yasuda, H., A. Barth, D. Stellwagen, and R. Malenka. "A developmental switch in the signalling cascades for LTP induction." *Nature Neuroscience* 6 (2002): 15-16.

Zal, T., and R. Gascoigne. "Photobleaching-corrected FRET efficiency imaging of live cells." *Biophysical Journal* 86 (2004): 3923-39.